Thermophysical Study of Phenanthroline Derivatives

A Contribution for the Development of New Charge Transport Materials

José Miguel Silva Ferraz
Master's Degree in Chemistry – Specialization in Functionalized Materials and Surfaces for Sustainability
Faculty of Sciences, University of Porto
2022-2023

Supervisor
Vera Lúcia de Sousa Freitas, Researcher, Faculty of Sciences of the University of Porto
Co-supervisor
Maria das Dores Melo da Cruz Ribeiro da Silva, Associate Professor, Faculty of Sciences of the University of Porto


U.PORTO
FACULDADE DE CIÊNCIAS
UNIVERSIDADE DO PORTO

“Success is not final; failure is not fatal:
it is the courage to continue that counts.”

Winston Churchill

Dedicated to my parents and sister

Acknowledgements

Esta dissertação e o trabalho apresentado nela só foi possível devido ao apoio e às contribuições de pessoas e instituições às quais quero expressar a minha gratidão.

Primeiro, queria agradecer à minha orientadora, a Doutora Vera Feitas e à minha coorientadora, a Professora Doutora Maria das Dores Ribeiro da Silva não só por terem concordado em acolher e orientar este projeto, mas também por todo o apoio científico e pessoal que me deram. É um motivo de orgulho poder dizer que trabalhei convosco.

A todos os membros do grupo *Molecular and Supramolecular Thermodynamics* (RG2, CIQUP-IMS) pela calorosa receção e por todo o apoio fornecido durante a duração desta dissertação.

To Professor Stefano Vecchio Ciprioti, to Professor Andrea Ciccioli, and to Doctor Lorenza Romagnoli for receiving me in their laboratories at La Sapienza University of Rome, for being such gracious hosts, and for your continued support.

Ao Departamento de Química e Bioquímica da Faculdade de Ciências pela Universidade do Porto, ao Centro de Investigação em Química da Universidade do Porto, aos FCUP|DQB Lab&Services e à Universidade "La Sapienza" de Roma pelo apoio e pelas condições disponibilizadas para a execução deste trabalho.

Ao programa Erasmus+ pela concessão da bolsa de mobilidade de longa duração que tornou a minha estadia em Roma possível.

Aos meus amigos que têm estado sempre ao meu lado desde que esta aventura começou. A ouvir, a conversar, a discutir e a apoiar de uma forma incansável. A vocês, obrigado por me darem o privilégio de vos ter na minha vida e de fazer parte das vossas.

Por fim, é muito importante dizer que não teria sido capaz de perseguir o meu sonho de fazer química, de estudar, de fazer esta dissertação e tudo o que a envolveu sem o apoio infindável da minha família. A minha mãe, o meu pai e a minha irmã são as pessoas mais importantes na minha vida e não existem formas que cheguem na língua portuguesa ou em qualquer outra para conseguir expressar o quão grato estou por tudo o que fazem e fizeram por mim.

Obrigado!

Resumo

No contexto do nosso interesse na caracterização termodinâmica de compostos heterocíclicos de azoto, esta dissertação incide em estudos termofísicos experimentais recentemente desenvolvidos para dois compostos derivados da fenantrolina: a batofenantrolina e a batocuproina. Estes compostos exibem propriedades com relevância em química de coordenação e são potenciais candidatos para o uso no transporte de cargas em materiais constituintes de dispositivos semicondutores orgânicos.

O comportamento térmico dos dois compostos foi estudado utilizando várias técnicas, nomeadamente a calorimetria diferencial de varrimento e a análise termogravimétrica. Para determinar as respetivas entalpias de sublimação, foram realizadas medições de pressão de vapor utilizando diferentes métodos, incluindo o método de efusão de Knudsen (por perda de massa e por espectrometria de massa), a termogravimetria isotérmica e a termogravimetria baseada numa microbalança de cristal de quartzo. Além disso, a entalpia de sublimação para cada composto também foi medida calorimetricamente usando a microcalorimetria Calvet de alta temperatura.

Os resultados obtidos fornecem uma compreensão mais profunda do comportamento de transições de fase para estes compostos, da fase condensada para a fase gasosa, esclarecendo a possível decomposição e as forças intermoleculares inerentes às espécies. Este conhecimento contribui para a caracterização abrangente das propriedades termofísicas destes compostos heterocíclicos de azoto.

Palavras-chave: fenantrolina, semicondutores orgânicos, comportamento térmico, pressão de vapor, estudo termofísico.

Abstract

In the context of our interest on the thermodynamic characterization of nitrogen heterocyclic compounds, this thesis focuses on the recently developed experimental thermophysical studies of two phenanthroline derivatives: bathophenanthroline and bathocuproine. These compounds exhibit properties that make them relevant ligands in coordination chemistry and potential candidates for use as charge carrier transporting materials in organic semiconductor devices.

The thermal behaviour of the two compounds has been studied using several techniques, namely, differential scanning calorimetry and thermogravimetric analysis. In order to determine the respective enthalpies of sublimation, vapor pressure measurements were carried out using different methods, including Knudsen effusion mass loss/mass spectrometry, isothermal thermogravimetry, and a quartz crystal microbalance technique. Additionally, the enthalpy of sublimation for each compound was measured calorimetrically using high-temperature Calvet microcalorimetry.

The results obtained provide a deeper understanding of the phase transition behavior for these compounds from the condensed phase to the gaseous phase, shedding light on molecular decomposition and the inherent intermolecular forces of the species. This knowledge contributes to the comprehensive characterization of the thermophysical properties of these nitrogen heterocyclic compounds.

Keywords: phenanthroline, organic semiconductors, thermal behaviour, vapour pressure, thermophysical study.

Table of Contents

List of Tables

List of Figures

List of Abbreviations and Symbols

BCP	Bathocuproine
BP	Bathophenanthroline
CM	Calvet Microcalorimetry
Δ	Change
CCTM	Charge Carrier Transporting Materials
μ	Chemical Potential
cr	Crystalline
DQB	Department of Chemistry and Biochemistry
DSC	Differential Scanning Calorimetry
DTA	Differential Thermal Analysis
E	Energy
H	Enthalpy
S	Entropy
FCUP	Faculty of Sciences of the University of Porto
f	Formation
FTIR	Fourier Transform Infrared
f	Frequency
g	Gas
GC	Gas Chromatography
G	Gibbs Free Energy
Q	Heat
C_p	Heat Capacity at Constant Pressure
ICP-MS	Inductively Coupled Plasma Mass Spectrometry
instr	Instrumental
U	Internal Energy
I-TG	Isothermal Thermogravimetry
KF	Karl-Fischer Titration
KTG	Kinetic Theory of Gases
KEML	Knudsen Effusion Mass Loss
KEMS	Knudsen Effusion Mass Spectrometry
KEM	Knudsen Effusion Method
l	Liquid
m	Mass
OSC	Organic Semiconductor

phen	Phenanthroline
p	Pressure
QCM	Quartz Crystal Microbalance
QCMG	Quartz Crystal Microgravimetry
rms	Root Mean Square
RT	Room Temperatore
SC	Semiconductor
STA	Simultaneous Thermal Analysis
T	Temperature
TG	Thermogravimetry
t	Time
trs	Transition
UP	University of Porto
VDM	Vacuum Drop-Microcalorimetry
XRD	X-Ray Crystallography

1. Introduction

The thermodynamic characterization of organic substances yields valuable insights into their molecular structure and reactivity, which is of great value to many other fields within Chemistry. This thesis aims at doing an in-depth thermophysical analysis of selected phenanthroline derivatives. To achieve this goal, experimental studies were conducted using various techniques available in two specialized research centres.

1.1. General Considerations on Phenanthroline and its Derivatives

The molecular family under the scope of this thesis derives from phenanthroline, a nitrogen containing heterocyclic molecule whose structure consists of three fused aromatic rings with two nitrogen heteroatoms that may vary in their positions originating several isomers. The most common and subsequently the most studied one is the 1,10-phenanthroline (phen) [1, 2], whose structural formula is represented on figure 1.1.

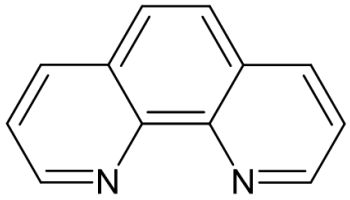

Figure 1.1 - Molecular structure of 1,10-phenanthroline (phen).

The synthesis of 1,10-phenanthroline involves Skraup reactions using glycerol and *o*-phenylenediamine as reactants, in the presence of a catalyst and an oxidizing agent.[2, 3] The reaction details are depicted in figure 1.2. Wherein glycerol undergoes a dehydration to produce acrolein, which subsequently condenses with *o*-phenylenediamine. This is followed by cyclization, resulting in the formation of the final compound. Furthermore, the original Skraup reaction can be modified to produce other ligands by introducing substituent groups added to the phenanthroline structure. [1-5] These substituent groups may include, but are not limited to NO_2, CH_3, phenyl and ether groups, such as methoxy groups.

.

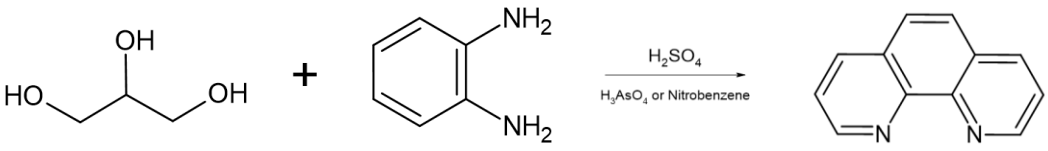

Figure 1.2 - Formation reaction of phenanthroline.[2]

The process of dehydration of glycerol will lead to the formation of acrolein which will then condense with the *o*-phenylenediamine subsequently followed by a cyclization which will form our final compound. It is also possible to alter the original Skraup reaction to form other ligands with substituent groups added to the phenanthroline structure.[1-5] Such substituent groups include but are not limited to NO_2, CH_3, phenyl and ether groups such as methoxy groups.

The juxtaposition of the nitrogen atoms and the rigidity of the three ringed planar structure, makes the molecules suitable for chelation.[6] Most phenanthroline complexes usually have the $[M(phen)_3]$ molecular formula with an octahedral geometry. Commonly studied phenanthroline complexes include Fe(II), Ni(II) and Ru(II) as their metallic centres. These complexes have interesting properties of their own such as the bioactivity of $[Ru(phen)_3]^{2+}$ and the luminescence of $[Cu(phen)_3]^{2+}$.[7, 8]

However, the electronic properties of these molecules gives rise to some other interesting applications. Of particular significance and relevance to this thesis is their use as charge carrier transporting molecular materials. This aspect is further explored in the next section.

1.2. Charge Carrier Transporting Materials

Most of the developments in this modern field depend on the better understanding of materials. One of the main focuses of research and investment in this area is regarding substances that can be useful for energy generation and transport. It is possible to distinguish several different kinds of classes of materials that have diverse electrical properties. However, some of the most fascinating and important fall under the purview of semiconductor (SC) materials.

1.2.1. Semiconductors

In the late 19th century, the first developments in the field of semiconductors emerged, marked by the development of a rectifier i.e., an AC/DC converter. Since then, the interest in this field grew significantly. Another major breakthrough occured in the 1940s when the first transistors were developed at Bell Labs. The research conducted by John

Bardeen, Walter H. Brattain and William Shockley on semiconductors and transistors would be awarded the 1956 Nobel Prize in Physics.[9] These devices act as switches and amplifiers for electrical signals and have since become a significant part of electronics. In figure 1.3, it is possible to see the three-point transistor, representing a significant milestone in the history of semiconductors. Afterward, the field experienced rapid expansion, and since the middle of the 20th century, semiconductors have become the very core and driving force of technological development.[9, 10]

Figure 1.3 - Point contact transistor. Adapted from ref. [10]

Semiconductors do not conduct electricity very well due to the presence of a gap between their valence band and conduction band, which is known as the energy gap, E_g. Figure 1.4 provides a visual representation of this phenomenon. In pure semiconductor materials, there are no energy levels in this region; therefore, it is considered a forbidden region. However, the size of E_g can be easily manipulated by changing the species that form the semiconductor. The bond interaction between elements is the main factor responsible of the size of E_g, with stronger bonds leading to a larger bandgap. It is important to note that external factors, such as temperature and pressure, can also affect E_g.[9-12]

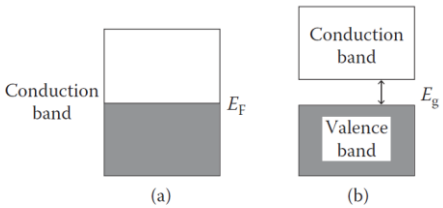

Figure 1.4 - Energy bands in a metal (a) and in a semiconductor (b). Adapted from ref. [9]

In metals, electrons are excited at all temperatures above 0 K, which allows the smooth conduction of electricity. However, in the case of semiconductor materials, conduction

occurs only when there is enough energy available to promote (excite) electrons from the valence band to the conduction band. This energy can come from thermal input but also from the absorption of light. When an electron moves to the conduction band, it leaves behind an absence of an electron in the valence band, which is known as a hole (considered to be a quasiparticle). It is important to note that the electrical charge of a hole is equal and opposite to that of an electron.[11]

However, this excitation is not permanent, and the electron can "fall back" into the empty state i.e., the hole in the valence band. This process is known as recombination and it leads to the annihilation of the charge carrier particles, resulting in the release of energy, usually in the form of a photon. Preventing recombination is crucial for energy generation purposes as the separation of electrons and holes generates an electrical potential. In most semiconductor materials, these two charge carriers (electron and holes) are the primary contributors to the conduction of electricity, with the exception of organic semiconductors, where positive or negative ions can also take part in the conduction process.[9-11]

It is also important to note that there are several types of semiconductors based on the composition of a particular material. If they consist of pure semiconducting materials, they are considered *intrinsic semiconductors*. However, in cases where impurities are present, they are known as *extrinsic semiconductors* and can be divided into two classes: positive (*p*-type) and negative (*n*-type) semiconductors. The '*n'* and '*p'* symbols represent the charge density present in a semiconductor, where '*p'* pertains to a larger density of holes and '*n'* corresponds to a larger density of electrons.[9, 11]

The impurities mentioned in the previous paragraph are known as dopants, which generally means that a chemical is inserted into the structure of the pure semiconductor with the intent of altering its properties, as shown in figure 1.5. This doping process opens the way for a massive universe of possible semiconductors. Each with different properties. Their high versatility and fascinating properties are the reasons why they brought the advent of integrated circuits and revolutionized computer industry, which deeply affects our daily lives.[9-11]

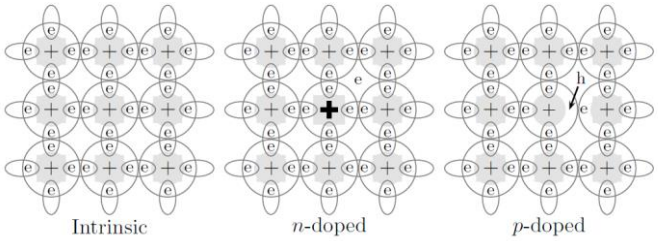

Figure 1.5 - Left: intrinsic semiconductor. Middle: *n*-type semiconductor (note the presence of an extra electron). Right: *p*-type semiconductor (note the absence of an electron i.e., the presence of a hole). Adapted from ref. [11]

1.2.2. Organic Semiconductors

Within semiconductors, various types of charge carrier transporting materials (CCTM) exist. However, this work will only focus on small organic molecules and molecular crystals.

Organic semiconductors (OSC) are solids materials composed of π-bonded molecules containing carbon and hydrogen atoms as their fundamental building blocks. In addition to carbon and hydrogen, heteroatoms like nitrogen, sulphur, and oxygen are frequently incorporated into these molecules. These heteroatoms play essential roles in both charge generation and charge transport within organic semiconductors.

These molecules have a major distinction from their inorganic or semi-metallic counterparts, particularly in the way that charge is transported through the material. In atomic solids, transport occurs intra-molecularly within the conduction band, as previously mentioned. However, in the case of molecular solids, charge transport is considered inter-molecular, often referred to as hopping transport.[13, 14] For instance, a temporary positive charge can be induced in a molecule before hopping to the next molecule, and this process continues through the material.

There are various ways to categorize these materials, depending on the property used for grouping. When considering their organization states, one can classify the sample into single crystals, polycrystals, liquid crystals, or amorphous glasses.[12, 15] This classification holds significance as the morphology of a material directly impacts its functionality in devices like organic light-emitting diodes (OLED).

Additionally, physical characteristics, such as grain size, grain boundaries, and molecular orientations, also play a crucial role in the performance of OSC devices. Consequently, the methods used to construct a specific CCTM layer are of particular importance.[12, 16] Organic CCTM can also be categorized based on the type of charge

carriers they transport, either as hole-transporting materials or electron-transporting materials.[15] Hole-transporting materials accept carriers with a positive charge and facilitate their transport and electron-transporting materials accept carriers with a negative charge and enable their movement. Figure 1.6 showcases some examples of charge transporting molecular materials.

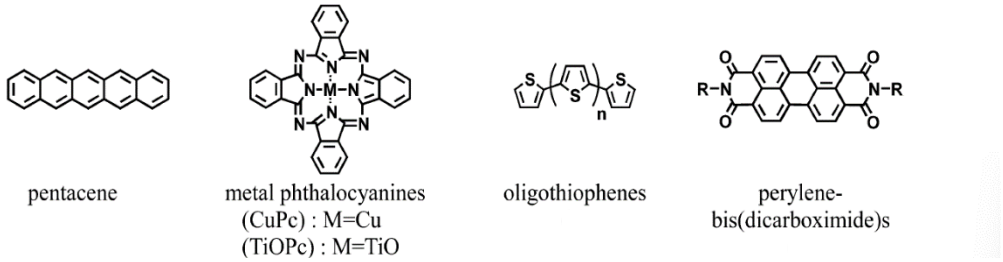

Figure 1.6 - Examples of charge carrier transporting materials used in OSC devices. Adapted from ref.[15]

It is worth emphasizing the significance of blocking charge carriers, which stands in contrast to charge carrier transport. Blocking electrons and holes plays a crucial role as it prevents their recombination, thereby promoting the generation of an electrical current. This property is of utmost importance in various semiconductor devices, as it enhances their efficiency and overall performance.

1.2.3. Applications of phenanthrolines in OSCs and in optoelectronics

When searching through literature, one finds very little information about the 1,10-phenanthroline in this field. Research has shown that 1,10-phenanthroline itself is a weakly emissive compound. However, when the search is extended to its derivatives the same does not apply.[4] The high synthetic versatility of this molecule opens up a wide range of possibilities, yielding different molecules with significantly different optoelectronic and charge carrier transporting properties. Extensive research efforts have been made to improve not only the electronic properties of pristine 1,10-phenanthroline but also to develop new chelating agents for photoluminescent metallic complexes.[17] Several functional groups have been studied, with those positioned at the 2,9 and 4,7 positions exhibiting the most promising synthetic approaches.[4, 18, 19] These functional residues typically aim to extend the π-conjugation or to introduce additional electrons into the system.[18] Systematic spectroscopic and theoretical studies of aryl-substituted phenanthrolines have shown significant variations in luminescence and

electronic properties depending on the substituents. The symmetry of the substitution seems to be the most important factor, along with the presence of electron-donating groups and dihedral torsion angles.[4, 18] These findings highlight the importance of substituent effects in tailoring the optoelectronic characteristics of phenanthroline derivatives. Another particularly interesting application that is also found in more general semiconductors is the control of the direction of energy/electron transfer. Studies have reported that by leveraging energy decrease of the singlet excited states of protonated phenanthrolines, it is possible to fine-tune the direction of energy transfer in appropriately designed arrays.[4, 18-20] Figure 1.7 illustrates one such case, showcasing the potential of these derivatives in directing energy transfer processes.

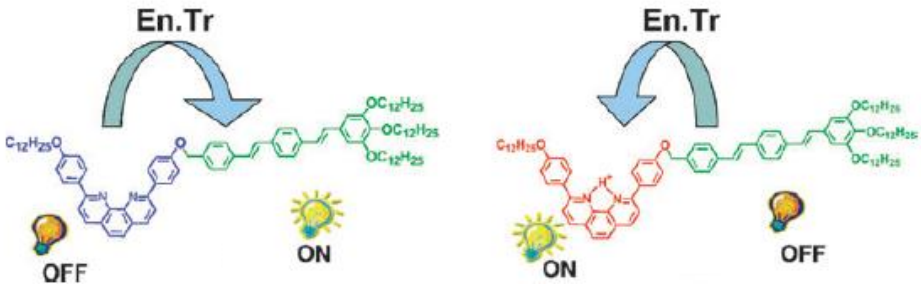

Figure 1.7 – Energy transfer direction in two oligophenylenevinylene functionalized phenanthrolines. Adapted from ref.[4]

In recent years, phenanthroline and its derivatives have shown distinct charge mobility properties, excelling in both electron and hole transport, as well as in blocking their passage.[15, 16, 20] Notably, bathophenanthroline and bathocuproine have been reported to exhibit high electron mobilities, comparable to other electron-transporting materials.[8, 21, 22] Additionally, these molecules have been found to serve as effective hole-blocking layers for energy generation purposes. In figure 1.8, two phenanthroline derivatives are presented, designed specifically as cathode interface layers. These materials have demonstrated their ability to enhance the efficiency of energy conversion in organic solar cells.[23]

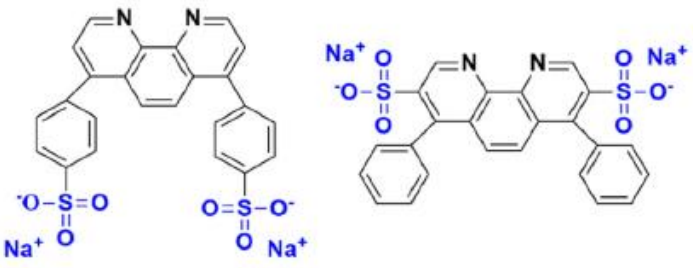

Figure 1.8 - Phenanthroline derived sulphonate salts used as cathode interface layers. Adapted from ref.[23]

The research on thin films of phenanthroline derivatives has yielded interesting results, as reported by Charas et al.[24] The study demonstrated that bathophenanthroline and bathocuproine form nanostructured layers when thermally deposited on the presence of LiF.

The use of 1,10-phenanthroline derivatives as tunable luminescent molecules and organic semiconductors is an ever-increasing field of research. These compounds have shown to be promising new charge carrier transporting materials.

1.3. Thermodynamics of the Studied Compounds: an Overview

The study of nitrogen heterocyclic compounds has been the focus of many research groups over the years and is the main topic of this thesis. As it will be further explored in this section, there is a severe lack of thermodynamic information regarding this molecular family. This work rises as a thorough analysis, focusing on two derivatives: 4,7-diphenyl-1,10-phenanthroline (bathophenanthroline, BP) and 2,9-dimethyl-4,7-diphenyl-1,10-phenanthroline (bathocuproine, BCP). The molecular formulae of these molecules is shown on figure 1.9.

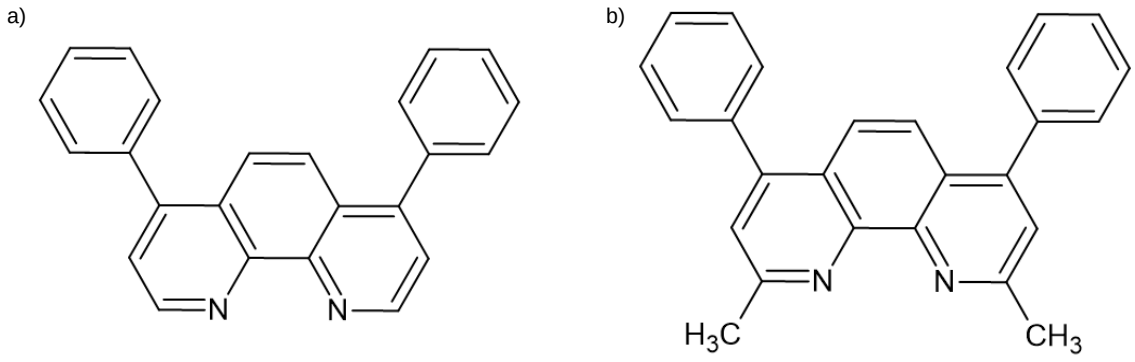

Figure 1.9 - Studied molecules. a) Bathophenanthroline; b) Bathocuproine.

The first thermodynamic study of phenanthroline and one of its derivatives was published by Vecchio et al.[25] in 2007. This analysis focused on determining the heat capacities and molar enthalpies and entropies of fusion of anhydrous 1,10-phenanthroline and 2,9-dimethyl-1,10-phenanthroline (neocuproine). The study yielded the following values for temperature, molar enthalpy, and molar entropy of fusion: (391.1 ± 0.1) K, (11.8 ± 0.1) $kJ \cdot mol^{-1}$, (30.0 ± 0.3) $kJ \cdot K^{-1} \cdot mol^{-1}$ for 1,10-phennathroline, and (435.9 ± 0.3) K, (17.6 ± 0.3) $kJ \cdot mol^{-1}$, (40.3 ± 0.6) $J \cdot K^{-1} \cdot mol^{-1}$ for neocuproine.[27] Additionally, it is noteworthy

that both phenanthroline and neocuproine exhibited single sharp endothermic peaks, corresponding to melting, and no solid-solid transitions were observed within the studied temperature range. Upon further searching the literature, a study conducted by Chickos et al. [26] in 2010 determined the vaporization enthalpy at 295.15 K and vapour pressures for the 1,7 and 4,7 phenanthroline derivatives. Only one other thermodynamic study of phenanthroline derivatives was found in the literature, focusing on determining the sublimation enthalpies of 5-substituted-1,10-phenanthrolines (as shown in figure 1.10), this study used Knudsen effusion mass loss and solution calorimetry.[27]

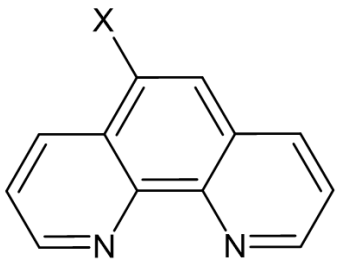

X = Cl, CH_3, CN, OCH_3, NH_2 & NO_2

Figure 1.10 - 5-Substituted-1,10-phenanthrolines studied by Brunetti et al.[27]

When searching for more thermodynamic studies of phenanthroline and its derivatives, a significant gap becomes evident. There is a clear lack of thermochemical and thermophysical data for other molecules in this family. This gap is particularly notable for the molecules bathophenanthroline and bathocuproine.

1.4. Goals and Methodology

In the context of a continuous study of the phenanthroline molecular family, this dissertation aims to develop the thermophysical study of two phenanthroline derivatives. This research is part of a broader study that also includes a thermochemical approach. The work presented in this dissertation focuses on the transition from the condensed phases to the gaseous phase and has three main goals: studying the thermal behaviour, understanding the phase stability of the molecules under investigation, and the determining thermophysical parameters.

Furthermore, it is worth mentioning that the research undertaken in this dissertation adopts a multitechnique approach to accomplish the stated objectives. By employing a diverse set of techniques, a deeper understanding of the phase transition processes is achieved, and valuable insights into molecular forces or potential molecular

decomposition processes (if any) are gained. The thermal behaviour of the proposed compounds has been studied using techniques such as differential scanning calorimetry and thermogravimetrical analysis. A significant number of vapour pressure techniques have been used to indirectly analyse the sublimation process. These methods include Knudsen effusion mass spectrometry/mass loss, isothermal thermogravimetry, and quartz crystal microgravimetry. Furthermore, vacuum drop-microcalorimetry has been used to directly study the energetics of sublimation.

Indeed, the thermodynamic characterization of these substances will yield valuable insights into their molecular structure and reactivity, which holds significance in various fields within Chemistry. By combining well-established and time-proven experimental methods, it becomes feasible to accurately determine all the parameters mentioned above. Moreover, this approach will shed light on molecular interactions and deepen our comprehension of molecular stability, making a significant contribution to the advancement of scientific knowledge in the field.

2. Physical Changes of Pure Substances

Perhaps the most fundamental way to study chemical systems is by examining the relationship between heat and work during the chemical or physical changes of substances within the constraints of the laws of thermodynamics. This field is known as chemical thermodynamics and involves not only the application of mathematical models to chemical and physical changes but also experimental determinations of various thermodynamic properties.

Chemical Thermodynamics has its origins in the late 19th century with the works of Rudolf Clausius when he first suggested that there was a relation between thermochemistry and thermodynamics in his "*Mechanical Theory of Heat"* [28]. Building on this, Josiah Willard Gibbs wrote and published a series of papers in which he described how the first two laws of thermodynamics could be used to determine the thermodynamic equilibrium of chemical reactions and their tendencies to occur or not. His most famous work was "*On the Equilibrium of Heterogenous Substances*" [29] and would become a defining milestone for chemical thermodynamics.

During the early 20th century, other works by Gilbert Lewis, Merle Randall and Edward Guggenheim would became paramount in defining modern chemical thermodynamics and still serve as the foundations for the merging between thermodynamics and chemistry today.[30]

Thermodynamics has been defined as the study of energy, its different forms, transformations and interactions between it and matter. In chemistry this translates to the study of energy changes in chemical reactions, phase changes, and solvation processes. These processes are characterized by state functions such as internal energy (*U*), enthalpy (*H*), entropy (*S*), and Gibbs energy (*G*).

Chemistry is usually known as the science that studies matter and its transformations. These transformations are usually associated with chemical change. However, chemistry also studies physical transformations, such as transitions between phases of pure substances. These changes occur without changing the chemical composition or identity of a substance. This section provides some insights into the states of matter, physical transformations, and phase boundaries, with the purpose of applying this knowledge to the experimental techniques used in this thesis.

2.1. States of Matter and Phase Transitions

One of the simplest ways to characterizing matter is by defining the state in which it exists at a particular temperature and pressure. However, it is important to first define what a phase or state of matter is.

A phase or state of matter is a form of matter that is uniform in terms of chemical composition and physical state. The most common states of matter are solid, liquid, gas, and plasma. However, many others exist, such as liquid-crystalline states, several solid phases such as the various allotropes or polymorphs, and some that only exist under rather extreme conditions, like the Bose-Einstein Condensate, which only exists at extremely low temperatures.

The three more common states: solid, liquid, and gas are differentiated from each other by the way atoms or molecules are distributed in a sample. In solids, atoms or molecules are arranged in an orderly fashion and close together. There are strong interactions between them (usually intermolecular forces), and there is little to no freedom of motion (depending on the type of solid under considering). Liquids are close together, but the "bonding" between the molecules is not as strong as in solids, allowing for greater freedom of movement. These two states, along with all their variations such as different polymorphs or liquid crystals, have their own unique characteristics and are the focus of study in a separate branch of physics known as condensed matter physics.

Gases, however, are of special importance. In this state, the particles are widely spaced apart, leading to limited interactions between. This gives rise to the concept of an ideal gas and to the differences between real or non-ideal gases. When working with an ideal gas, it is important to consider that these gases have zero density and infinite volume. At infinite volume, the volume occupied by the gaseous particles becomes negligible compared to the overall volume of the gas, so the gaseous atoms or molecules themselves are considered to have zero volume. At zero density, the atoms or molecules are infinitely far apart, resulting in zero intermolecular forces. Therefore, deviations from ideality (real gases) are primarily due to intermolecular forces and nonzero volume. For experimental purposes, there is an approximation that can be applied to treat real gases as ideal. Using very low pressures reduces the gas density, thereby diminishing the strength and presence of intermolecular interactions.

The spontaneous transformation from one phase to another, known as a phase transition, occurs at a specific pressure and at a characteristic transition temperature, T_{trs}. At these temperature and pressure coordinates, the two phases are in equilibrium

with each other. In the following table, there are the names of the main phase transitions between the previously described states of matter.

Table 2.1 - Denominations of phase transition processes between solids, liquids, and gases.

From/To	Solid	Liquid	Gas
Solid	-	Melting	Sublimation
Liquid	Freezing	-	Vaporization
Gas	Deposition	Condensation	-

Each transition and phase have its own characteristic coordinates, which are summarized below.

- Normal Point/Temperature (p = 1 atm)
- Standard Point/Temperature ($p = 10^5$ Pa)
- *"Phase Transition"* Point/Temperature

Additionally, there is a set of conditions where three different phases can coexist instead of the usual two. This point is known as the triple point (T_3), where the boundaries of the three phases intersect.

There is also the critical point. The temperature (T_c) and pressure (p_c) at which the density of the vapour equals the density of the liquid, and the boundary between them disappears. At and above this point, a supercritical fluid is formed. It is also important to note that this point helps determine whether the gaseous phase is a gas or a vapour, with the difference being that the latter can be compressed into a solid or a liquid, whereas the former cannot.

These phase transitions and specific points can be experimentally detected through thermal analysis methods. These methods use the heat transfer involved in a phase transition process to determine the temperature at which it occurs, and the energy required for the process. For instance, when a sample is heated at steady rate and the transition is endothermic, there will be a temporary halt in the temperature rise during the phase transition process.

With the aim of better understanding and studying phases, phase diagrams appear as the most concise way to illustrate which phase exists under specific condition of pressure, volume, temperature, and so on. These diagrams provide a rationale for the occurrence or coexistence of thermodynamically stable phases and assist in

summarizing all the previously described properties and coordinates. The most common type of phase diagrams are the ones that relate temperature and pressure such as the one seen in figure 2.1.

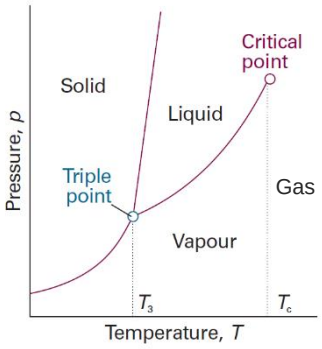

Figure 2.1 - The general regions of pressure and temperature where solids, liquid and gases are thermodynamically stable. Adapted from ref.[30]

It is also important to mention that at these boundaries between phases, the Gibbs energy of the system reaches its minimum. This parameter is of such importance that when defined for one mole, it has a specific name and symbol: the chemical potential, denoted as μ. For a system comprised of a single, pure substance, the molar Gibbs energy is equal to its chemical potential, $\mu = G_m$. The chemical potential is usually defined as a measure of the potential for a substance to undergo change. In this context, it represents the potential for a substance to undergo a physical change. This implies that, for a system in equilibrium, the chemical potential of a substance must be the same in every phase present.

In an argument widely considered elegant, Gibbs deduced a rule that determines the number of parameters that can be varied while keeping the number of phases in equilibrium constant.

Let's consider a system which P phases, each consisting of C components, all in equilibrium, and with no chemical process occurring between the components. The number of intensive variables, such as temperature and pressure, is two. The composition of each phase is specified by providing the molar fraction of C. Since the sum of molar fractions must equal one, there are C – 1 independent mole fractions. Therefore, the number of composition variables for P phases is P (C - 1), and when considering, temperature and pressure, there are P (C – 1) + 2 variable in total. For each component, there are P -1 equations for P phases, and since there are C components,

the total number of equations is C(P-1). Thus, the total number of the degrees of freedom is given by F = P(C-1) +2-C(P-1). Simplifying, the result is:

$$\mathrm{F} = \mathrm{C} - \mathrm{P} + 2 \;\; (Gibbs\ Phase\ Rule) \qquad \text{Equation 2.1}$$

This is the Gibbs phase rule for systems without reactions. As an example, consider a system in which two phases are in equilibrium. In this case, F = 1 is obtained, indicating that either temperature or pressure is not freely variable when the other is set. If the system involves ongoing reactions, the rule is applied as follows.

$$\mathrm{F} = \mathrm{C} - \mathrm{P} + 2 \text{ - r} \qquad \text{Equation 2.2}$$

Where r is the number of independent reactions (reactions that cannot be written as the combination of others).

2.2. Thermodynamics of Phase Boundaries

As explore beforehand, during the phase transition process, a phase α and another phase β are in equilibrium. Therefore, their chemical potential are equal at a pressure *p* and at a temperature *T*.

$$\mu(\alpha; p, T) = \mu(\beta; p, T) \qquad \text{Equation 2.3}$$

Solving this equation for *p* in terms of *T* will give rise to the mathematical definition for the phase boundary. This is known as the coexistence curve. If infinitesimal changes to *p* and *T* are made in such a way that the phases remain in equilibrium with each other, their chemical potentials will change, but they will remain equal. So, logically, the change in chemical potential of phase α is the same as that in phase β, $d\mu(\alpha) = d\mu(\beta)$.The variation of the Gibbs free energy, *G* with *p* and *T* is given by equation 2.4:

$$dG = Vdp - SdT \qquad \text{Equation 2.4}$$

So, by assuming that $\mu = G_{\mathrm{m}}$, $d\mu = V_{\mathrm{m}}dp - S_{\mathrm{m}}dT$ can be obtained for each phase. Using this and equation 2.3, the equality for the change in chemical potential can be rewritten as follows,

$$V_{\mathrm{m}}(\alpha)dp - S_{\mathrm{m}}(\alpha)dT = V_{\mathrm{m}}(\beta)dp - S_{\mathrm{m}}(\beta)dT$$ Equation 2.5

where V_{m} and S_{m} are the molar volumes and entropies of both phases, respectively. By rearranging the equation, can be obtained

$$[S_{\mathrm{m}}(\beta) - S_{\mathrm{m}}(\alpha)]dT = [V_{\mathrm{m}}(\beta) - V_{\mathrm{m}}(\alpha)]dp$$ Equation 2.6

This is equivalent to the changes in the parameters *S* and *V* during phase transition.

$$\Delta_{\mathrm{trs}}SdT = \Delta_{\mathrm{trs}}Vdp$$ Equation 2.7

This relation can be arranged into a more familiar form, known as the Clapeyron equation.

$$\frac{dp}{dT} = \frac{\Delta_{\mathrm{trs}}S}{\Delta_{\mathrm{trs}}V} \quad (Clapeyron\ Equation)$$ Equation 2.8

This equation is an exact representation of the slope of the tangent to the phase boundary at any temperature and pressure where two phases of a pure substance are in equilibrium. This, of course, forms the basis for defining the boundaries between the condensed phases and the gaseous phase.

2.3. The Solid-Liquid Equilibrium

Continuing from the Clapeyron equation, let's define the boundary between the solid and liquid phases. The melting process involves a molar enthalpy change, $\Delta^{\mathrm{l}}_{\mathrm{cr}}H^{\circ}_{\mathrm{m}}$. The fusion also occurs at a specific temperature, *T*; therefore, the following can be defined: $\Delta^{\mathrm{l}}_{\mathrm{cr}}S = \frac{\Delta^{\mathrm{l}}_{\mathrm{cr}}H}{T}$. This leads to

$$\frac{dp}{dT} = \frac{\Delta^{\mathrm{l}}_{\mathrm{cr}}H}{T\Delta^{\mathrm{l}}_{\mathrm{cr}}V}$$ Equation 2.9

which is the definition of the boundary between the solid and the liquid phases. However, this expression can still be manipulated to obtain the enthalpy dependency on pressure.

From the integration of equation 2.9, the following is obtained:

$$p_2 = p_1 + \frac{\Delta^{\mathrm{l}}_{\mathrm{cr}} H_{\mathrm{m}}}{\Delta^{\mathrm{l}}_{\mathrm{cr}} V_{\mathrm{m}}} ln \frac{T_2}{T_1}$$ Equation 2.10

This equation was originally derived by The Lord Kelvin (William Thompson) and is the approximation of the solid-liquid boundary.

2.4. The Solid/Liquid-Vapour Equilibrium

When the molecules in the condensed phases have sufficient energy to escape from the surface, a phase change takes place. For a solid, it is called sublimation, and for a liquid, it is called vaporization. In both processes, as clarified previously, there is a transformation into a vapour.

During this process, the gaseous molecules exert a pressure – vapour pressure. Note that this process does not continue indefinitely, eventually, it will come to a halt. At the molecular, this corresponds to a dynamic equilibrium between the process of vaporization/sublimation and condensation/deposition. Here, the vapour pressure is attained. This parameter is temperature dependent, as it will be subsequently shown.

The process of transitioning from a condensed phase to a vapour is accompanied by a change in enthalpy, $\Delta^{\mathrm{g}}_{\mathrm{cr},s} H$. If this transition occurs at a temperature, *T*, it can consider that $\Delta^{\mathrm{g}}_{\mathrm{cr,l}} S = \frac{\Delta^{\mathrm{g}}_{\mathrm{cr,l}} H}{T}$. With this, the Clapeyron equation can be converted to represent the slope of the boundary between a condensed phase and the gas phase.

$$\frac{dp}{dT} = \frac{\Delta^{\mathrm{g}}_{\mathrm{cr,l}} H}{T \Delta^{\mathrm{g}}_{\mathrm{cr,l}} V}$$ Equation 2.11

Now, considering that the molar volume of a gas is much larger than the molar volume of both the crystalline and liquid phases, it can be approximated that $\Delta^{\mathrm{g}}_{\mathrm{cr,l}} V \approx V_{\mathrm{m}}(\mathrm{g})$. Additionally, if one assumes that the gas behaves ideally (for instance, under extremely high vacuum conditions), the following relation can be used: $V_{\mathrm{m}}(\mathrm{g}) = \frac{RT}{p}$. Applying these two approximations to the Clapeyron equation results in:

$$\frac{dp}{dT} = \frac{\Delta^{\mathrm{g}}_{\mathrm{cr,l}} H}{T\left(\frac{RT}{p}\right)} = \frac{p \Delta^{\mathrm{g}}_{\mathrm{cr,l}} H}{RT^2}$$ Equation 2.12

Using $\frac{dx}{x} = d\ lnx$, the previous expression can be arranged into the Clausius-Clapeyron Equation.

$$\frac{d\ lnp}{dT} = \frac{\Delta^{g}_{cr,l}H}{RT^2}\ (\text{Clausius} - \text{Clapeyron Equation}) \qquad \text{Equation 2.13}$$

This equation is an approximation, but it is essential for understanding phase diagrams, particularly highlighting the solid/liquid-vapour boundaries. It is also important to note that this equation forms the fundamental basis for all of the vapour pressure methods used in this work. This will be further explored in chapter three.

The enthalpic parameter obtained from the Clausius-Clapeyron relation can either be the molar enthalpy of vaporization or the molar enthalpy of sublimation. These parameters are defined as the energy (usually in $kJ{\cdot}mol^{-1}$) required to vaporize/sublimate one mol of a liquid or a solid. Both can serve as measures of the intermolecular forces present in the condensed phases. If the energy required for this transition is high, one can infer that the intermolecular attraction is strong. Such samples will have low or very low vapour pressures.

2.5. Units, Nomenclature and Standard States

There is a significant effort within the scientific community, particularly in chemistry, led mainly by IUPAC (International Union of Pure and Applied Chemistry) to establish a common ground and a universal language that any scientist in the world can understand. Therefore, before delving into the description of the methodologies used in this work, it is essential to first define the fundamental aspects that apply universally to all of them. These aspects includes units, nomenclature, and standard states. This section aims to define these fundamental concepts to provide a better understanding of what is discussed within the realms of physical chemistry and chemical thermodynamics.

Firstly, a *physical quantity Q* can be expressed as the product of a *numerical value* $\{Q\}$ and a *unit* $[Q]$

$$Q = \{Q\}\,[Q] \qquad \text{Equation 2.14}$$

This is valid for all quantities determined and analysed in this work. It is important to note that in some cases, there are no units associated with numerical values (dimensionless quantities). Units, numerical values, and all physical quantities can be manipulated using the normal rules of algebra.

IUPAC and its Physical Chemistry Division recommend the use of the International System of Units (SI) in all scientific and technical publications. [31] However, in some cases, specific units derived from the SI system are used. In chemical thermodynamics, some of the primary units include not only the kelvin (K) for the thermodynamic temperature and mole (mol) for quantity of substance, but also the SI unit of energy, the joule (J), and the pascal (Pa) as the SI unit of pressure. As an example of particular cases (and also because both units are used in this work), the electronvolt (eV) and the Hartree (E_h) are non-SI units that are commonly accepted and used in some specialized fields.[32]

The names and symbols of physico-chemical quantities are also provided and recommended by IUPAC.[31]. The usual symbols for internal energy (*U*), enthalpy (*H*), Gibbs energy (*G*), entropy (*S*) and heat capacity at constant pressure (C_p) are adopted and used in this work. A change in these (and other) quantities is indicated by the Greek capital letter for delta (Δ) accompanied by either a subscript indicating the process or a subscript and a superscript indicating the initial and final state. The latter form is preferred in this work. For example, the sublimation entropy is represented as $\Delta_{\mathrm{sub}}S$ or $\Delta_{\mathrm{cr}}^{\mathrm{g}}S$.It is

also important to note that within the field of calorimetry and thermal analysis, there are recommendations provided by IUPAC and the International Confederation for Thermal Analysis and Calorimetry (ICTAC). This work follows the 2014 recommendations [33]

Another important aspect to consider is that different states in which a sample can exist, or a process occur are possible. To ensure comparability, *standard states* have been introduced by IUPAC and ICTAC.[31] These *standard states* are the ones in which thermochemical and thermophysical values should be presented. In Physical Chemistry, the standard state of a pure solid refers to the pure substance in the solid phase under a pressure of 0.1 MPa. The standard state of a pure liquid refers to the pure substance in the liquid phase at 0.1 MPa. When referring to pure gases, the standard state is that of an ideal gas at a pressure of 0.1 MPa. Note that temperature is not included in the definition of standard state. However, the "reference" temperature of T = 298.15 K has been used for some years now.

2.5.1. Standard Enthalpies of Phase Transition

As much of this work revolves around physical changes, it is also important to define the standard enthalpies of phase transition. The enthalpies of fusion ($\Delta_{\mathrm{fus}}H$ or $\Delta_{\mathrm{cr}}^{\mathrm{l}}H$), vaporization ($\Delta_{\mathrm{vap}}H$ or $\Delta_{\mathrm{l}}^{\mathrm{g}}H$) and sublimation ($\Delta_{\mathrm{sub}}H$ or $\Delta_{\mathrm{cr}}^{\mathrm{g}}H$) are usually regarded as thermophysical properties (hence the title) because only physical changes occur, and no chemical cleavage or addition takes place.

The thermodynamic definition of standard enthalpy of phase transition comes into play when a substance A undergoes a transition from a phase α to a phase β, where A is in its standard state in both phases.

$$A(\alpha) \rightarrow A(\beta) \qquad \text{Equation 2.15}$$

If one is considering the process of sublimation or the process of vaporization, then equations 2.16 and 2.17 are used to represent the process.

$$A(\mathrm{cr}) \rightarrow A(\mathrm{g}) \qquad \text{Equation 2.16}$$

$$A(\mathrm{l}) \rightarrow A(\mathrm{g}) \qquad \text{Equation 2.17}$$

Experimental measurements for determining the enthalpies of sublimation and vaporization are conducted at a saturation vapour pressure, p, of the condensed substance and at a temperature T. Figure 2.2 provides a representation of the

thermochemical cycle that relates the enthalpies of phase transition at a given *T* for different pressures.

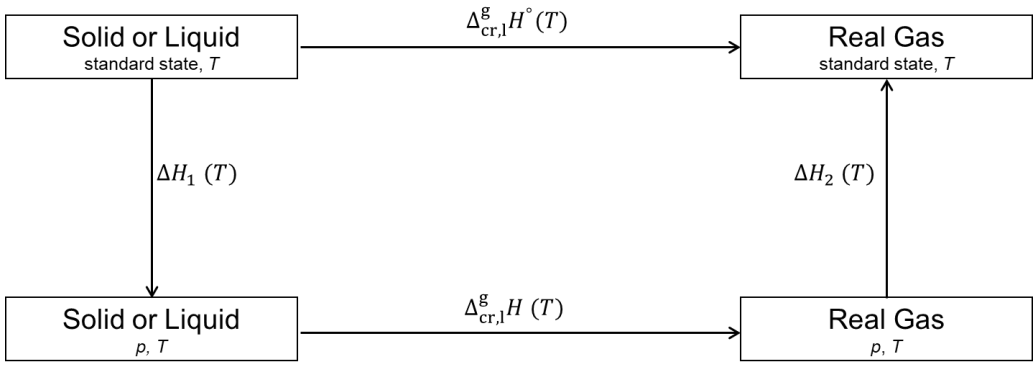

Figure 2.2 - Thermochemical cycle that relates the enthalpies of phase transition at a given *T* for different pressures.

By applying the first law of thermodynamics, the following equation can be written.

$$\Delta^{g}_{cr,l}H^{\circ}(T) = \Delta H_1\ (T) + \Delta^{g}_{cr,l}H(T) + \Delta H_2\ (T) \qquad \text{Equation 2.18}$$

The contributions of the enthalpic factors 1 and 2 are directly dependent on the vapour pressure. Since, for most organic compounds, including the ones studied in this work, their vapour pressures are very small, these values can be neglected without introducing significant errors. Therefore, equation 2.19 is obtained and will be used jointly with the experimental techniques.

$$\Delta^{g}_{cr,l}H^{\circ}(T) \approx \Delta^{g}_{cr,l}H(T) \qquad \text{Equation 2.19}$$

2.5.2. Temperature Dependence of Phase Change Enthalpies

The enthalpy of a substance increases with temperature. This happens because, as temperature rises, the molecules become excited to higher energy states, resulting in an overall increase in their total energy. The same principle applies when transitioning between different states of matter. The temperature dependence of enthalpy is based on the condition of the system, whether it is at constant volume or constant pressure.

Experimentally, enthalpy changes are usually studied under constant pressure conditions. The property that relates these changes is the heat capacity at constant

pressure. When examining an experimental range of temperatures, it transforms into the following equation:

$$\Delta H = C_p \Delta T \qquad \text{Equation 2.20}$$

This definition can also be extended to encompass changes not only in temperature but also in the state of matter.

It is important to note that experimental determinations of heat of sublimation/vaporization, for instance, are typically carried out with samples that have relatively low volatility at the reference temperature (T = 298.15 K). Therefore, measurements are often conducted at temperatures significantly higher than the reference temperature, depending on the nature of the material. This introduces an error on the calculation of the phase transition enthalpy, which needs to be adjusted if one wishes to obtain the value at the reference temperature. This adjustment is made using the Kirchhoff equation.

$$\Delta^{\mathrm{g}}_{\mathrm{cr,l}} H^{\circ}_{\mathrm{m}}(298.15K) = \Delta^{\mathrm{g}}_{\mathrm{cr,l}} H^{\circ}_{\mathrm{m}}(<T>) - \int_{298.15K}^{<T>} \left(C_P^{\circ}(\mathrm{cr,l}) - C_P^{\circ}(\mathrm{g})\right) dT \qquad \text{Equation 2.21}$$

This equation is based on a thermochemical cycle that relates the experimentally determined standard molar enthalpy of sublimation/vaporization, $\Delta^{\mathrm{g}}_{\mathrm{cr,l}} H^{\circ}_{\mathrm{m}}(<T>)$, to the standard molar enthalpy of sublimation/vaporization at the reference temperature, $\Delta^{\mathrm{g}}_{\mathrm{cr,l}} H^{\circ}_{\mathrm{m}}(298.15\ \mathrm{K})$, through their respective heat capacities. This cycle is shown below.

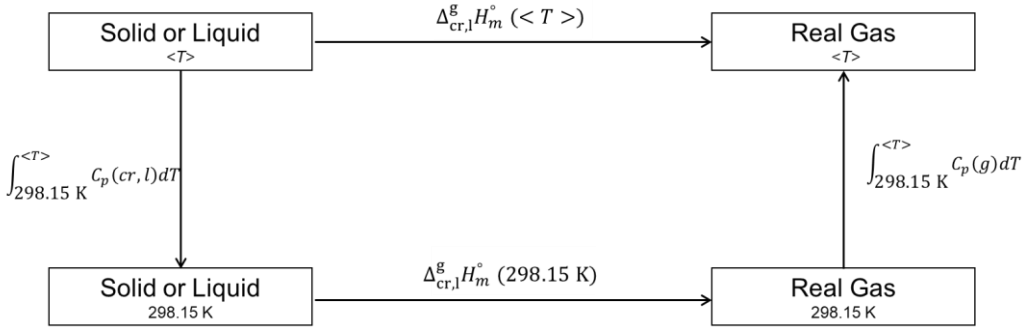

Figure 2.3 - Temperature dependence of the heat of sublimation or vaporization.

Integrating equation 2.21 yields:

$$\Delta^{\mathrm{g}}_{\mathrm{cr,l}}H^{\circ}_{\mathrm{m}}(298.15K) = \Delta^{\mathrm{g}}_{\mathrm{cr,l}}H^{\circ}_{\mathrm{m}}(<T>) - [C^{\circ}_{P}(\mathrm{cr,l}) - C^{\circ}_{P}(\mathrm{g})][<T> - 298.15]$$ Equation 2.22

Using this equation, it is easy to adjust the experimentally determined value to the one at the reference temperature. However, there are some issues with this approach, mainly the lack of heat capacity values for the samples and at the various working temperatures. This can be somewhat overcome through different methods, including quantum chemistry for the gas phase [34, 35] and group additivity schemes for the condensed phases[36, 37].Note that while this is describing sublimation and vaporization, the same reasoning applied here can also be used for fusion[36, 37]. During this work, the method described by Chickos[36, 37] was used to calculate $\Delta^{\mathrm{g}}_{\mathrm{cr}}C^{\circ}_{p}$ yielding the values of -57.1 J·K^{-1}·mol^{-1} and -68.1 J·K^{-1}·mol^{-1} for bathophenanthroline and bathocuproine, respectively. And also the giving a value of $\Delta^{\mathrm{g}}_{\mathrm{l}}C^{\circ}_{p}$ -143.9 J·K^{-1}·mol^{-1} for bathophenanthroline.

2.5.3. Temperature and Pressure Dependence of the Standard Molar Entropy of Sublimation

Considering that vapour pressure experiments, i.e., with the Knudsen Effusion Method are done at conditions different that those of the standard and reference state, adjustments to the reference temperature and state are required.

The sublimation process from the crystalline state to the gaseous state is characterized by a particular temperature, <*T*>, and a given vapour pressure at that temperature, *p*(<*T*>). These two factors, along with the change in heat capacity, need to be considered when adjusting to the reference temperature. This is done according to the following equation.

$$\Delta^{\mathrm{g}}_{\mathrm{cr,l}}S^{\circ}_{\mathrm{m}}(298.15) - \Delta^{\mathrm{g}}_{\mathrm{cr,l}}S^{\circ}_{\mathrm{m}}(\langle T\rangle, p\langle T\rangle) = \int_{\langle T\rangle}^{298.15} (C^{\circ}_{P}(cr,l) - C^{\circ}_{P}(g))\frac{dT}{T} - \int_{p\langle T\rangle}^{p^{\circ}} R\frac{dp}{p}$$ Equation 2.23

Integration of the previous equation yields the following.

$$\Delta^{\mathrm{g}}_{\mathrm{cr,l}}S^{\circ}_{\mathrm{m}}(298.15K) = \Delta^{\mathrm{g}}_{\mathrm{cr,l}}S^{\circ}_{\mathrm{m}}(\langle T\rangle, p\langle T\rangle) + \Delta^{g}_{cr}C^{\circ}_{p}\left(\frac{298.15}{\langle T\rangle}\right) + Rln\left(\frac{p^{\circ}}{p\langle T\rangle}\right)$$ Equation 2.24

3. Experimental Methodologies

As mentioned in the first chapter, the main objective of chemical thermodynamics is to study energy changes in chemical reactions, phase changes and solvation. Experimental chemistry and its many techniques serve as a means to determine these parameters. This assessment is accomplished through a myriad of different techniques and methodologies based on scientific principles, as explored in the chemical thermodynamics section.

All experimental techniques operate within the same approach: a system is subjected to a particular condition, and a change is observed through detectors that monitor a specific signal, usually an electrical signal such as current or resistance.

This chapter aims to describe the experimental techniques used in this thesis to observe the chemical and physical processes and to make the measurements necessary to determine the thermodynamic parameters.

3.1. Knudsen Effusion Method

In the early 1900s[38-40], Martin Knudsen studied the effusion of gases through a nearly ideal circular or cylindrical orifice. These studies consisted of applying the kinetic theory of gases to study the flow of the effusing gas. Etymologically, the word effusion has its origins in Latin in the word *effundo*, which means “shed” or “pour forth”. Scientifically, effusion is the process in which a gas escapes from a container through a small orifice. Not only did he prove the kinetic model of gases but also demonstrated the soundness and validity of the Maxwell’s distribution of speeds.

This section aims at describing the foundational theoretical work behind KEM and the different forms of measuring the equilibrium vapour pressures of low volatile samples namely through mass loss and mass spectrometry measurements.

3.1.1. Kinetic Theory of Gases

The kinetic theory of gases (KTG) is one of the most significant models in physical chemistry. It aims at describing the thermodynamic behaviour of gases and also at explaining macroscopic properties like pressure, temperature, and volume from a molecular point of view. This of course is done for perfect gases, i.e., molecules that are

in constant, chaotic motion that do not experience any mutual attraction but elastic collisions.

This model is based on three assumptions:

1. The gas is comprised of molecules of mass m in constant, random motion defined by classical mechanics.
2. Molecules are “point like”. Their diameters are much smaller than the average distance travelled between collisions so, their sizes are negligible.
3. The only interaction between molecules are short elastic collisions (total conservation of translational kinetic energy).

From this set of assumptions, one can reach important conclusions and define the macroscopic properties of gases such as pressure. The following relation is derived from the assumptions presented above.

$$pV = \frac{1}{3}nM{v_{rms}}^2 \qquad \text{Equation 3.1}$$

Here *p* is the pressure, *V* is the volume of the gas, *n* is the quantity of gas, *M* its respective molar mass and v_{rms}^2 is the root-mean-square speed (rms) of the molecules of the gas. If we consider that the rms depends only on temperature and molar mass, then, at a constant temperature, the following relation rises. Note that it is the same as Boyle’s law of gases.

$$pV = constant \quad \text{(Boyle’s Law)} \qquad \text{Equation 3.2}$$

From equation 3.1, we can now alter it to derive the equation of perfect gases. By considering the Maxwell-Boltzmann distribution of speeds we obtain the following relation for the root-mean-square speed.

$$v_{rms} = \left(\frac{3RT}{M}\right)^{1/2} \qquad \text{Equation 3.3}$$

If we substitute the previous equation into equation 3.1, we obtain the equation of state of a perfect gas.

$$pV = nRT$$ Equation 3.4

So, it is possible to conclude that the KTG can be regarded as a model of a perfect gas. From it, we can also calculate several other values related with speed and collisions. One such parameter is the mean free path, *λ*. It is the average distance a molecule travels between collisions and it is given by equation 3.5.

$$\lambda = \frac{kT}{\sigma p}$$ Equation 3.5

Where *k* is the Boltzmann constant, *T* is temperature, *σ* is the collision frequency, and *p* is pressure. In a sample of constant volume, pressure is proportional to temperature. So, *T/p* remains constant. As a consequence, the mean free path is independent of temperature at a constant volume which means that the number of collisions depends only on the number of molecules present. However, for the purposes of this work, we will not go into any further detail.

3.1.2. General Considerations on the Knudsen Effusion Method

The typical Knudsen Effusion Method (KEM) experiments consists of the measuring the equilibrium vapour pressure of condensed compounds. This is done through observations of a signal resultant of the flux of the molecules in the gaseous phase from a temperature-controlled cylindrical cell (the Knudsen Cell – figure 3.1) through orifices of a very reduced size at a specific temperature. Depending on the technique, this signal may be the mass loss rate, or the electrical current produced from the ions resulting from ionizations of the effusing molecules. In both cases, from this signal it is possible to evaluate the gas pressure inside the cell.

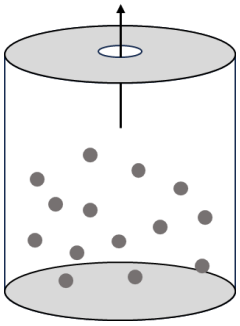

Figure 3.1 - Representation of the effusion of gas molecules through an effusion hole.

Afterwards, by plotting the function ln *p* = f(*1/T*), it is possible to derive the enthalpy of phase transition from the condensed phase to the gaseous phase using the Clausius-Clapeyron relation (defined in section 2.2).

$$\frac{dlnP}{dT} = \frac{\Delta^{g}_{cr,l}H_{m}}{RT^{2}} \qquad \text{Equation 3.6}$$

During his studies, Knudsen deduced the following equation for when the width of a tube is much larger than orifice through which the gas escapes and for when the pressure outside of the cell is much lower than the pressure inside the cell.

$$P = \frac{m}{A_0 t}\left(\frac{2\pi RT}{M}\right)^{1/2} \qquad \text{Equation 3.7}$$

Where m is the mass of the gas species, A_0 is the area of the orifice, *t* is time interval and *M*, *R* and *T* represent molar mass, ideal gas constant and temperature, respectively. This equation is only applicable on a set of conditions of which it is important to outline the following:

1) saturated vapour in the cell
2) null thickness of the orifice
3) isothermal equilibrium between the cell and the sample
4) molecular flow regime (mean free path larger than the effusion diameter)

Of course, in reality, it is not possible to attain all of these requirements. This leads to an error in the measurements. So, it is imperative that corrections are inserted into equation 35. With the inclusion of a factor that evaluates the probability of transmission of molecules through the orifice, considering its radius and its thickness, i.e., the Clausing factor, ω_0, we get equation 3.8.

$$P = \frac{1}{\omega_0}\cdot\frac{m}{A_0 t}\left(\frac{2\pi RT}{M}\right)^{1/2} \qquad \text{Equation 3.8}$$

There are, evidently, other corrections such as the condensation coefficient and even the existence of reactions such as dimerization but equation 3.8 remains the most useful for experimental use with of course a highlight to the mass loss method which will be described in the next subsection.

This technique requires careful measurements and detailed processes as it is easy to propagate experimental errors associated to the measurements of pressure and temperature.

However simple this description may be, it gives a general idea of what KEM is. Nevertheless, the technique is quite intricate and will be further explored on the subsequent sections.

3.1.3. The Clausius-Clapeyron Relation for the Knudsen Effusion Method

In section 2.2, we explored the boundary between the condensed phases and the gas phase and derived the Clausius-Clapeyron Equation.

$$\frac{dlnP}{dT} = \frac{\Delta^{\mathrm{g}}_{\mathrm{cr,l}} H_{\mathrm{m}}}{RT^2} \qquad \text{Equation 3.9}$$

This particularly useful equation can be used to predict how the vapour pressure varies with temperature and is the basis of several effusion techniques with Knudsen Effusion appearing as the most relevant one. However, to be used to experimentally determine the enthalpies of sublimation and vaporization, one needs to assume that $\Delta^{g}_{cr,l} H_m$is constant. With this assumption, we can integrate the Clausius-Clapeyron relation, and we obtain the following equation.

$$ln\frac{p2}{p1} = \frac{\Delta^{\mathrm{g}}_{\mathrm{cr,l}} H_{\mathrm{m}}}{R}\left(\frac{1}{T_1} - \frac{1}{T_2}\right) \qquad \text{Equation 3.10}$$

If, p_2 is the saturation vapour pressure at T_2 and if p_1 if the standard vapour pressure, equation 3.10 changes into the following form.

$$ln\left(\frac{P}{P^{\circ}}\right) = a - \left(\frac{b}{T}\right) \qquad \text{Equation 3.11}$$

$$a = \frac{\Delta^{g}_{cr,l} S^{\circ}_{m}(P^{\circ})}{R}$$

$$b = \frac{\Delta^{g}_{cr,l} H^{\circ}_{m}}{R}$$

Thus, from the linear regression of the graphical representation of ln *p* vs 1/*T* one not only can accurately derive the enthalpy of sublimation/vaporization of a given sample but also its entropy. The latter is done through the following equation. Corrections to the reference temperature and corresponding vapour pressure are done as explained in section 2.5.3.

$$\Delta^{g}_{cr,l} S_{m}(p, \langle T \rangle) = \frac{\Delta^{g}_{cr,l} H_{m}}{T} \qquad \text{Equation 3.12}$$

From the values adjusted to the reference temperature, the Standard Molar Gibbs Energy of Sublimation can be calculated according to the Gibbs-Helmholtz equation.

3.1.4. Knudsen Effusion Mass Loss

The classical approach to the Knudsen effusion method is based on observing a mass change rate at a previously defined temperature (Knudsen effusion mass loss - KEML). This leads to a direct usage of the Knudsen equations shown in section 3.3.2 and reduced experimental errors.

Over the years, many methods have been developed to monitor the mass change. Some use mass measurements before and after exposing a sample at a temperature, *T*, and high vacuum.[41] Others use quartz crystal microbalances for continued monitoring.[42] For this work, a thermobalance based method was used as described in [43].

3.1.4.1. Equipment and Experimental Procedure

For this thesis, a Knudsen system with a Ugine-Eyraud Model B60 Setaram thermobalance was used along with a graphite resistor as the main heating element. A quartz tube with the measuring cell is placed inside this heat source. The system is described in figure 3.2.

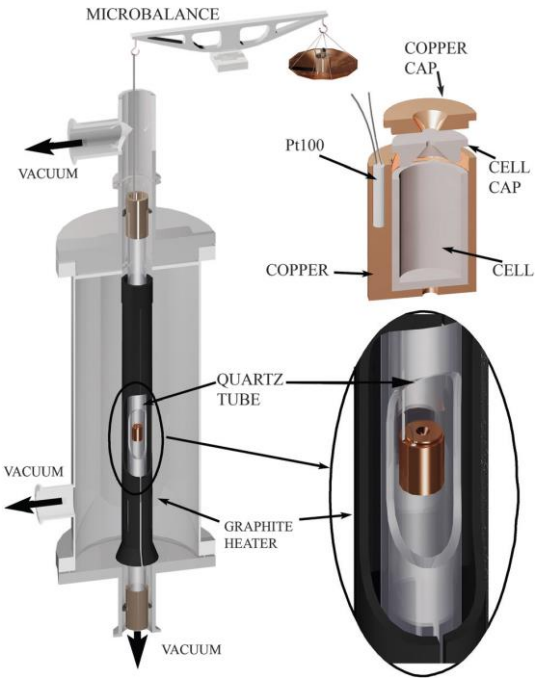

Figure 3.2 - Scheme of the KEML apparatus. Adapted from ref. [43]

This system was modified by inserting the Knudsen cell into a capped copper cylinder. The aforementioned was done with the purpose of homogenising the temperature of the effusion source which is made in pyrophyllite and can have different effusion hole diameters (0.3, 1 and 3 mm).

To have a better accuracy in the temperature measurement, a platinum resistance thermometer (Pt100) was inserted directly into the copper cylinder. It is also important to note that the system is connected to two vacuum systems, each constituted by a rotary and a diffusion pump. Temperature and mass loss data points are collected via a data logger (HP 34970A). This system is controlled via a homemade software based on the LabVIEW graphical programming environment. This software is capable of executing a temperature programme without the need for human supervision and thus, is capable of measuring the rate of mass loss at a defined temperature independently. The output file has the data gathered registered in it which will then be used in the ln p vs 1/T regression.

3.1.5. Knudsen Effusion Mass Spectrometry

As previously mentioned, there are several forms of detecting the flow of material from an effusion source. This current section will explore the Knudsen Effusion Mass Spectrometry (KEMS) method. This powerful technique combines the KEM with a mass

spectrometer providing insights not only into the thermodynamics of the process but also to the chemical composition of the sublimated sample. A multitude of materials can be analysed using this technique ranging from metals to ceramics and organic substances.[44, 45]

This technique has its origins in the late 1940s, but it was extensively used in the 1960s and 1970s where it gained a large popularity and even being used to study lunar rocks gathered in the Apollo lunar missions.[46] Originally it is a high temperature technique but it can also be used for lower temperature ranges like as the ones used for the study of organic substances such as ionic liquids or pure organic molecular materials as it is the case of the sample studied in this dissertation.

The current section aims to explore the general principles behind the technique and the system used in this thesis.

3.1.5.1. General Principles of KEMS

The basic principle behind KEMS is to subject a standard Knudsen cell to a given temperature at very low pressures in order to generate a molecular flow that is subsequently ionized via impact with an electron beam of a given energy and directed to a mass spectrometer. This ionized gas will give a particular signal intensity for each of the ionized species. This can be converted into vapour pressure and then, much like KEML, plotted in order to use the Clausius-Clapeyron relation.

In great similarity to Knudsen effusion mass loss, this technique is, obviously, based on the conditions defined by Martin Knudsen. This includes the mathematical equations that translate the obtained signal to pressures. Such translation is done under the basis of the following equation.

$$P_x = \frac{K_{\mathrm{instr}} I^{+}_{\mathrm{n}x} T}{\sigma_x \gamma_{\mathrm{n}x} \alpha_{\mathrm{n}x}} \qquad \text{Equation 3.13}$$

Where P is the partial pressure of a given species x in Pa, I^{+}_{nx} is the ion intensity of the isotope n of species X, K_{instr} is the instrumental constant of the ionization source, T is the temperature in K, σ_x is the ionization cross section which measures the probability of

ionization occurring when a molecule of the sample collides with an electron. γ_{nx} is the gain constant of the electron multiplier detector and α_{nx} is the isotopic abundance.

Note that, although it is not the main goal of this technique, it is also possible to determine some gas-phase ion energetic parameters such as the appearance energy, AE_0. This concept is commonly used as a threshold in mass spectrometry experiments. It is the minimum energy required to cause the ionization of the sample molecule. This parameter can either be directly determined through experimental measurements or via linear extrapolation of the ionization efficiency curve i.e., the number of ions produced, or the intensity of the signal produced by them as a function of the energy of the electrons used to produce ionization.

3.1.5.2. Equipment and Experimental Procedure

This type of devices include these main sections: the Ion source, the ion optics, the electromagnet, the electron multiplier detector as it is shown in the figure below.

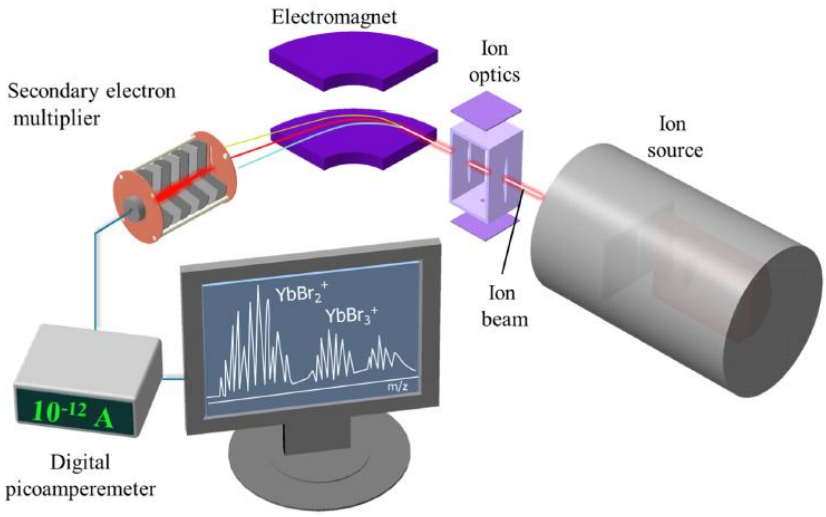

Figure 3.3 - Schematic of a KEMS system. Adapted from ref[47]

The system used for this work has a similar composition. A single focusing 90º magnetic sector mass spectrometer originally by PATCO that is equipped with a Knudsen molecular source. The effusion cell used in this work is made of platinum and has an effusion orifice with 1 mm diameter. This Knudsen cell is inserted into an outer tantalum crucible.

The effusion source is surrounded by a spiral-shaped tungsten heating element and tantalum shields that are placed in order to have a better thermal equilibrium. The temperature measurements are done with a Pt/Pt-13%Re thermocouple which is inserted in the bottom of the tantalum crucible. In figure 3.4, it is possible to see a schematic of a Knudsen molecular source that, in spite of not being the one used in this work, it is practically identical. The only significant difference is the heating element.

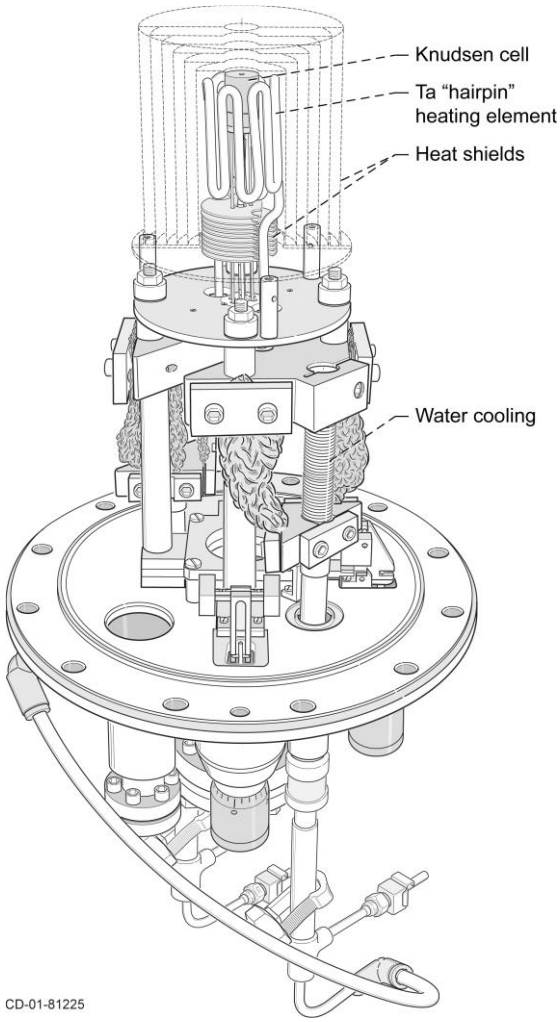

Figure 3.4 - Single-cell Knudsen molecular source used in the KEMS measurements. Adapted from ref[44]

The ionization of the vapours effusing from the Knudsen cell was accomplished by electron impact with an electron emission current generally regulated at 1.0 mA and the intensities were measured through a secondary electron multiplier.

The measurements were carried out by filling a Knudsen cell with enough sample to cover the bottom of it and by subsequently exposing it to a high vacuum. When low

background pressures are reached, the heating element is turned on. Here, temperature is generated by running a high current (10 – 200 A) through the tungsten heating element. The monitoring of the *T* of the sample is done via a thermocouple that is in contact with the bottom of the Knudsen effusion cell as mentioned before.

When the *T* is considered stable, the measurement of ion beam intensity can be carried out. A shutter is placed in the way of the molecular source to distinguish the ions produced by a sample from the background gases with the same mass-to-charge ratio. By measuring the intensity of the beam, it is possible to apply now equation x and build a ln*p* vs 1/*T* plot. With a sufficient number of points one can accurately derive the heat of sublimation or vaporization. It is also important to note that most measurements were done using a circa 20 eV electron energy. The same process is done for an appropriate calibrant which will produce an instrumental constant.

3.1.5.3. Treatment of Experimental Results

After measuring the ion intensity of a given isotope of the species being studied at various temperatures, the transformation of this variable to a partial pressure inside the cell has to be performed. This is done, as mentioned previously, through equation 3.13. This, however, introduces a number of constants that need to be carefully considered as they can potentially be a large source of error.

Firstly, the instrumental constant, K_{instr}, needs to be determined with a calibration experiment every time a new analysis is conducted. This is due to the nature of the electron source. As it is used, its geometry will be altered and as such, will produce electrons differently. This constant also covers any error that may come from the geometry of the apparatus and of the features of the cell.

Secondly, the ionization cross section, σ_x, can be a major source of error as for most organic samples, this variable is unknown. As a way of surpassing this issue with an approximation, one can use an empirical additivity rule and calculate σ_x by adding the known ionization cross section for each of its parts. An example is the σ_x of phenanthrene. By this additivity rule, $\sigma_{phenanthrene} = 3 \times \sigma_{benzene}$. Nevertheless, it remains only an approximation. One way of determining the ionization cross section is by using KEML to determine the partial pressure at a certain *T* and going backwards with a rearranged equation 3.12 and obtaining σ_x.

A normal assumption in KEMS is to assume that the multiplier gain is proportional to the square root of the molecular mass of the species. [43, 48] The isotopic abundance can easily be calculated.

3.2. Quartz Crystal Microgravimetry

As described in the last section and in section 2.2, it is possible to indirectly determine the enthalpy of change from a condensed phase to the gas phase (vaporization and sublimation) through vapour pressure experiments. In one of the Knudsen methods described earlier, mass measurements are done with a thermobalance to determine vapour pressures. There are, however, other ways of doing said measurements. This section aims at describing a method based on the change in frequency of a quartz resonator – Quartz Crystal Microgravimetry (QCMG).

This technique uses a quartz crystal microbalance (QCM) to determine the rate of mass deposition on a quartz crystal. This is equal the rate of mass-loss of a sample at a previously defined temperature. With a sufficient number of points over a large enough *T* range, it is possible to a ln*p* vs 1/*T* to determine the heat of change from a condensed phase to the gaseous phase with an adapted Clausius-Clapeyron relation.

3.2.1. General Principles of Quartz Crystal Microgravimetry

Quartz crystal-based microbalances have been used in microgravimetric techniques to determine the deposition of very small masses[49-51]. This can be done as the increase in thickness of the "load" on the quartz crystal leads to a decrease in its resonant frequency. The first developments of this technique appeared in 1959 when Sauerbrey introduced this new mass measuring method.[52] It has been shown that QCMG is very sensitive to small changes in mass of solid samples.[53]

As the device used in this work is originally designed for studying ionic liquids, its working principle is based on open cell conditions (non-equilibrium) rather than Knudsen conditions (effusion through an orifice, under equilibrium) Nevertheless, this technique employs an adapted Clausius-Clapeyron relation.[54, 55]

$$\ln\left(\frac{dm}{dt}\sqrt{T}\right) = -\frac{\Delta^{g}_{cr,l}H^{\circ}_{m}}{RT} + A \qquad \text{Equation 3.14}$$

The final step uses the Sauerbrey relation, $df = -Cf^2 dm S_C^{-1}$ [52],to consider that the change in frequency over time is directly proportional to the change in mass over time, $\frac{df}{dt} \approx \frac{dm}{dt}$, and as such, we obtain equation 3.14.

$$\ln\left(\frac{df}{dt}\sqrt{T}\right) = -\frac{\Delta^{g}_{cr,l}H^{\circ}_{m}}{RT} + A \qquad \text{Equation 3.15}$$

Note that this working equation only considers the process of phase change and not any other process that might occur such as condensation of the evolved gas. This of course introduces an error that needs to be considered when doing measurements with this technique. This will be further explored in the results chapter as the aim of these experiments was to test how appropriate this device was for low volatility solids.

3.2.2. Equipment and Experimental Procedure

The equipment used in this setup is comprised of both commercial and specially crafted parts. It was assembled at the department of basic and applied sciences for engineering of the La Sapienza University of Rome by Professor Stefano Vecchio Ciprioti, Professor Andrea Ciccioli, Doctor Bruno Brunetti, and Engineer Marco Magi.

Before going to details, it is important to note two facts. Firstly, this equipment is originally designed to study ionic liquids at lower temperatures than other devices found in literature. Its designed in based on the work developed by Verevkin et al.[55] And, secondly, this device is a prototype and it still is in its early stages of development. As such, the work developed for this thesis should be considered as test. In the results and discussion chapter, further comments and descriptions will be made and considered.

The equipment is mainly comprised of three main sections: the quartz crystal microbalance, the molecular vapour source, and the vacuum system. In figure 3.5, it is possible to find a schematic of the prototype device.

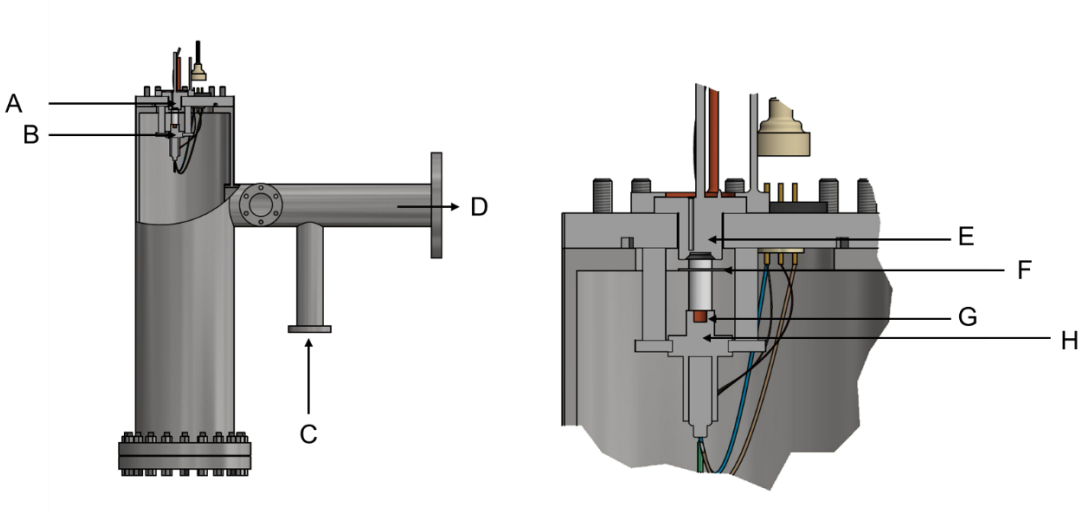

Figure 3.5 - Schematic of the quartz crystal microgravimetry setup. A) QCM; B) molecular vapour source; C) atmosphere inlet valve; D) vacuum system; E) QCM; F) shutter; G) sample holder; H) heating element.

The quartz monitor crystal is placed directly above the molecular vapour source. It is a gold plated, 6 MHz crystal and it is held in place against a sensor that measures its resonance frequency. This part is an adapted front load single sensor that is connected to a STM-2 USB thin film rate/ thickness monitor (figure 3.6). This monitor is held inside a Faraday cage to prevent any external influence on the measurements. It is important to note that all of these parts are Inficon products.

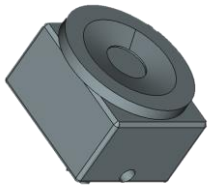

Figure 3.6 - Adapted front load sensor used to hold the QC.

The molecular vapour source is designed in accordance with reference [55]. As an attempt to determine vaporization enthalpies of ILs at lower temperatures, an open cell design was used, i.e., an open cavity where the sample is held. In our case, this cavity is an aluminium crucible that is held inside a copper block. This latter part is connected to a power source which provides a current that generates a specific temperature. This temperature is measured via a Pt100 thermocouple that is directly connected to the block. This is represented in the scheme below.

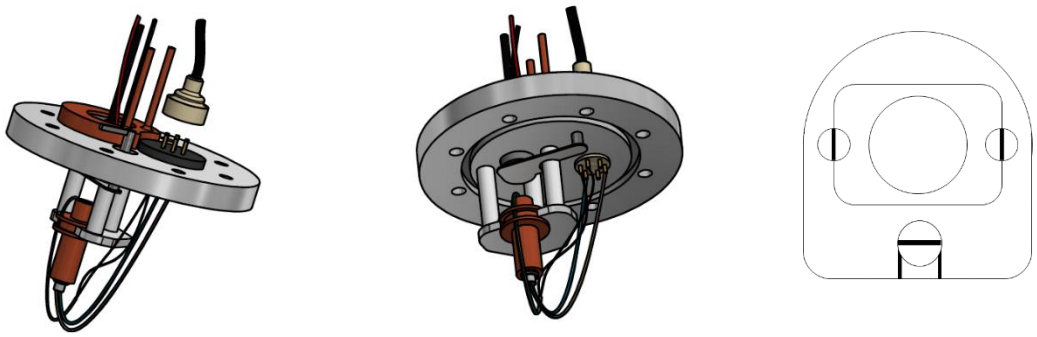

Figure 3.7 - Schematic of the molecular vapour source.

The evacuation system is comprised by two vacuum pumps. A rotary pump system responsible for doing a pre-evacuation of the chamber and an Adixen ADH turbomolecular pump. This system is capable of generating pressures on the nano Pascal scale after only an hour.

A typical QCMG experiment starts with the loading of a sample to an aluminium crucible. This sample needs to be enough to cover the bottom of the crucible and it will be further pressed with a glass rod to ensure a smooth surface and an even distribution of the sample. This step is done to ensure that all of the loaded sample is at the same temperature and that there is no significant temperature gradient present.

The next step is to close the vacuum chamber and tightly secure it with a number of bolts. Afterwards, the vacuum system is initiated with the pre-vacuum step done by the rotary pump. As the threshold pressure is reached, the vacuum seal is considered strong enough to turn on the turbomolecular pump safely. As the latter vacuum pump reaches its optimal working rpm, the temperature system can be engaged taking our system to a predefined *T*. When $P \leq 10^{-8}$ Pa, the experiment can begin.

The measurement procedure takes a step-temperature approach where a previously defined change in frequency is observed at a certain temperature. The duration of the change in frequency is recorded and from this we obtain our $\frac{df}{dt}$ which will be used in ln *p* vs 1/*T* plot. The frequency measurements are done with a shutter that exposes (or not) the QCM to the vapour of the sample.

3.3. Thermal Analysis

Thermal Analysis is described by the International Confederation of Thermal Analysis and Calorimetry as “the study of the relationship between a sample property and its temperature as the sample is heated or cooled in a controlled manner”.[33] Several properties are used in thermal analysis but the two explored with this thesis are heat flow and sample mass. These measurements are done with differential scanning calorimetry and thermogravimetric analysis. These techniques will be subsequently defined and detailed.

The usual approach with thermal analysis involves the application of a heating and cooling signal to a sample and measurement of temperature and energy associated with a thermal event: melting, crystallization, vaporization, glass transition, and decomposition reactions. The experimental techniques have a very wide temperature range in which they operate, it is usually from -180 and 600 ºC. It however depends on the device and attached modules such as different cooling systems.[33, 56, 57]

3.3.1. Differential Scanning Calorimetry

Differential scanning calorimetry (DSC) measures the energy transferred as heat at constant pressure. This measurement can be due to a chemical or physical change occurring in the sample subjected to a temperature program, usually an increase at constant heating rate. For this work, only physical changes have been studies with DSC.

This technique finds its origins in the differential thermal analysis (DTA) technique. The base components are quite similar between the two techniques. In DTA, a temperature-controlled furnace that contains sample and reference cells is used. Attached to the cells, you have thermocouples that record the temperature of both reference and sample.[56]

The ideal arrangement of the cells in these devices (figure 3.8) is having the cells symmetrically placed along with a symmetrical arrangement of the measuring sensors so when the heat capacity of the sample and reference are the exact same and the temperature difference is zero.[56, 58]

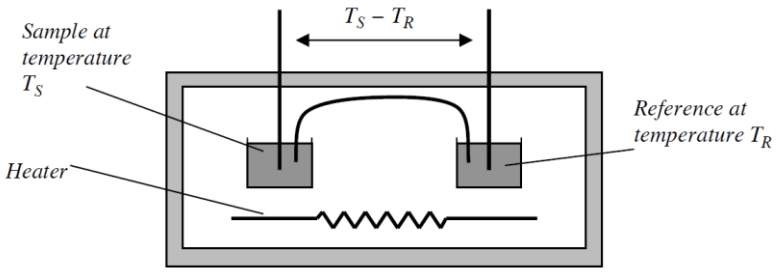

Figure 3.8 - Typical arrangement of a DTA apparatus. Adapted from ref [56].

DTA data can be plotted as a function of sample temperature, reference temperature or time. In both DSC and DTA, the measurement of a signal change relies on the temperature difference from both cells and a result, the detection of the thermal event that occurs.

As an example, when a sample undergoes a phase change, the rate of temperature increase will be lower than that of the reference as the energy transferred to the sample is being used to break the intermolecular bonds characteristic of the phase rather than just increasing the temperature. When the phase transition is complete, the cell temperature will be equal again. In figure 3.9, the characteristic thermograms are shown.

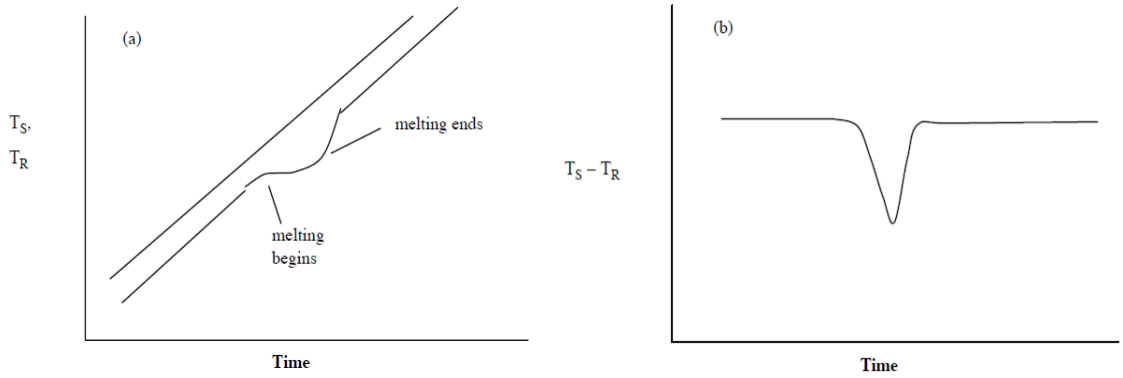

Figure 3.9 - DTA response showing a direct representation of the measured temperatures (a) and of their difference (b). Adapted from ref. [56]

Differential scanning calorimetry appeared in the 1960s as a way to surpass some of the difficulties encountered by DTA. [56, 58]

3.3.1.1. General Principles of Differential Scanning Calorimetry

Similarly to a DTA, a DSC consists of two small cells that are heated electrically at a constant rate. The temperature *T* at a time *t* during a linear heating or cooling program is given by $T = T_0 + \alpha t$, where T_0 is the starting temperature and α is the heating or cooling rate.

As defined in the second chapter, if no physical or chemical process occurs, then the heat transferred at constant pressure is related to the heat capacity of a given sample by $q_p = C_p \Delta T$. The assumption that heat capacity is independent of temperature is important as then a direct determination of the heat exchanged can be undertaken. From this assumption, the change in q_p can be plotted against temperature. This plot is called a thermogram and from the integration of the curve, the enthalpy change can be determined with equation 3.15.

$$\Delta H = \int_{T1}^{T2} C_p \, dT \qquad \text{Equation 3.16}$$

Where, T_1 and T_2 are the temperatures at which the process being studied starts and ends. To achieve the measurement described, the base signal in DSC is that of heat flow. There are two main different approaches used to measure heat flow: heat flux and power compensation.

The original innovation that gave rise to DSC was that the temperature difference between the sample and reference cells is kept at near zero. As such, the electrical power supplied to the sample furnace is varied as to keep the temperature difference near zero, hence the term power compensation. In a typical power compensation DSC experiment, the reference furnace is submitted to a linear temperature program. The control system forces the sample to remain in the same temperature program of the reference cell and as such, any differences in the power supplied to the cells must be from the heat capacity and from the enthalpy of transition that is being observed.[56, 58] This type of DSC is generally considered the most sensitive of the two main types.

Heat flux DSC is considered the simpler of the two approaches. Typically, two crucibles (sample and reference) are placed symmetrically within the same furnace with a thermocouple placed in close proximity with each. These are connected in such a way that the voltage developed from the pair is a direct measurement of the temperature difference between both cells. In figure 3.10, find a schematic of the heat flux apparatus.

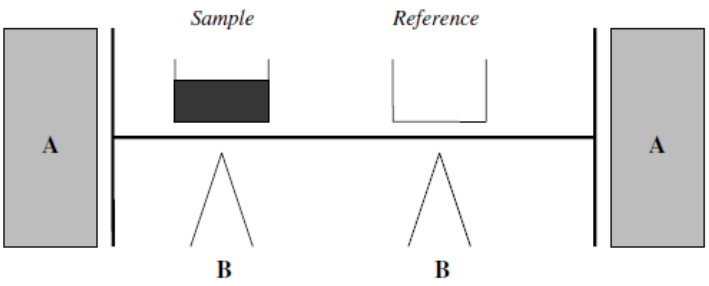

Figure 3.10 - Heat flux DSC schematic. A - Furnace, B - Thermocouple. Adapted from ref.[56]

The physical composition of the device is what gives rise to the equation used to define it. The thermal path, normally a metal membrane of armature where the crucibles are supported, gives rise to the following equation.

$$\frac{dQ}{dt} = \frac{\Delta T}{R}$$ Equation 3.17

Where Q is the heat, t is the time, ΔT is the temperature difference between the furnace and the crucible and R is the thermal resistance of the heat path between the furnace and the crucible. From this equation, the temperature difference arises as the difference in heat flow provided that the thermal paths are truly identical. As such, heat flow is a measure of the properties of the sample with all other influences discarded by comparison with the reference. The ΔT needs to be calibrated to provide a heat flow as a function of temperature. This calibration is done with known standards. This calibration needs to be done by considering the standard used but also the heating/cooling rate used.

The heat flow signal can be plotted as either a function of temperature or time. The shape of the signal changes however are typical and can be used to figure out what event is occurring. In figure 3.11, it is possible to find a thermogram with some of the more characteristic transitions.

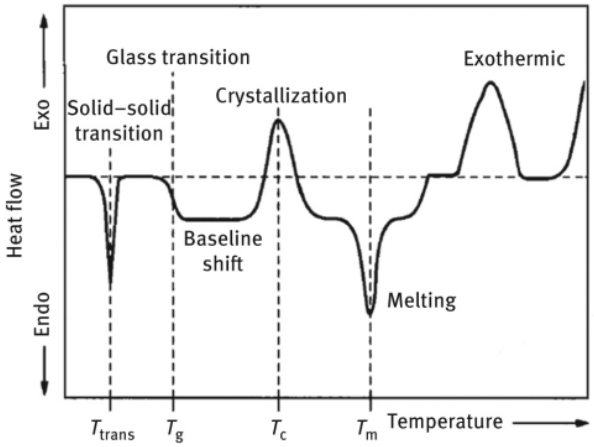

Figure 3.11 - Typical transitions in a DSC thermogram. Adapted from ref.[59].

The heat flow change can either be endothermic or exothermic in line with the event that is occurring. As an example, consider the melting of a sample. The transition from a solid to a liquid requires an energy input to break the solid-solid intermolecular bonds. This will result in an endothermic signal change. The shape and size of the peak is always indicative of what is happening with a sample. If the observed peak is sharp, it indicates that the transition occurs within a single step. If, however, a large peak or several can be observed, that transition can happen in more steps or different samples (polymorphs for instance) are present.

3.3.1.2. DSC Equipment

For the experiments carried out under this thesis, a single Heta Flux DSC device was used. This device was commercially obtained from Netzsch. It is a DSC 204 F1 Phoenix. It is equipped with a silver furnace which is capable achieving a maximum temperature range from -180 to 400 ºC. However, this device uses an intracooler colling system that limits the range from – 80 to 400 ºC. Hermetically sealed aluminium crucibles (Al purity 99.5 %) were used for our thermal behaviour experiments These have a large operating range with a maximum temperature of 600 ºC. A constant inert and protective gas-flow was used. In this case, the used gas was nitrogen and was subsequently controlled by an integrated mass flow controller and software. The device is automatically controlled via the Proteus software from Netzsch.

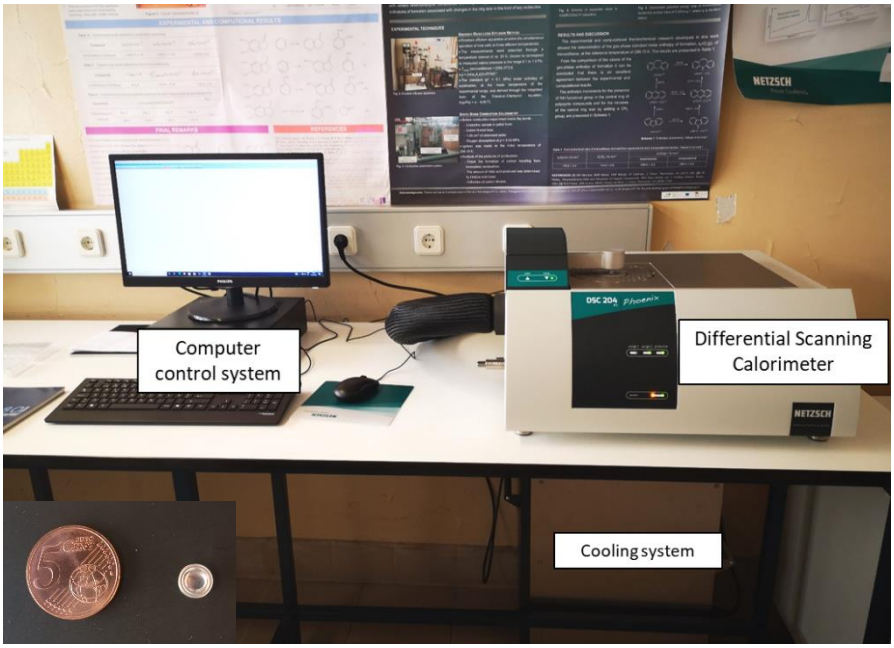

Figure 3.12 - Picture of the Heat Flux DSC apparatus used for this work shown along with the hermetically sealed aluminium crucibles.

Our device was calibrated with different standard samples for different heating rates. It is important to outline the calibration done with benzoic acid which provides the calibration for small organic molecules such as our samples.

3.3.2. Thermogravimetry

In order to have a good understanding of thermogravimetry (TG), one should consider thermogravimetry to be the continuous or repeated measurement in sufficient intervals of the mass of a given sample while it is heated or at a specific temperature.

This technique gives information regarding physical processes, mainly those in which sample mass changes but also gives insights into chemical phenomena such as chemisorption, oxidative degradation and decomposition which can work as an indication of phase stability but mainly as the stability of the sample itself. [57, 60, 61]

3.3.2.1. General Principles of Thermogravimetric Analysis

A basic TG device requires a precision balance and a furnace that is programmed for a linear rise of temperature through time. Original TG devices used manual measurements of mass. However, modern devices make automated and continuous measurements of

mass which guarantees that no mass change is overlooked.[61] In figure 3.13, a general schematic of a TG is shown along with typical position of thermobalances.

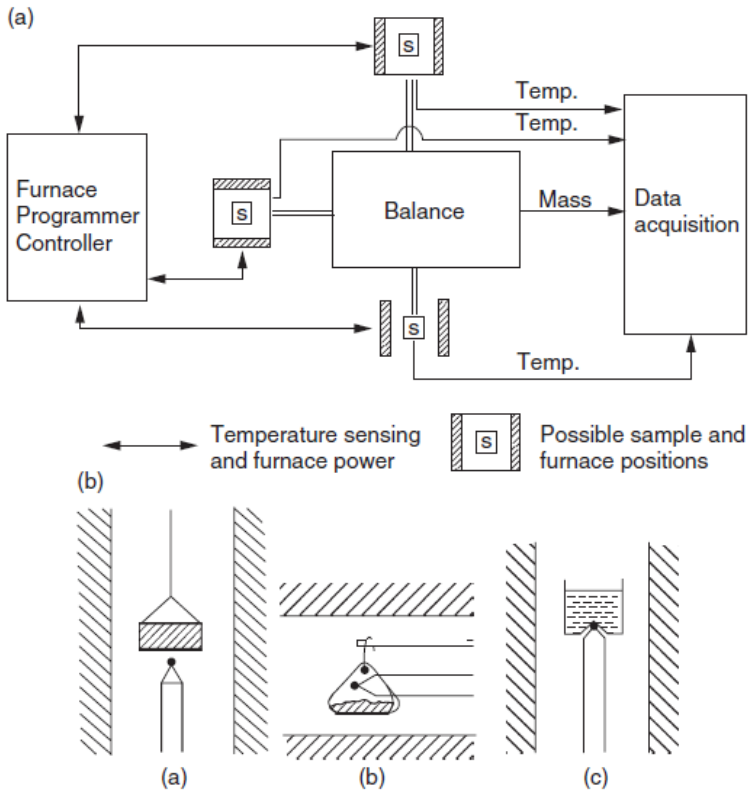

Figure 3.13 - a) general schematic of a TG device. b) Typical thermobalance configuration a) top-loading, b) side-loading and c) bottom-loading. Adapted from ref.[57]

It is also important to note that gases may be used during the experiment with different intents. Gases such as argon, nitrogen and synthetic air can be used to observe the thermal behaviour of a sample under different conditions.

Similarly, to DSC, one can plot the measured mass change versus the temperature thus creating a thermogram. Two different approaches can be taken: 1st by plotting the weight *versus* temperature (the thermogravimetric curve); 2nd by plotting the rate of mass loss *versus* temperature (differential thermogravimetric curve).[57, 61] Several different features can be identified in the first curve:

I. A horizontal section. Indicative of constant weight
II. A curved section. The steepness is indicative of the rate of weight loss $\left(\frac{dm}{dt}\right)$.
III. An inflection (where $\left(\frac{dm}{dt}\right)$ can reach a minimum) which can indicate the end of a phenomenon and/or the formation of an intermediate compound.

In figure 3.14, examples of the curves described beforehand can be found. The sections A are correspondent to the plateau (point I). B is an inflection point which corresponds to point III. In the DTG curve, the curved sections are where DTG ≠ 0. Here, lass loss is occurring. The inflection is represented were DTG has a minimum between the second and third DTG peak. The plateaus are where DTG = 0.

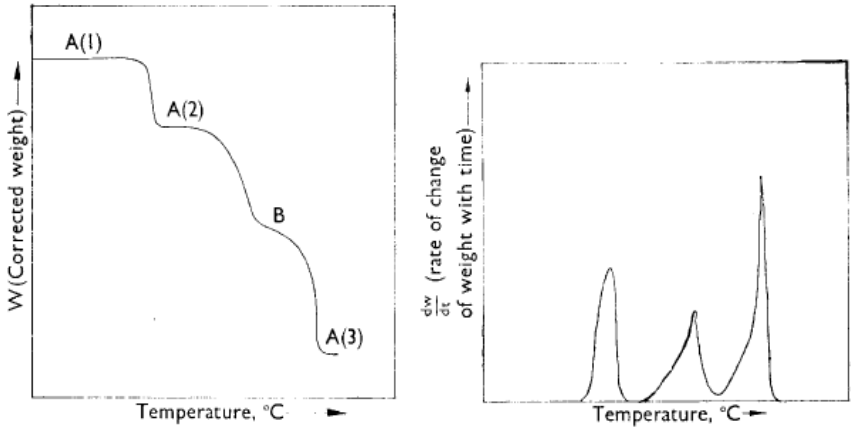

Figure 3.14 - Example of thermogravimetric and differential thermogravimetric curves. Adapted from ref. [61]

This highly versatile technique can be outfitted with several different attachments in order to gather more information. Mass spectroscopy and FTIR sets can be used to gather information from the evolved gases.[60, 61] As an example, to distinguish if a small mass loss is ascribed to water vaporizing or to another event.

However, the most important variation of TG for this work is when energetic information gathered with DSC in simultaneous. Simultaneous Thermal Analysis (TG/DSC) has several advantages over separate experiments. Besides saving time and costs, it provides cleared insights into the processes that are occurring preventing ambiguities that might arise.[57, 61]

3.3.2.2. Isothermal Thermogravimetry

Another variation of this technique that has been used in this work, isothermal thermogravimetry (I-TG). Here, the thermobalance is used to measure mass-change over a previously defined time period. This mass loss rate can then be manipulated to calculate the enthalpy of vaporization (or sublimation if the compound is volatile enough).[62] This temperature dependence of the vapour pressure is given by the following equation where, p is pressure, $\Delta m/\Delta t$ is the mass loss rate, M is the molecular weight, S is the surface area.

$$\mathrm{p} = \frac{\Delta m}{\Delta t}\sqrt{\frac{T}{M}} \cdot \frac{1}{S} = Q \qquad \text{Equation 3.18}$$

This is then plotted similarly to other vapour pressure techniques, ln *Q* vs *T* and from that slope, it is possible to derive the enthalpy of sublimation.

3.3.2.3. TG/STA Equipment

The TG and STA measurements carried out under this thesis were done on a Stanton-Redcroft 625 simultaneous TG/DSC connected to a 386 IBM-compatible personal computer. It was calibrated using several high purity standards – tin and indium depending on the explored temperature range.

Non-isothermal temperature experiments were carried out under a stream of synthetic air to observe the behaviour of the sample under more realistic conditions. I-TG experiments were done under an inert gas as to remove the evolved vapour during vapour pressure experiments. Heating rate is varied from experiment to experiment and is mentioned on each individual set. Open pan aluminium crucibles were used for the TG/DSC and I-TG experiments. Each TG/DSC experiments used 4 to 6 mg of sample compound.

3.4. Vacuum Drop-Microcalorimetry

As discussed in a previous chapter, the heat of sublimation is a particularly important parameter as it provides insights into the intermolecular forces present in a sample, serving as a measure of their intensity. The method described in section 3.1, uses an indirect approach through vapour pressures to determine this parameter. This section aims to describe a direct approach to this determination – vacuum drop-microcalorimetry (VDM) or Calvet microcalorimetry (CM). This involves the measurement of the energy necessary to isothermally vaporize or sublimate a well-known amount of sample.

3.4.1. General principles of vacuum drop-microcalorimetry

The history of this type of calorimetry dates back to 1923 when Tian first developed a calorimeter based on the measurement of the heat flow through a sample[32] . However, in the mid-20th century, in 1948, Calvet developed a calorimeter based on the same principle but with a twin-cell geometry. In essence, these calorimeters consist of two identical calorimetric cells inserted into two cavities in a metallic block. The details of the

experimental apparatus are better described further in this section, but first, it is important to understand the general principles of this technique.

There are two neighbourhoods that need to be considered: the internal and external. The external neighbourhood is at a constant temperature and is controlled very precisely. The internal neighbourhood has a variable temperature and is where the vaporization/sublimation process occurs. This apparatus has two thermopiles: one is used to detect any temperature changes, and the other is used to compensate for these changes with the goal of maintaining the system isothermal. This device is equipped to handle both exothermic and endothermic processes. The compensation of heat changes is accomplished via the Peltier and Joule effects respectively. This is particularly important as the process to compensate for temperature changes is what is used to determine the energy of a process.

The device operates on a differential basis with twin cells, one for the sample itself and the other as a reference. This differential approach eliminates any interference from internal temperature fluctuations or from the materials used to support the sample (such as glass capillary tubes). The presence of the reference cell also enables the establishment of a “reference” temperature against the sample cell, further enhancing the sensitivity of temperature shifts. Additionally, the cell geometry and the nearly complete coverage of the cell with thermopiles increases the precision of the temperature control.

The remarkable sensitivity of the Calvet microcalorimeter allows it to e measure exceedingly small amounts of heat and of slow processes, hence the “micro” designation.

3.4.2. Equipment and Experimental Procedure

For this work, an adapted Tian-Calvet type microcalorimeter was used. The equipment described in this section has been installed, adapted, and tested in our laboratory at the Centro de Investigação em Química da Universidade do Porto - CIQUP. This setup is well-documented in the literature.[63] In figure 3.15, it is possible to see a schematic representation of the apparatus, and in figure 3.16, there is an image of the actual system.

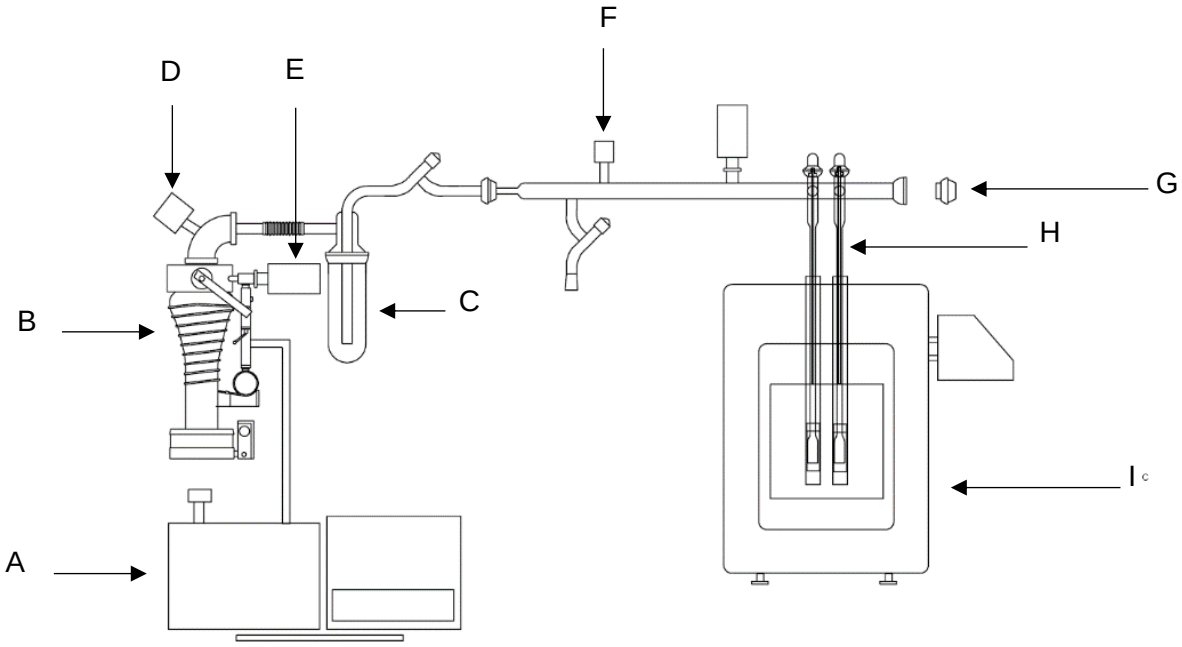

Figure 3.15 - Schematic of the Vacuum Drop-Microcalorimeter used in this work. A) Rotary Vacuum Pump; B) Diffusion Vacuum Pump; C) Glass Trap; D) Penning Gauge; E) Pirani Gauge; F) Atmosphere Inlet Valve; G) Vacuum Line; H) Glass Extensions of the Calorimetric Cells; I) HT1000D Calorimetric Block. Adapted from ref.[63]

Figure 3.16 - Photograph of the vacuum drop-microcalorimeter apparatus.

The system consists of two major components: the calorimeter and calorimetric cells, and the vacuum system.

The calorimeter is a Calvet-type microcalorimeter from Setaram, model HT1000D. This device comprises several parts, all designed to enhance the sensitivity of the measuring chamber, particularly the conduction device. This device connects the outer wall of the measuring chamber to the isothermal block. Heaters are placed on both the bottom and on the top of the cell to ensure a uniform distribution of heat. The measuring chamber can be accessed through two extensions (item G in figure 3.15). Temperature measurement is carried out using 16 sheets, each containing 31 thermocouples, totalling 496 Pt-Pt/Rh thermocouple units. This is well illustrated in figure 3.17.

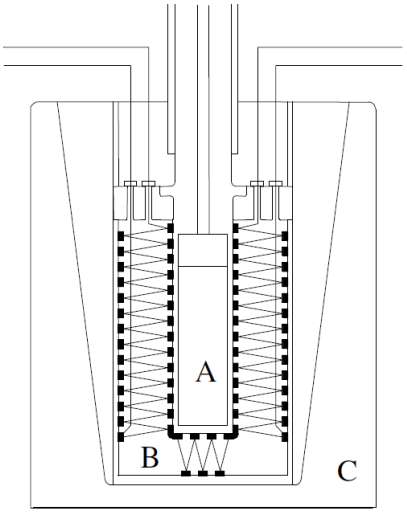

Figure 3.17 - Representation of the calorimetric cell (A) surrounded by the thermocouple system (B) inside the isothermal metallic block (C). Adapted from ref.[63].

Inside the calorimeter, it is possible to find the bulk of the calorimetric cells. These cells consist of Pyrex glass cylinders enclosed within highly conductive alloy cylinders known as Kanthal. The cells are connected to the vacuum line through Pyrex extensions, which can be easily accessed by the user, enabling multiple experiments without the need to disassemble the calorimetric chamber. This setup is illustrated in figure 3.18.

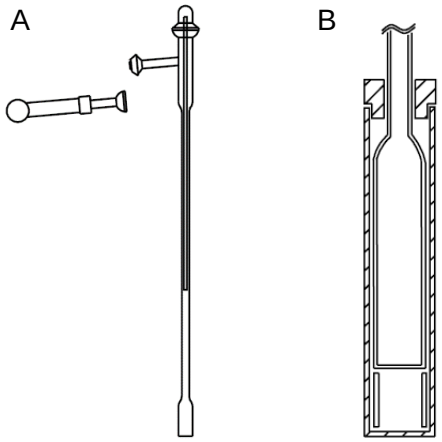

Figure 3.18 - A) Calorimetric Cell Assembly; B) Bottom of the calorimetric cell.

The next section of the device is the vacuum system (labelled A to F in figure 3.15) which consists of two pumps, a glass trap, a vacuum line, and pressure gauges. The pumping system includes a rotary pump (Edwards RV5) and a diffusion pump (Edwards Diffstak 63). The glass trap can be filled with liquid nitrogen and act as a cold condensation spot. Two types of pressure gauges are used: a Pirani gauge (Edwards APG-M) for the pre-vaccum sequence and a Penning (AIM-S) for the vaporization/sublimation experiments. A typical vacuum drop-microcalorimetry technique starts by selecting suitable pairs of glass capillary tubes, one for reference (blank) and one for the sample. The mass of each capillary tube is determined using a Mettler-Toledo UMT 2 microbalance with a resolution of ± 0.1 μg. Then, the powdered sample is loaded into the sample capillary tube, and its mass is re-measured with the same microbalance. Each sample capillary should contain between 3 to 5 mg of the sample. After these steps, the two tubes are simultaneously dropped into the calorimetric cels. This drop occurs after temperature stabilization at T = 298.15 K. Once thermal stability is achieved, the chamber is exposed to high vacuum to induce sublimation. In figure 3.19, it is possible to observe a typical thermogram obtained from measuring the heat flow through our sample.

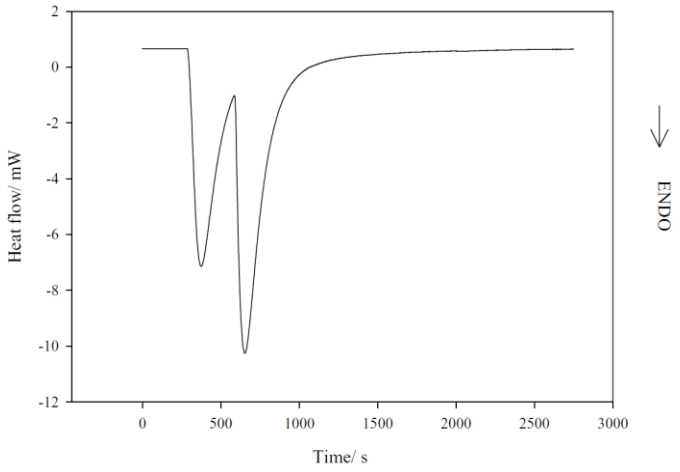

Figure 3.19 - Typical vacuum drop-microcalorimetry thermogram.

The integration of the thermogram yields the total observed enthalpy change of the process, $\Delta H_{observed}$. It is important to note that the observed enthalpy change includes the entire process and not only the phase change.

The device was properly tested and calibrated, as described in reference [63].

Reference [63] also showed that the uncertainty of the described method is circa 2 %. This uncertainty is influenced by three main factors: the thermal stability of the compound, the purity of the sample and the enthalpy correction from the working temperature to the reference temperature of 298.18 K.

3.4.3. Treatment, calibration, and correction of experimental results

As mentioned in the previous sections, the measurements are conducted under conditions significantly different from standard and reference conditions. Therefore, data treatment and corrections are of paramount importance. To understand the corrections, one must first understand the treatment of experimental data.

From the integration of a thermogram, like of the one shown in figure 3.19, one obtains the total enthalpic change, as mentioned in the previous subsection. The contribution from the fall of the capillary tubes, the sensitivity response of the cells, and the heating of the sample and the glass from room temperature to the working temperature are included in the $\Delta H_{observed}$. Therefore, a correction factor obtained from blank

experiments needs to be introduced - $\Delta H_{corr}(blanks)$. From this, the following equation is obtained:

$$\Delta H_{corrected} = \Delta H_{observed} + \Delta H_{corr}(blanks) \quad \text{Equation 3.19}$$

However, there are some other factors that need to be considered when correcting our experimental results. One such factor arises from the fact that there is a small area on the top of the cell that is not covered by the thermocouple system. This can result in the loss of some heat. This loss is temperature-dependant, and as such, an *in-situ* calibration is always required when a new working temperature is defined. The calibration step is conducted by performing experiments on substances with well-known heats of sublimation and with similar vapour pressure to that of the analysed sample. When treated with equation 3.18 and the following equation, where *M* and m_{am} are the molar mass and sample mass, respectively, the enthalpy of sublimation for the calibration experiment is obtained.

$$\Delta^{g,T}_{cr,l,298.15K} H^{\circ}_{m} = \frac{\Delta H_{corrected} \times M}{m_{am}} \quad \text{Equation 3.20}$$

After the enthalpic correction to the reference *T* of 298.15 K, it is possible to compare the obtained value with the literature value, through which one obtains the calibration constant, k_{cal}, for the operating conditions of the Calvet microcalorimeter. This is described by equation 3.20.

$$k_{cal} = \frac{\Delta^{g,T}_{cr,l,298.15K} H^{\circ}_{m}}{\Delta^{g,T}_{cr,l,298.15K} H^{\circ}_{m}(calib)} \quad \text{Equation 3.21}$$

Now, it is possible to calculate the enthalpy of sublimation for the sample being analysed. This is achieved through equation 3.21, where k_{cal} is the calibration constant, m_{am} is the sample mass, *M* is the molar mass, and ΔH_{corr} is the corrected obtained enthalpy.

$$\Delta^{g,T}_{cr,l,298.15K} H_{m} = \frac{k_{cal} \Delta H_{corrected} \times M}{m_{am}} \quad \text{Equation 3.22}$$

As described in [64], some assumptions are made to correct the obtained enthalpic value to the standard value. However, the error introduced by these assumptions is negligible and can be disregarded. Temperature adjustments and corrections are carried out according to the method described in the 2.5 section of this thesis. The values of the enthalpic correction are obtained from the heat capacities in the gas state of the working

molecule, which are determined computationally through the B3LYP/6-31G(d) computational method.

4. Results and Discussion

The present chapter aims to present and discuss the results obtained for the compounds studied in this work – bathophenanthroline and bathocuproine. All the calibration essays conducted are also documented, along with tests performed.

This chapter is divided into three major sections: one focusing on bathophenanthroline, another on bathocuproine, and a third on the vapour pressure analysis.

4.1. Bathophenanthroline

The results pertaining to bathophenanthroline (figure 4.1) are presented and further discussed under this section. As explored in this first chapter, this molecule has several applications in the field of organic semiconductor devices. To the best of our knowledge, there is no thermophysical information regarding this molecule in the literature and as such, this work aims at providing a complete thermophysical profile.

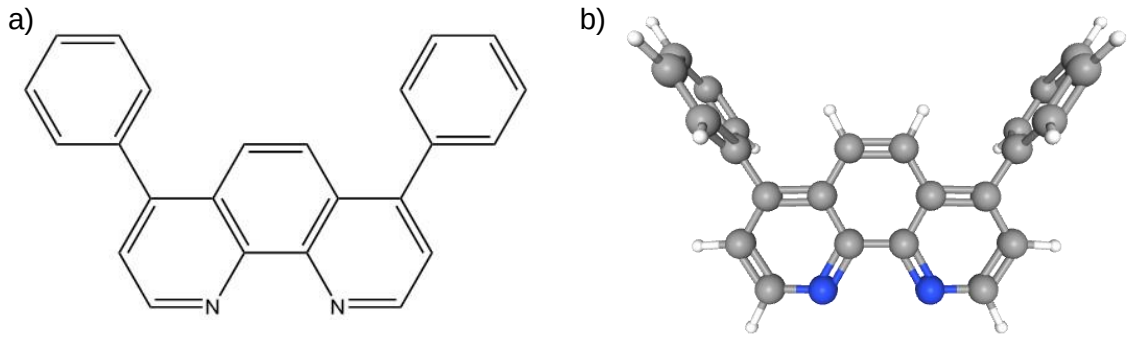

Figure 4.1 - a) Structural formula of bathophenanthroline. b) 3D representation of bathophenanthroline.

4.1.1. Sample Details: Source and Characterization

This section aims at presenting the characterization and, when appropriate, further treatment of the commercially obtained samples of bathophenanthroline. In table 4.1, it is possible to find details on the sample, its source and results of purity and water content analysis.

Table 4.1 - Purification and source details of bathophenanthroline.

Compound	Bathophenanthroline		
[IUPAC name]	[4,7-diphenyl-1,10-phenanthroline]		
[CAS RN]	[1662-01-7]		
Molecular Formula	$C_{24}H_{16}N_2$		
Molecular Weight	332.4 $g \cdot mol^{-1}$		
Source/Batch	Alfa Aesar	ThermoFisher Scientific	Alfa Aesar
	1	2	3
Initial purity [a]	0.997	0.991	0.997
Appearance	White powder	Pale cream crystals	White powder
Actual purity [b]	0.9998	0.9978	0.9993
Purification method	-	Sublimation	-
Final mass fraction purity	-	0.9999	-
Analysis method	GC	GC	GC
% H_2O[c]	0.049	-	0.034

[a]According to the analysis certificate of the supplier.

[b]Obtained from Gas chromatography (GC) analysis (with FID);

[c]Determined via Karl-Fischer Titration.

Before going into details, it is important to underline that the purity analysis was performed using gas-chromatography (GC), which determines the mass fraction of a given sample. The percentage of water was determined via Karl-Fischer titration (KF).

Using GC, it was found that the first and third batches had a sufficiently high purity (≥0.9990) for all the analysis conducted in this work. However, the second batch had a lower purity than what is required (≤0.9990) and needed to be purified. This purification process was carried out by vacuum sublimation, resulting in a final mass fraction close to one. The small amount of water present in the different batches also indicated that all the samples could be used without any further treatment.

Note that only the first batch was used for this work.

FTIR measurements were carried out to ascertain if any change occurred in the sublimated sample. Measurements were done on a PerkinElmer Spectrum Two (ATR

module) with four scans per spectrum. Data were analysed using the PerkinElmer software Spectrum. FTIR analysis was conducted at FCUP|DQB Lab& Services.

In figure 4.2, it is possible to see the complete FTIR spectrum of bathophenanthroline from the original sample compared with the sample purified by sublimation. In figure 4.3, there is a zoomed-in view of the fingerprint region. As it is seen, the spectra are identical. This is a clear indication that no chemical changes occurred in the purified bathophenanthroline sample, aside from the increase in purity.

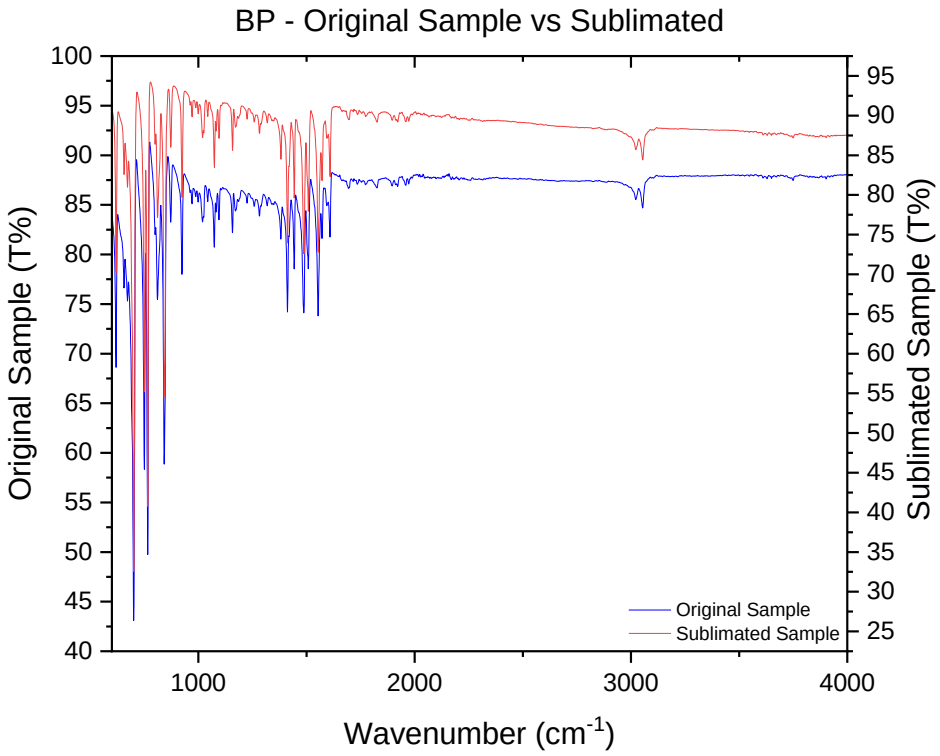

Figure 4.2 - Bathophenanthroline FTIR spectra. Original Sample versus Sublimated sample.

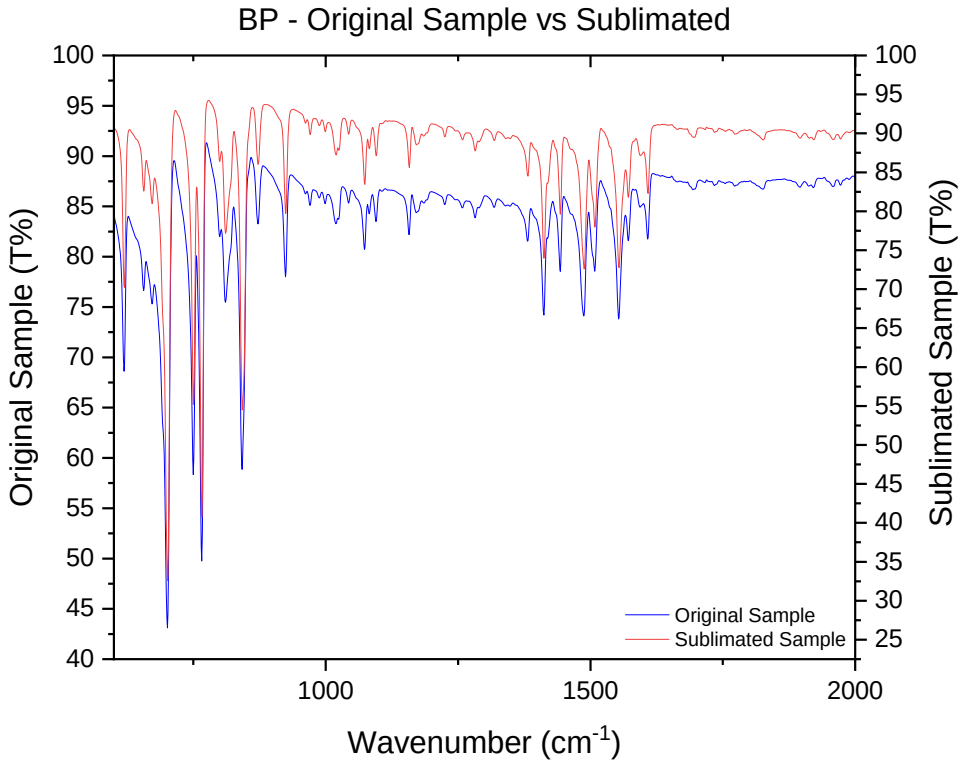

Figure 4.3 - Bathophenanthroline FTIR spectra. Original Sample versus Sublimated sample. (Fingerprint region)

4.1.2. Thermal Analysis

This section aims to present and discuss the experimental results obtained from differential scanning calorimetry (DSC) and thermogravimetric analysis (TG) for the previously discussed sample. Various scans were conducted under different conditions, such as different scanning rates or with different temperature programmes, and these will be specified in each case.

An initial scan was conducted on the original sample at a rate of 10 $K \cdot min^{-1}$ to determine if any solid-solid transitions were present, as different crystalline states can have different thermophysical and thermochemical properties. This is particularly important for the subsequent thermodynamic measurements. In figure 4.4 the DSC curve that refers to that scan can be found. As it is possible to observe, only one process is identified.

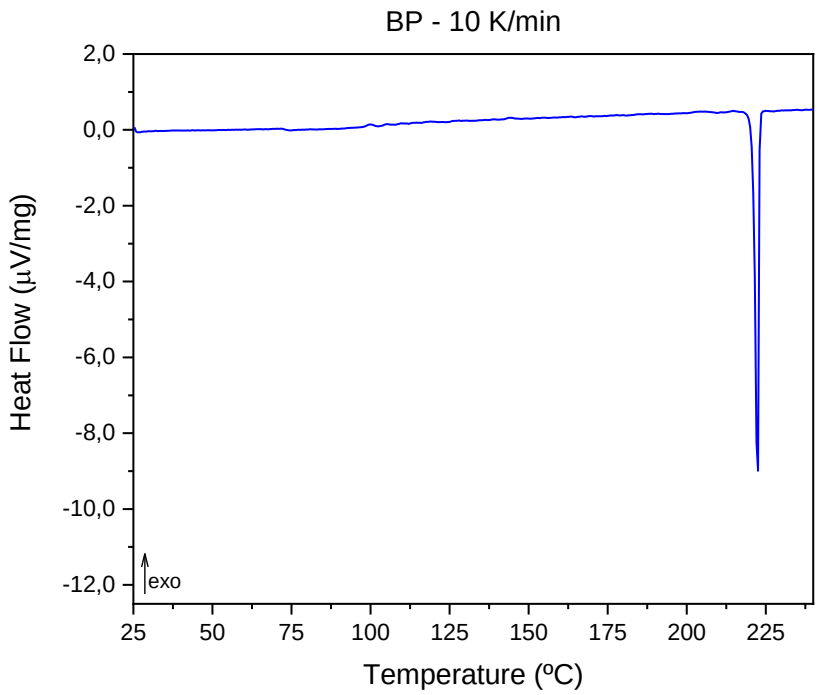

Figure 4.4 - Thermogram of a 10 K·min^{-1} scan of the original bathophenanthroline sample. Analysis conducted with a hermetically sealed alluminium crucible under a constant nitrogen flow.

From this scan, a single fusion event was identified. The shape of the peak indicates that fusion happens in one single quick step for the only crystalline form that can be identified. Since there only is one fusion event, experiments to determine the temperature and heat of fusion can be easily carried out.

4.1.2.1. Heat and Temperature of Fusion

The experiments to determine the heat and temperature of fusion were conducted in the temperature range of [473.15 – 513.15] K at heating rate of 2 K·min^{-1}. Additionally, a hermetically sealed aluminium crucible was used under a purge and protective N_2 flow. From four different experiments using fresh samples, a value of (492.46 ± 0.78) K was obtained for the temperature of fusion, along with a value of (41.0 ± 0.4) kJ·mol^{-1} for the standard molar enthalpy of fusion. The results are presented in table 4.2, including the values adjusted to the reference temperature of 298.15 K.

Table 4.2 - Experimentally obtained values for the temperature and heat of fusion of bathophenanthroline.

	Bathophenanthroline	
Essay	T_{fusion} **(K)**	$\Delta_{cr}^{l}H_m^{\circ}$ **<T_{fusion}> (kJ·mol^{-1})**
1	492.27	41.1
2	492.26	41.1
3	492.55	40.9
4	492.77	40.8
Average Values	⟨492.46 ± 0.78⟩	⟨41.0 ± 0.4⟩
$\Delta_{cr}^{l}H_m^{\circ}$ **(298.15 K) (kJ·mol^{-1})**	30.4 ± 0.4	

In figure 4.5, it is possible to observe a close-up view of the fusion peak. As said before, this is a single sharp endothermic peak, indicating the presence of a single crystalline form that undergoes rapid melting in a single step.

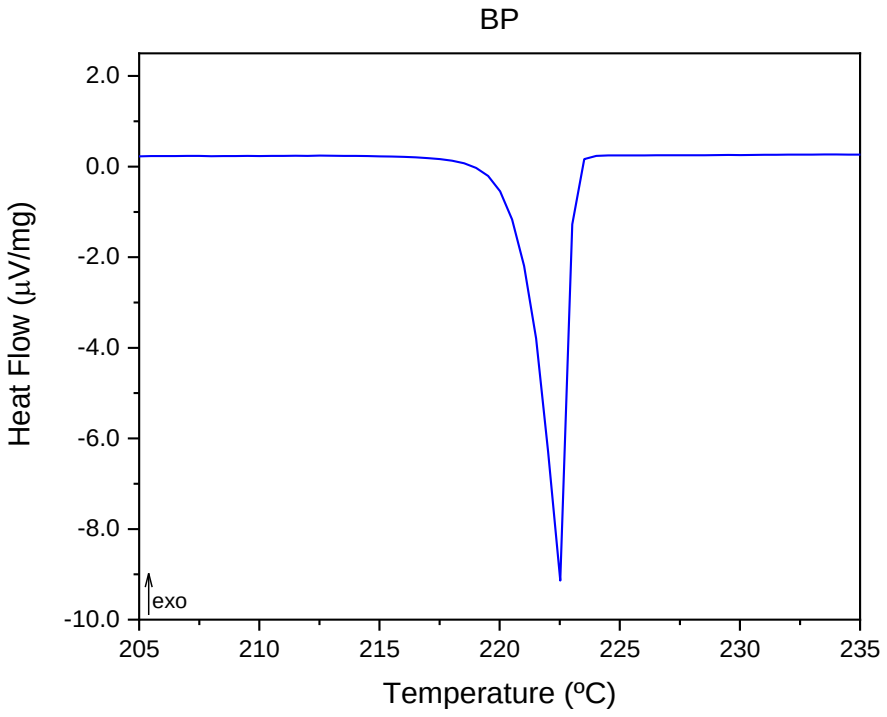

Figure 4.5 - DSC curve of the fusion process of bathophenanthroline.

4.1.2.2. Thermal Behaviour Analysis

Additional scans were conducted with the purpose of ascertaining if any other thermophysical processes occurred on the liquid and solid phases.

A 10 K·min^{-1} scan between [513.15 - 213.15] K and subsequently between [213.15 – 513.15] K signalled the presence of several thermophysical phenomena that deserved further study. In order of occurrence, these were a (a) change in the baseline of the DSC signal, (b) a small but significant exothermic peak, (c) a small but significant endothermic peak followed by (d) a large exothermic peak, and finally (e) a large endothermic peak. This is further detailed in figure 4.6.

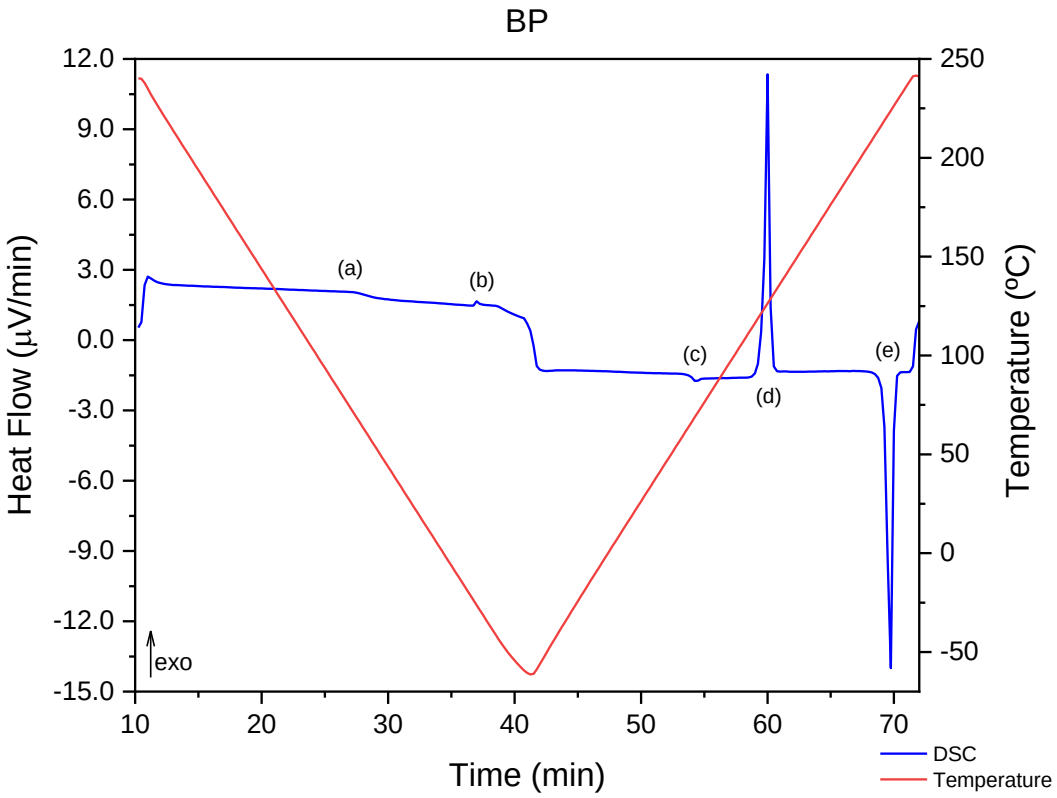

Figure 4.6 - DSC curve of the thermal behaviour analysis of bathophenanthroline. Hermetically sealed Al crucible under N_2 flow

A DSC experiment with an identical temperature program was conducted to observe if any of the events were artifacts, and event (a) was identified as one. It can be ascribed to the cooling control or to some characteristic inherent to the intracooler device.

To analyse the remaining events, a new sample was prepared and subjected to the same temperature program, and it was stopped between events (b) and (c) at 298.15 K as the DSC signal indicated that the sample was in the solid state. The crucible was opened, and the treated sample was analysed visually and with FTIR-ATR. It appeared to be a translucent solid. When removed from the crucible, it turned into a white powder. In figure 4.7 is the FTIR spectrum obtained from the treated sample compared with the original sample.

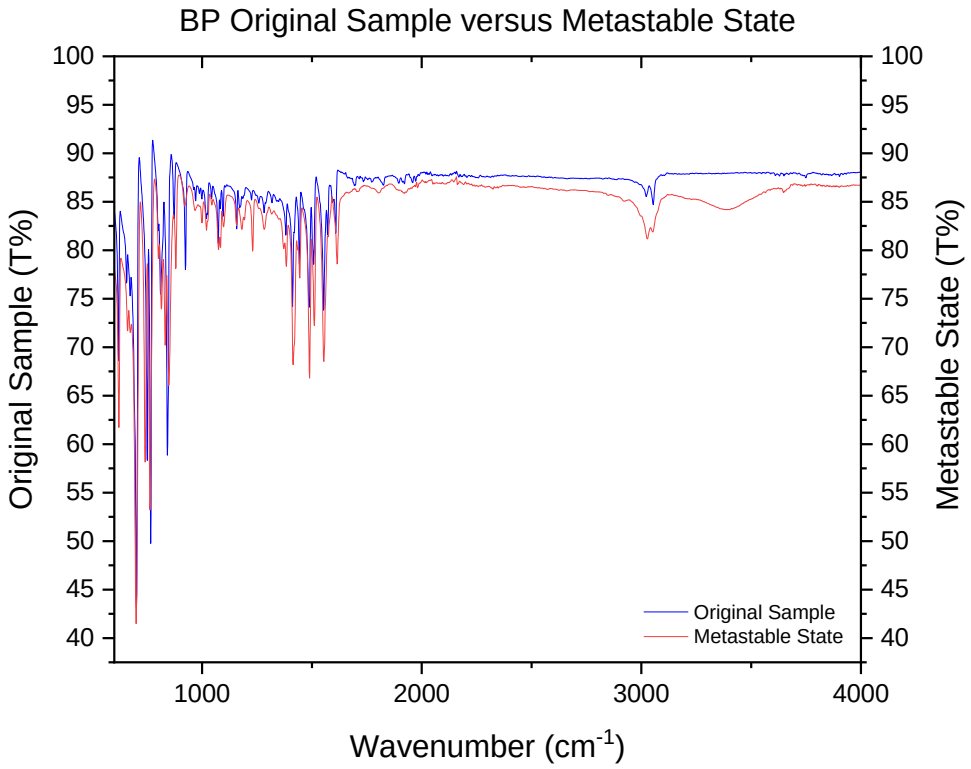

Figure 4.7 - Bathophenanthroline FTIR spectra. Original sample versus metastable sample.

As it is possible to observe, there is a significant change in the IR spectrum. This indicates a change in the structure of the observed sample. The most significant change is in the 3400 cm^{-1} range. This portion of the infrared region is usually ascribed to N–H stretching. This suggests that a possible metastable state is formed where there is a significant interaction between nitrogen and hydrogen atoms. This interaction can be either intramolecular or intermolecular in nature. The latter possibility seems the most likely as this bond is usually highly directional.

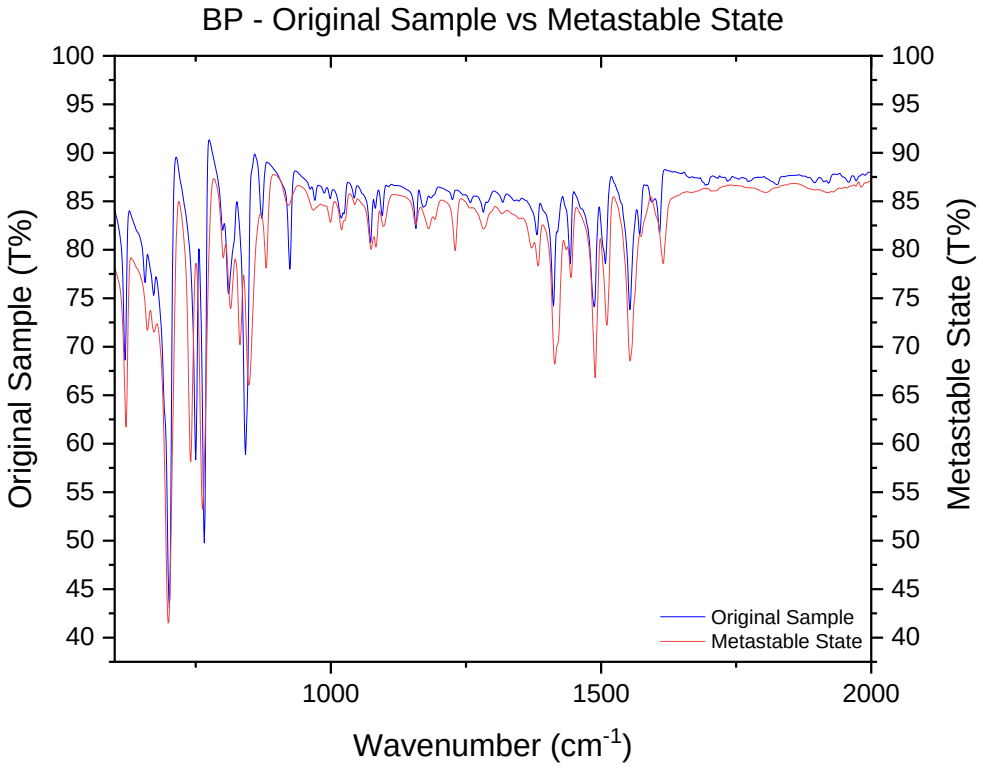

Figure 4.8 - Bathophenanthroline FTIR spectra. Original sample versus metastable sample. (Fingerprint region)

Further analysis of the fingerprint region (figure 4.8) suggests that its molecular motions triggered by infrared radiation are not significantly different, which suggests that the N-H interactions described previously are responsible for the metastability of this state.

Returning to figure 4.6 and to the thermophysical events, the (c) event has a more recognizable peak shape that is usually ascribed to the formation of an isotropic liquid (but not as energetic as fusion). So, a change from a metastable, solid state to a liquid state is observed. This change, which will give enough mobility to the molecules of the sample to then crystallize in their normal crystalline state, can be ascribed to event (d). This behaviour is called cold crystallization, and it happens when a sample is cooled and does not crystallize but rather change into a metastable state. This state, upon heating, is turned into one with higher molecular mobility (usually a liquid) which will then have enough energy to solidify into an organized crystalline state. Peak (e) has been identified as fusion.

Infrared analysis of the sample after cold crystallization was also performed, and the spectrum (figure 4.9) is identical to the one from the original sample, which is an indicative of the same chemical and structural features.

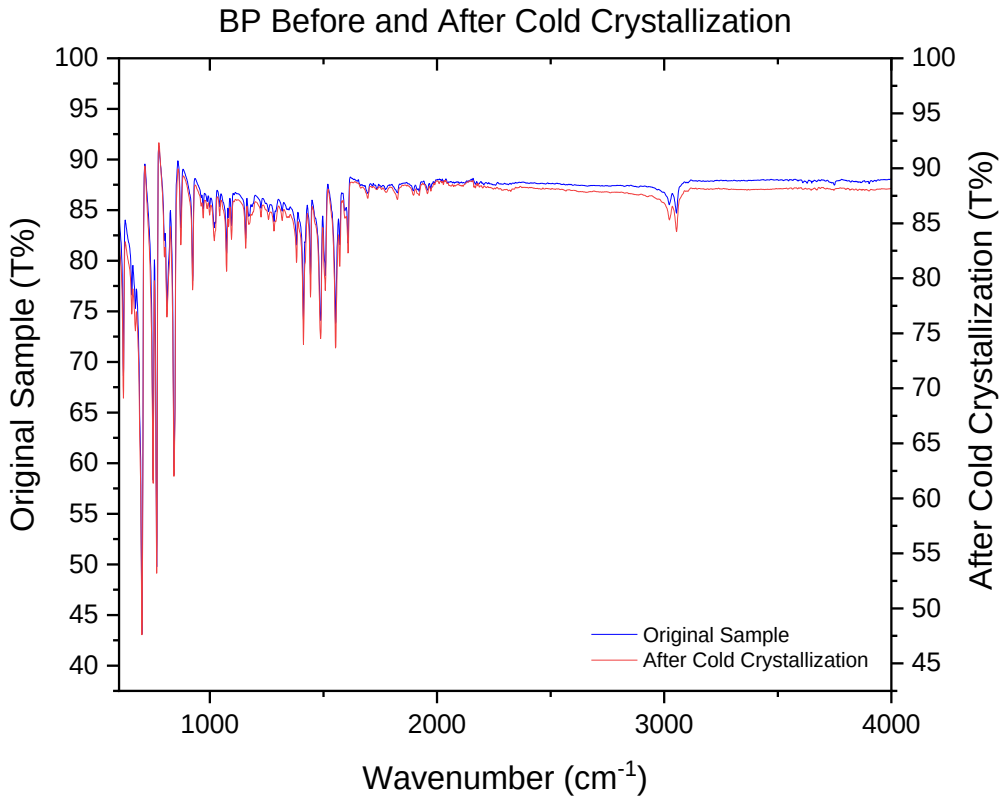

Figure 4.9 - Bathophenanthroline FTIR spectra. Original sample versus treated sample (after cold crystallization).

Further experiments were conducted in order to ascertain the reproducibility of the behaviour between different heating and cooling cycles and also between different cooling rates.

Firstly, a fresh sample was subjected to a temperature program with two cycles with temperature varying between [213.15 – 513.15] K at 10 K·min^{-1}. The goals were to see if the events described earlier were reproducible through several cycles, if the shape of the fusion peak was the same, and if the T_{fusion} was equal to that of the original sample.

Figure 4.10 is a DSC curve of the experiment described in the previous paragraph. As it is possible to observe, the thermophysical events explored earlier are reproducible not only between fresh samples but also within the same sample through several cycles.

This indicates that the sample stays the same chemically, and that there are only physical changes present.

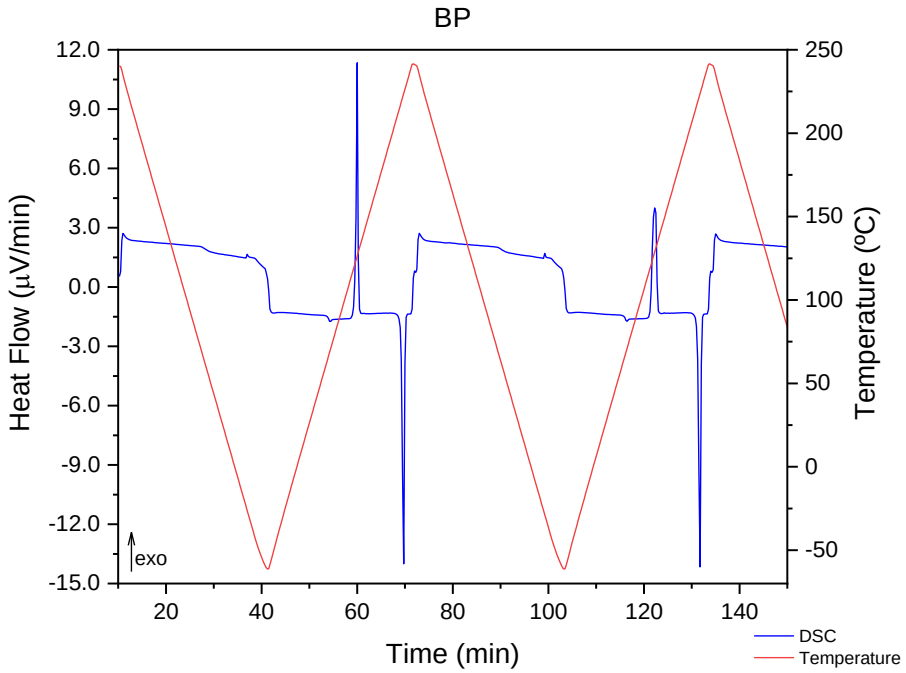

Figure 4.10 - DSC curve of the thermal behaviour analysis of bathophenanthroline through two heating and cooling cycles.

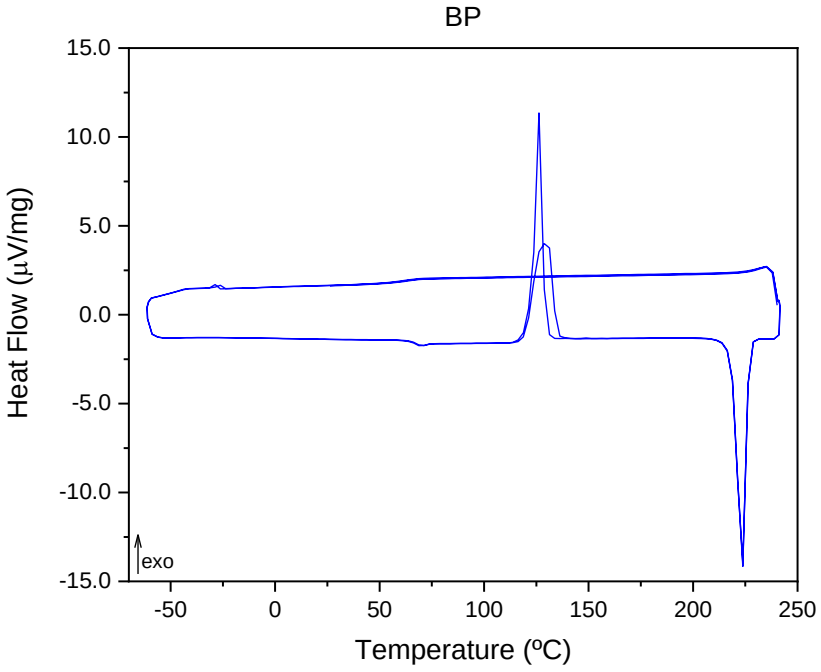

Figure 4.11 - DSC curve of the thermal behaviour analysis of bathophenanthroline through two heating and cooling cycles.

In figure 4.11, a DSC curve of the same experiment as in figure 4.10 is presented, but this time with temperature (*T)* on the x-axis. In the cold crystallization, a difference in the peak shape is observed, but the onset temperature remains the same. This behaviour is common, as crystallization depends on various factors, such as seeding and molecular diffusion on the liquid sample. However, fusion is only dependent on the heating rate and the temperature. The shape and onset points of the fusion process are nearly identical, which supports the hypothesis that the sample crystallizes into a single, thermodynamically stable crystalline form.

DSC experiments were conducted at different cooling rates to investigate whether the metastable state described earlier would still form. The corresponding DSC curves are explicitly presented in figure 4.12, and the results indicate that this metastable state formed at cooling rates of 10 $K \cdot min^{-1}$ and 5 $K \cdot min^{-1}$. However, it did not occur at 2 $K \cdot min^{-1}$. This absence can be attributed to the slow cooling rate, which likely resulted in the generation of an undercooled liquid.

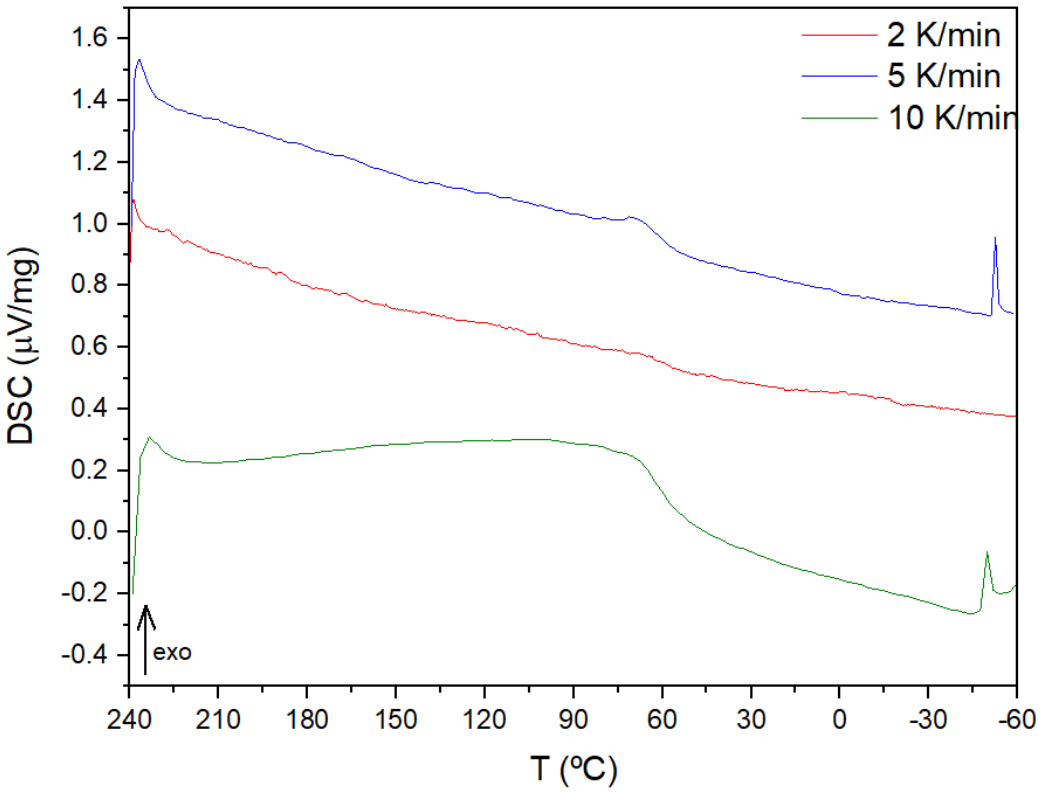

Figure 4.12 – DSC cooling curve of bathophenanthroline at several cooling rates.

The change in the heat flow baseline, previously ascribed to a cooling control issue, also decreases in magnitude as the cooling rate decreases, which further supports the artifact hypothesis.

4.1.2.3. Simultaneous Thermal Analysis

Simultaneous heat flow and mass measurements were undertaken to investigate the thermal behaviour of bathophenanthroline under open crucible conditions and synthetic air (an 80/20 nitrogen/oxygen mixture). These conditions are more representative of real-world scenarios. The device described in chapter three has a temperature range of [RT – 873.15] K, and in figure 4.13, a complete thermogram within the available range is presented.

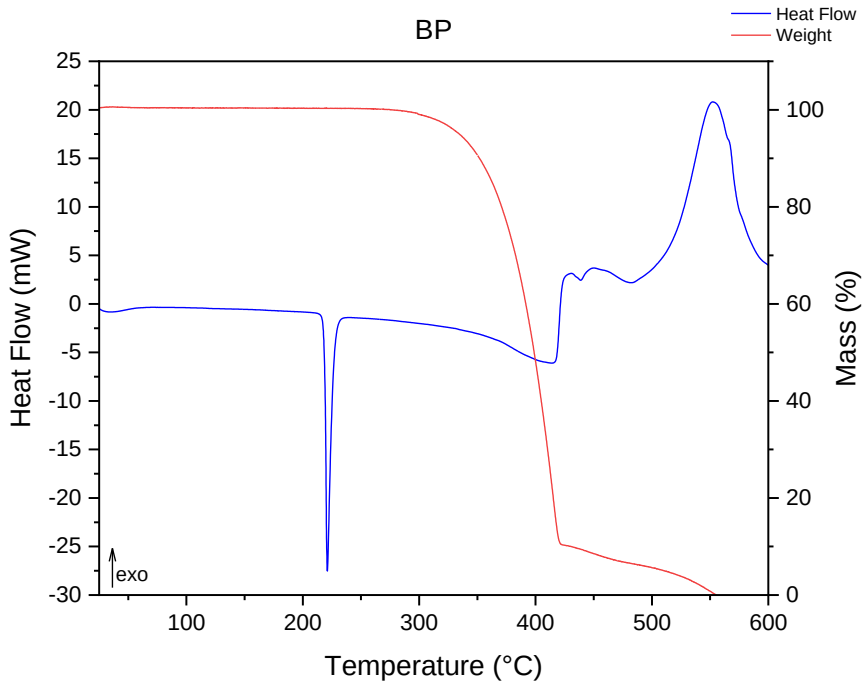

Figure 4.13 – DSC and TG curves of bathophenanthroline under open Al crucible and synthetic air conditions. [RT - 873.15] K range.

Before fusion, stable heat flow and mass signals indicate that no detectable change is observed in the sample, i.e., no significant decomposition and no significant sublimation occur.

After fusion, a constant decrease in the heat flow of the sample is observed. The heat flow change is indicative of vaporization of the sample, i.e., an endothermic loss of mass.

Although decomposition cannot be completely ruled out, the signal indicates that none occurs as no exothermic events are observed. It is also important to note a 90% decrease in the mass sample.

The 90% decrease in mass ends around $T \approx 700.15$ K, after which a substantial exothermic heat flow change is observed. This change indicates the decomposition of the remaining sample, which occurs in three steps. At $T \approx 823.15$ K, the experiments reaches its conclusion with a complete mass loss. Figure 4.14 provides a detailed thermogram of bathophenanthroline, covering the period from just before fusion to the end of the experiment.

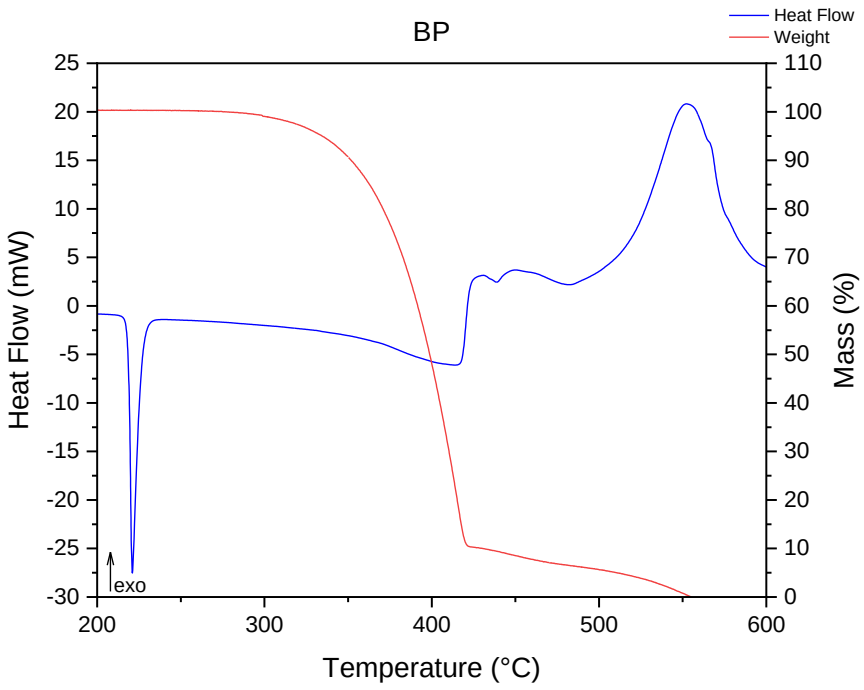

Figure 4.14 – DSC and TG curves of bathophenanthroline under open crucible and synthetic air conditions. [473.15 - 873.15] K range.

This experiment was repeated several times, and the behaviour observed is reproducible. It's worth noting that the chemical stability of the sample after fusion is crucial, as it opens up the possibility of conducting vapour pressure measurements to determine heat of vaporization.

4.1.3. Vacuum Drop-Microcalorimetry

The sample under discussion underwent direct sublimation analysis using vacuum drop-microcalorimetry. Tests performed with this sample indicated that the operating temperature of the device should be set at 503.15 K. The experimentally obtained results, along with further corrections based on an instrumental constant, are recorded in table 4.3 along with the final result obtained from the mean of six independent experiments.

Table 4.3 - Experimentally obtained results on the sublimation study of bathophenanthroline with the vacuum drop-microcalorimetry technique.

Bathophenanthroline	**1**	**2**	**3**	**4**	**5**	**6**
T**/ K**	511.28	511.18	511.42	511.18	511.18	511.34
T_{amb}**/ K**	298.15	298.25	298.15	298.15	298.15	298.25
$m_{samplecap}$**/ mg**	24.6285	22.9686	22.7055	22.5858	22.4085	23.4417
m_{ref}**/ mg**	24.5424	22.9937	22.6849	22.6550	22.4719	23.4313
m_{sample}**/ mg**	3.177	2.948	2.792	2.826	2.431	3.171
ΔH_{corr}**(blanks)/ mJ**	31.215	52.423	46.514	60.047	59.714	45.834
$\Delta H_{observed}$**/ J**	2.232	2.057	1.940	1.981	1.652	2.184
$\Delta H_{corrected}$**/ J**	2.263	2.109	1.987	2.041	1.711	2.230
$\Delta^{g,T}_{cr,298.15}H^{\circ}_{m}$ **/kJ·mol^{-1}**	258.7	259.8	258.4	262.3	255.6	255.4
$\Delta^{T}_{298.15}H^{\circ}_{m}$ **/kJ·mol^{-1}**	74.6	74.6	74.7	74.6	74.6	74.7
$\Delta^{g}_{cr}H^{\circ}_{m}$**(298.15 K) /kJ·mol^{-1}**	184.1	185.2	183.7	187.7	181.0	180.8
$\langle\Delta^{g}_{cr}H^{\circ}_{m}$**(298.15 K)$\rangle$ = 183.7 ± 4.2 kJ·mol^{-1}**						

4.1.3.1. Calibration with triphenylbenzene for bathophenanthroline and tests with 9-acridanone

A molecule with similar vapour pressure was selected to do *in situ* calibration for the selected temperature. The molecular structure of the calibration compound is depicted in figure 4.15.

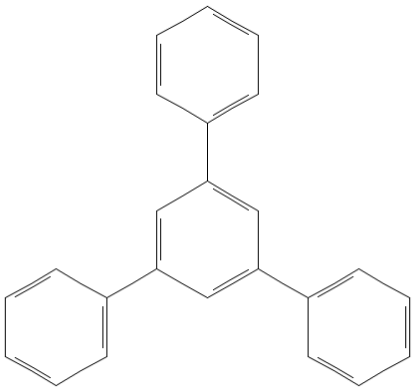

Figure 4.15 - Molecular structure of 1,3,5-triphenylbenzene.

The results for the 1,3,5-triphenylbenzene calibration are in table 4.4. The l constant is determined from the mean of seven different assays.

Table 4.4 - Experimentally obtained results on the calibration experiments with 1,3,5-triphenylbenzene with the vacuum drop-microcalorimetry technique at 503.15 K.

Triphenylbenzene	**1**	**2**	**3**	**4**	**5**	**6**	**7**
***T*/ K**	510.85	511.08	511.18	511.27	511.06	511.05	511.36
T_{amb}/ K	298.25	298.15	298.15	298.15	298.15	298.05	298.25
$m_{samplecap}$/ mg	22.401	21.046	21.885	20.292	24.800	24.696	23.234
m_{ref}/ mg	22.410	21.043	21.954	20.248	24.884	24.702	23.205
m_{sample}/ mg	3.0318	2.6843	3.4560	3.1326	3.7020	3.5202	4.3798
ΔH_{corr}(blanks)/ mJ	51.616	53.945	61.984	50.092	55.696	44.633	43.680
$\Delta H_{observed}$/ J	2.080	1.914	2.526	2.250	2.590	2.487	3.168
$\Delta H_{corrected}$/ J	2.131	1.968	2.588	2.300	2.646	2.532	3.212
$\Delta^{g,T}_{cr,298.15}H^{\circ}_{m}$ /kJ·mol^{-1}	215.4	224.6	229.5	224.9	219.0	220.4	224.7
$\Delta^{g,T}_{cr,298.15}H^{\circ}_{m}$ /kJ·mol^{-1} (expected)	243.0	243.1	243.2	243.2	243.1	243.1	243.3
K	1.1282	1.0825	1.0597	1.0812	1.1101	1.1032	1.0828
	<K> = 1.0925 ± 0.0218						

It is worth noting that the constant obtained is unusually large, required confirmation. To verify this value, tests were conducted using a previously studied sample with a similar working temperature. 9-acridanone (figure 4.16) was selected for this purpose, and the data from these experiments are registered in table 4.5.

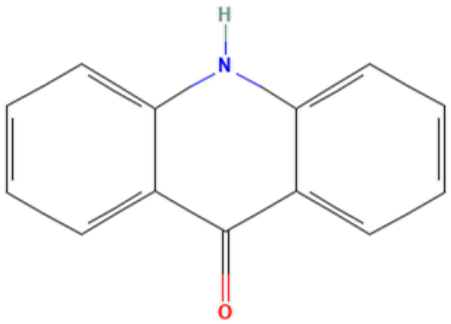

Figure 4.16 - Molecular structure of 9-acridanone.

The apparent increase of the constant, compared to previous calibration experiments, can be due to several factors. The most significant factor is the unusually working temperature for this device although it still falls within the experimental temperature range of the calorimeter. This elevated temperature results in greater heat loss through the top section of the calorimetric cells. As explained in chapter three, this section of the cell lacks thermocouples, leading to an unaccounted heat loss that must be considered on the *in-situ* calibration, hence the higher constant.

Table 4.5 - Experimentally obtained results on the test experiments with 9-acridanone with the vacuum drop-microcalorimetry technique at 503.15 K.

9-acridanone	**1**	**2**	**3**	**4**
T**/ K**	511.18	511.39	511.42	511.25
T_{amb}**/ K**	298.35	298.15	298.15	298.15
$m_{samplecap}$**/ mg**	24.3813	24.2619	23.6669	23.4206
m_{ref}**/ mg**	24.3432	24.2732	23.5870	23.4585
m_{sample}**/ mg**	2.3715	3.4095	2.3916	1.7132
ΔH_{corr}**(blanks)/ mJ**	20.317	30.540	23.027	46.635
$\Delta H_{observed}$**/ J**	2.065	2.944	2.080	1.432
$\Delta H_{corrected}$**/ J**	2.085	2.975	2.103	1.478
$\Delta^{g,T}_{cr,298.15}H^{\circ}_{m}$ **/kJ·mol^{-1}**	55.5	55.6	55.6	55.5
$\Delta^{T}_{298.15}H^{\circ}_{m}$ **/kJ·mol^{-1}**	187.5	186.1	187.5	184.0
$\Delta^{g}_{cr}H^{\circ}_{m}$**(298.15 K) /kJ·mol^{-1}**	132.0	130.5	131.9	128.5
$<\Delta^{g}_{cr}H^{\circ}_{m}(298.15\ K)>$ **= 130.7 ± 3.2 kJ·mol^{-1}**				
$<\Delta^{g}_{cr}H^{\circ}_{m}(298.15\ K)>$**lit = 131.8 ± 2.9 kJ·mol^{-1}**				

4.1.4. Knudsen Effusion Method

Bathophenanthroline underwent vapour pressure studies using the two techniques described in section 3.1. In this section, the raw and treated results are presented, along with their interpretation and comments. Further discussion will be provided in the “vapour pressure analysis” section at the end of this chapter.

4.1.4.1. Knudsen Effusion Mass Loss

In table 4.6, the obtained and treated results for bathophenanthroline using the KEML method are recorded. These results include the temperature and accompanying vapour pressures, along with the calculated 1/T and ln p. The latter values are used in a graphical representation of the Clausius-Clapeyron slope, from which parameters a and b can be derived (figure 4.17). As explained in chapter three, these parameters enable the calculation of the vapour pressure at the mean temperature, $p(<T>)$, the enthalpy of

sublimation at mean temperature, $\Delta_{cr}^{g}H_{m}^{\circ}$ (<*T*>), and the entropy of sublimation at mean temperature, $\Delta_{cr}^{g}S_{m}^{\circ}$ (<*T*>). These parameters are presented in table 4.7.

Considering the thermodynamic parameters obtained at the average temperature, it is possible to adjust these values to the reference temperature of 298.15 K, resulting in $\Delta_{cr}^{g}H_{m}^{\circ}$, $\Delta_{cr}^{g}S_{m}^{\circ}$. These latter parameters can be used Gibbs free energy of the sublimation process at 298.15 K, $\Delta_{cr}^{g}G_{m}^{\circ}$. Additionally, the previous described plot can be used to extrapolate the vapour pressure at the reference temperature. All of the values mentioned in this paragraph are registered in table 4.8.

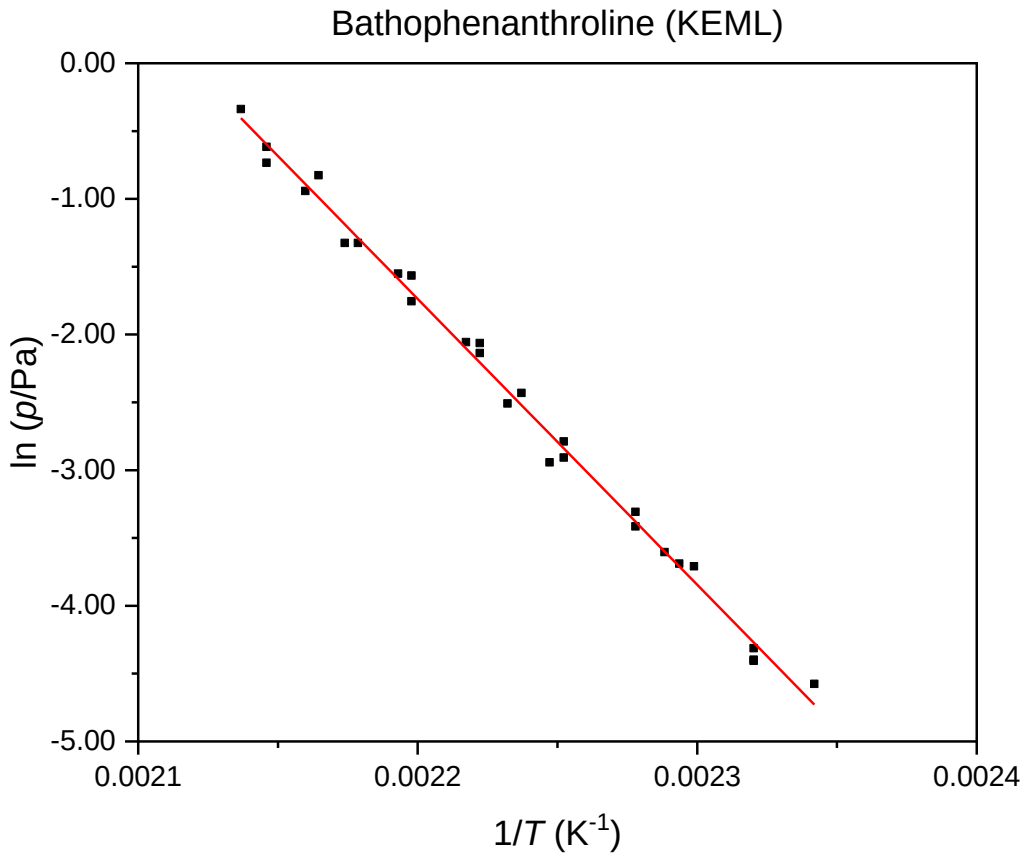

Figure 4.17 - Graphical representation of ln *p* vs 1/*T* obtained through the Knudsen effusion mass loss method for bathophenanthroline.

Table 4.6 - Experimental and treated results obtained for bathophenanthroline through the KEML method.

T **(K)**	***p*** **(Pa)**	**1/*T*** **(K^{-1})**	**ln (*p*/Pa)**
427	0.010	2.34E-03	-4.58
431	0.012	2.32E-03	-4.40
431	0.012	2.32E-03	-4.41
431	0.013	2.32E-03	-4.31
435	0.025	2.30E-03	-3.71
436	0.025	2.29E-03	-3.69
437	0.027	2.29E-03	-3.60
439	0.037	2.28E-03	-3.31
439	0.033	2.28E-03	-3.41
444	0.055	2.25E-03	-2.91
444	0.062	2.25E-03	-2.79
445	0.053	2.25E-03	-2.94
447	0.088	2.24E-03	-2.43
448	0.081	2.23E-03	-2.51
450	0.127	2.22E-03	-2.06
450	0.118	2.22E-03	-2.14
451	0.128	2.22E-03	-2.06
455	0.173	2.20E-03	-1.75
455	0.209	2.20E-03	-1.57
456	0.212	2.19E-03	-1.55
459	0.266	2.18E-03	-1.32
460	0.266	2.17E-03	-1.32
462	0.438	2.16E-03	-0.83
463	0.390	2.16E-03	-0.94
466	0.540	2.15E-03	-0.62
466	0.480	2.15E-03	-0.73
468	0.713	2.14E-03	-0.34
$\langle T \rangle = 448$ K			

Table 4.7 - Clausius-Clapeyron equations parameters obtained for bathophenanthroline with the KEML method at the mean temperature.

Technique	a	b	R^2	p(<*T*>)	$\Delta_{cr}^{g}H_m^{\circ}$ (<*T*>)	$\Delta_{cr}^{g}S_m^{\circ}$ (<*T*>)
				Pa	kJ·mol^{-1}	J·K^{-1}·mol^{-1}
KEML	44.63±0.75	-21076±334	0.9935	0.074	175.2 ± 2.8	391.2 ± 6.2

Table 4.8 - Standard molar enthalpy, entropy and Gibbs free energy and vapour pressure at the temperature of 298.15 K for bathophenanthroline obtained with the KEML method.

Compound	$\Delta_{cr}^{g}H_m^{\circ}$ /kJ·mol^{-1}	$\Delta_{cr}^{g}S_m^{\circ}$ /J·K^{-1}·mol^{-1}	$\Delta_{cr}^{g}G_m^{\circ}$ /kJ·mol^{-1}	*p* / Pa
Bathophenanthroline	183.8 ± 2.8	255.0 ± 6.2	107.8 ± 3.1	3.49 x 10^{-10}

4.1.4.2. Knudsen Effusion Mass Spectrometry

In table 4.9, the experimentally obtained and treated results for bathophenanthroline using the KEMS method are recorded. It is important to note, however, that the apparatus used for this study has a significant limitation when it comes to studying organic samples like the one under discussion. Its original design is intended for high temperature chemistry, and therefore, it takes a long time to stabilize at low temperatures. Consequently, it is practically impossible to collect a significant number of experimental points in a single experiment. This limitation accounts for the small number of experimental points and the relatively large experimental error. Nevertheless, it is worth highlighting the remarkable sensitivity of this method, which boasts a much smaller detection limit and enables experiments at much lower temperatures compared to other vapour pressure techniques.

The KEMS results include the temperature and accompanying vapour pressures along with the calculated 1/*T* and ln *p*. The latter values are used in a graphical representation of the Clausius-Clapeyron slope from which parameters *a* and *b* can be obtained (figure 4.18). As described in chapter three, from these values it is possible to calculate the vapour pressure at the mean temperature, *p*(<*T*>), the enthalpy of sublimation at mean temperature, $\Delta_{cr}^{g}H_m^{\circ}$ (<*T*>), and the entropy of sublimation at mean temperature, $\Delta_{cr}^{g}S_m^{\circ}$ (<*T*>). These parameters are in table 4.10.

Considering the thermodynamic parameters obtained at the average temperature, it is possible to adjust the values to the reference temperature of 298.15 K, $\Delta_{cr}^{g}H_m^{\circ}$, $\Delta_{cr}^{g}S_m^{\circ}$. These latter parameters can be used to calculate the Gibbs free energy of the

sublimation process at 298.15 K, $\Delta_{cr}^{g} G_{m}^{\circ}$. The plot described earlier can also be used to extrapolate the vapour pressure at the reference temperature. These parameters are presented in table 4.11, along with the appearance potential of our sample, which was corrected by measuring the appearance potential of water, a known constant. This correction is also represented in figure 4.19.

The instrumental constant was determined by measuring the vapour pressure values of triphenylbenzene and comparing them with values from literature. As explained in section 3.1.5, this comparison is necessary due to the changing experimental conditions of Knudsen effusion mass spectrometry from one experiment to another. The resulting values are presented in table 4.12.

Table 4.9 - Experimental and treated results obtained for bathophenanthroline through the KEMS method.

Essay 1			
***T* (K)**	***p* (Pa)***	**1/*T* (K^{-1})**	**ln (*p*/Pa)**
353	1.08E-06	0.0028	-13.7
362	4.16E-06	0.0028	-12.4
369	1.36E-05	0.0027	-11.2
378	5.15E-05	0.0026	-9.87
$\langle T \rangle$= 365			
Essay 2			
***T* (K)**	***p* (Pa)***	**1/*T* (K^{-1})**	**ln (*p*/Pa)**
346	6.30E-07	0.0029	-14.3
354	2.30E-06	0.0028	-13.0
362	1.08E-05	0.0028	-11.4
371	3.54E-05	0.0027	-10.3
$\langle T \rangle$= 358			

*Obtained with an instrumental constant from 1,3,5-triphenylbenzene; sigma (bathophenanthroline) = 3*sigma (benzene) + 2 sigma (pyridine) ≅5*sigma (benzene) = 75

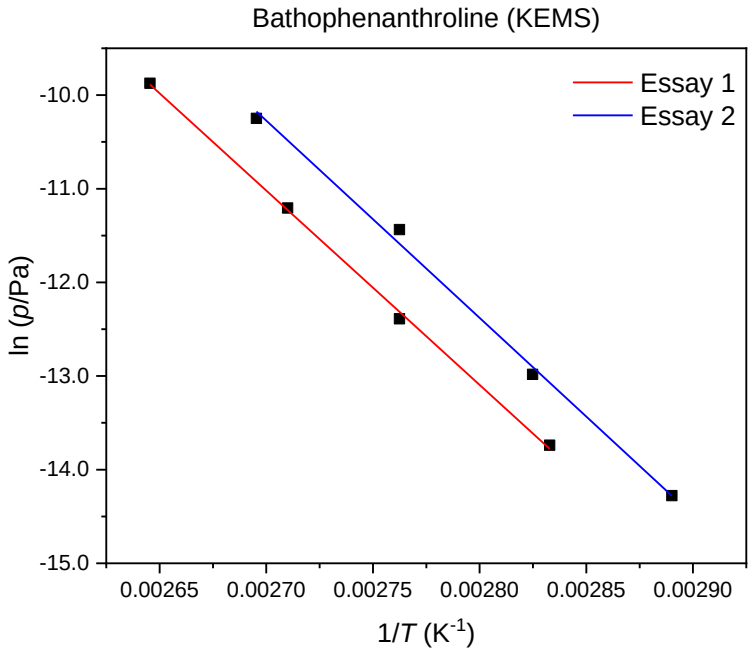

Figure 4.18 - Graphical representation of ln *p* vs 1/*T* obtained through the Knudsen effusion mass spectrometry method for bathophenanthroline.

Table 4.10 - Clausius-Clapeyron equations parameters obtained for bathophenanthroline with KEMS at the mean temperature.

KEMS	a	b	R^2	p(<*T*>)	$\Delta_{cr}^{g}H_m^{\circ}$ (<*T*>)	$\Delta_{cr}^{g}S_m^{\circ}$ (<*T*>)
				Pa	kJ·mol^{-1}	J·K^{-1}·mol^{-1}
Essay 1	45.04±1.24	-20762±453	0.9991	5.45 x 10^{-6}	172.6 ± 3.8	472.2 ± 10.3
Essay 2	46.60±2.55	-21064±911	0.9963	1.74 x 10^{-6}	175.1 ± 7.57	488.9 ± 21.1

Table 4.11 - Standard molar enthalpy, entropy and Gibbs free energy and vapour pressure at the temperature of 298.15 K along with the appearance potential for bathophenanthroline obtained with the KEMS method.

Essay	$\Delta_{cr}^{g}H_m^{\circ}$ /kJ·mol^{-1}	$\Delta_{cr}^{g}S_m^{\circ}$ /J·K^{-1}·mol^{-1}	$\Delta_{cr}^{g}G_m^{\circ}$ /kJ·mol^{-1}	*p* / Pa	AE_0 /eV
1	176.5 ± 3.8	387.6 ± 10.3	60.9 ± 2.1	5.08 x 10^{-11}	-
2	178.6 ± 7.6	416.8 ± 21.1	54.3 ± 3.6	8.50 x 10^{-11}	-
Mean	176.9 ± 3.4	393.2 ± 9.3	59.3 ± 1.8	6.79 x 10^{-11}	8.1

Table 4.12 - Instrumental constant values obtained with 1,3,5-triphenylbenzene.

T (K)	*p* (bar)*	$K_{instrum}$
372	2.87e-8	0.0089
354	2.57e-9	0.0124
345	7.07e-10	0.0106

*Values from Verevkin et al. JCT (1997) 29, 1495.

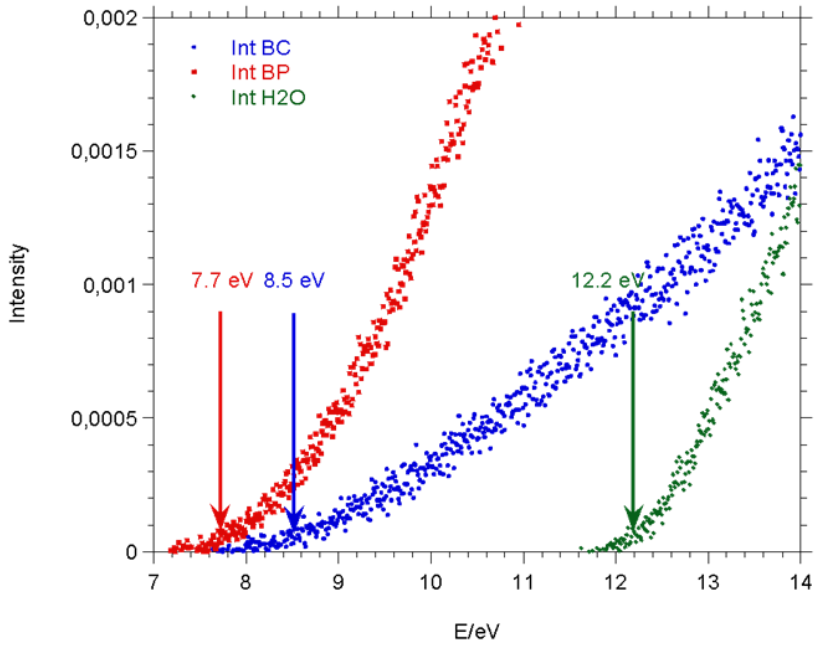

Figure 4.19 - Ionization intensity measurements for the determination of the appearance potential of bathophenanthroline.

During Knudsen effusion mass spectrometry experiments, the only significant experimental mass spectrometry signals detected are the ones corresponding to the mass of bathophenanthroline and its isotopes. So, it is possible to surmise that no decomposition occurs, only sublimation. Although, a change in the volume of the sample, similar to the sintering effect was observed. X-ray crystallography and FTIR experiments were conducted to ascertain if any changes occurred. The results are presented in figure 4.20 and 4.21, respectively. These indicate that no change occurred, only a decrease in the volume of the sample.

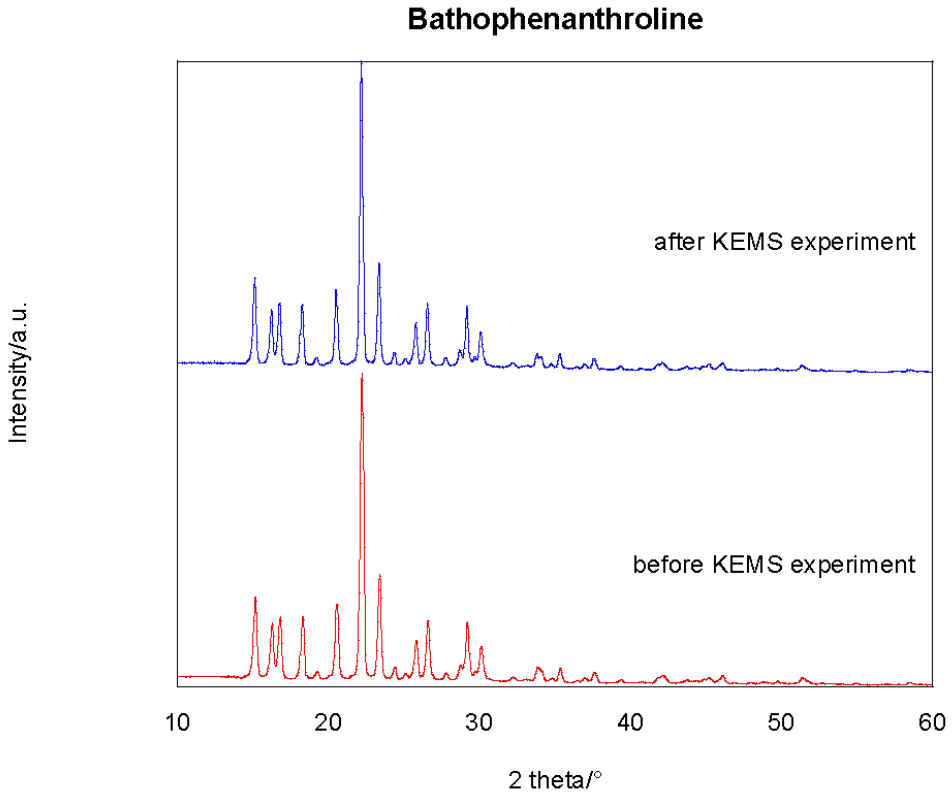

Figure 4.20 - XRD spectra of bathophenanthroline before and after a KEMS experiment.

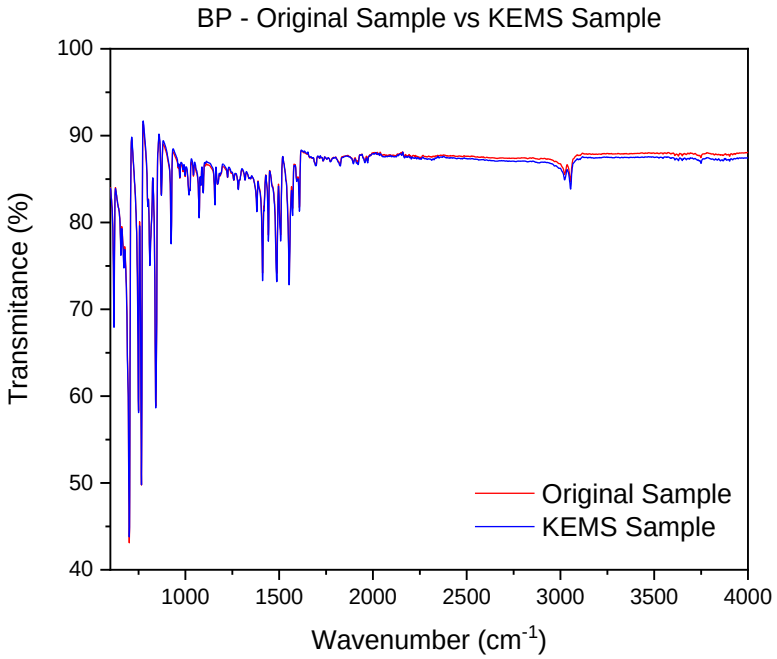

Figure 4.21 - FTIR spectra of a bathophenanthroline sample from before and after a KEMS experiment.

4.1.5. Quartz Crystal Microgravimetry

Bathophenanthroline was also submitted to vapour pressure analysis with the quartz crystal microgravimetric technique described on section 3.2. This technique uses a different approach to the study of sublimation/vaporization. Here, non-equilibrium conditions are used as such, only the enthalpy change can be determined.

In this section the raw and treated results are presented. The values for d*f*/d*t*, *T*, 1/*T*, and ln Q are registered in table 4.13. In figure 4.22 we have a graphical representation of the ln Q vs 1/*T* plot. As described in chapter three, from these values it is possible to calculate the enthalpy of sublimation at mean temperature, $\Delta_{cr}^{g}H_{m}^{\circ}$ (<*T*>) (table 4.14), and from that the enthalpy of sublimation at the reference temperature of 298.15 K, $\Delta_{cr}^{g}H_{m}^{\circ}$. Only the values from the second and third essays were considered as the first essay has a very significant experimental error. This sustains the decision not to use it when calculating the final mean value (table 4.15).

The initial results obtained with this technique were significantly different from those obtained with the other vapour pressure techniques. This spurred the need of doing experiments with a test sample of a similar vapour pressure to that of studied compound. The results from the tests with 1,3,5-triphenylbenzene are registered in table 4.16 and presented in figure 4.23. A significant deviation from the literature value of $\Delta_{cr}^{g}H_{m}^{\circ}$ 1,3,5-triphenylbenzene indicates that some factors may not be considered when calculating the enthalpy of sublimation value of our samples or that some experimental systematic errors are being introduced. So, to correct the slope obtained a correction constant was by measuring the d*f*/d*t* values of 1,3,5-triphenylbenzene, calculating the obtained sublimation enthalpy and comparing it with the value from literature (tables 4.17 and 4.18). The obtained instrumental constant can be used to correct the ln Q vs 1/*T* slope of the sample. These experiments should be done with a similar *T* program, but TPB is too volatile to do so under the conditions used by this technique.

As the device is not capable of directly measuring vapour pressures, it is not possible to say with full certainty what factors are affecting the results. However, it is possible to speculate. A common error in this type of measurement is deviations in temperature control. If there is a deviation, it could be due to incorrect values of temperature being recorded, and this needs to be addressed by recalibrating the temperature sensor.

Another possible factor is also a background shift, i.e., the frequency shift caused by condensation of non-sample compounds that remain in the vacuum chamber or by a normal shift in the resonant frequency of the crystal. Although previous experiments during the assembly of the QCM device indicate that the temperature of the quartz crystal remains the same, it is entirely possible that the heat that radiates from the molecular source at high temperatures can affect the frequency shift of the sensor. This can be overcome with an internal temperature control. For instance, a water flow that maintains the quartz crystal temperature stable. Experiments with empty crucibles and with the same temperature program are recommended. The value of the background shift can be removed from the experimentally obtained value for the sample like such $\frac{df}{dT}_{corr} = \frac{df}{dT} - \frac{df}{dT}_{blank}$. Future experiments should consider this correction factor.

Table 4.13 - Experimentally and treated results obtained for bathophenanthroline with the QCM method.

Essay 1			
d*f*/d*t*	***T* (K)**	**1/*T* (K^{-1})**	**ln *Q***
0.1000	453	0.00221	0.755
0.0539	448	0.00223	0.131
0.0316	443	0.00226	-0.406
0.0223	438	0.00228	-0.761
0.0148	433	0.00231	-1.179
Essay 2			
d*f*/d*t*	***T* (K)**	**1/*T* (K^{-1})**	**ln *Q***
0.1582	463	0.00216	1.225
0.0954	458	0.00218	0.714
0.0607	453	0.00221	0.257
0.0388	448	0.00223	-0.197
0.0251	443	0.00226	-0.637
0.0165	438	0.00228	-1.063
Essay 3			
d*f*/d*t*	***T* (K)**	**1/*T* (K^{-1})**	**ln *Q***
0.0833	461	0.00217	0.582
0.0579	457	0.00219	0.213
0.0383	453	0.00221	-0.205
0.0291	449	0.00223	-0.483
0.0201	445	0.00225	-0.858

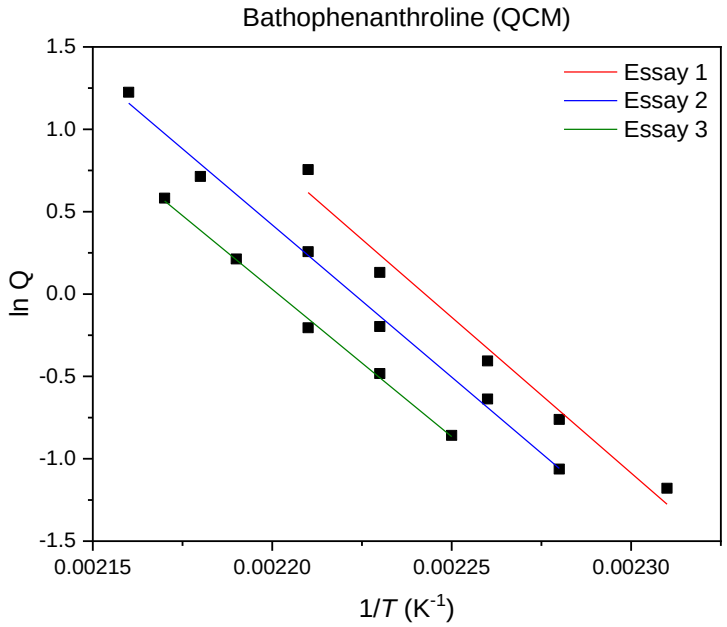

Figure 4.22 - Graphical representation of ln Q vs 1/*T* obtained through the QCM method for bathophenanthroline.

Table 4.14 - Clausius-Clapeyron equations parameters obtained for bathophenanthroline with the QCM method at the mean temperature.

Bathophenanthroline	**<T> /K**	**m**	**R^2**	**$\Delta_{cr}^{g}H_{m}^{\circ}$ (<*T*>)**
				kJ·mol^{-1}
Essay 1	443	-18717 ± 1314	0.9854	155.6 ± 10.9
Essay 2	450	-18286 ± 358	0.9985	152.0 ± 3.0
Essay 3	453	-18477 ± 708	0.9956	153.6 ± 5.9

Table 4.15 - Standard molar enthalpy at the mean temperature and at the temperature of 298.15 K before and after correction for bathophenanthroline obtained with the QCM method.

Essay	**$\Delta_{cr}^{g}H_{m}^{\circ}$ (<*T*>)**	**$\Delta_{cr}^{g}H_{m}^{\circ}$ (*T* = 298.15 K)**	**$\Delta_{cr}^{g}H_{m}^{\circ}(T = 298.15\ K)_{corr}$ ***
	kJ·mol^{-1}	**kJ·mol^{-1}**	**kJ·mol^{-1}**
Essay 1	155.6 ± 10.9	163.9 ± 10.9	185.6 ± 10.9
Essay 2	152.0 ± 3.0	160.7 ± 3.0	182.0 ± 3.0
Essay 3	153.6 ± 5.9	162.5 ± 5.9	184.0 ± 5.9
Mean of Essay 2 and 3	-	161.6 ± 2.7	182.4 ± 2.7

*Obtained with an instrumental constant from triphenylbenzene.

Table 4.16 - Experimentally and treated results obtained for 1,3,5-triphenylbenzene with the QCM method.

Essay 1			
d*f*/d*t*	***T* (K)**	**1/*T* (K^{-1})**	**ln *Q***
0.2296	423	0.00236	1.552
0.1518	418	0.00239	1.133
0.0996	413	0.00242	0.705
0.0632	408	0.00245	0.244
0.0421	403	0.00248	-0.168
Essay 2			
d*f*/d*t*	***T* (K)**	**1/*T* (K^{-1})**	**ln *Q***
0.0406	403	0.00248	-0.205
0.0613	408	0.00245	0.215
0.0919	413	0.00242	0.625
0.1399	418	0.00239	1.051
0.2246	423	0.00236	1.530
0.3571	428	0.00234	2.000

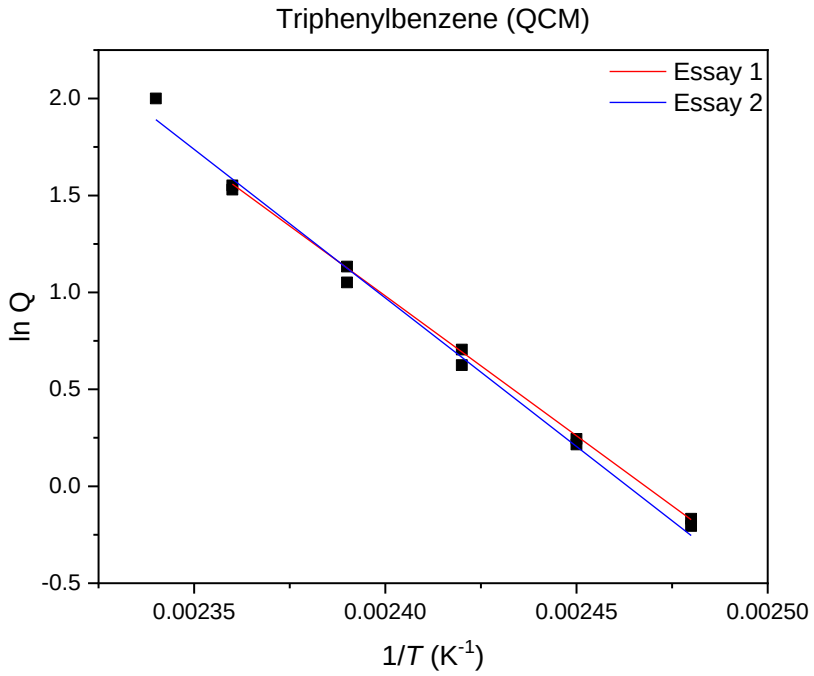

Figure 4.23 - Graphical representation of ln Q vs 1/*T* obtained through the QCM method for 1,3,5-triphenylbenzene.

Table 4.17 - Clausius-Clapeyron equations parameters obtained for 1,3,5-triphenylbenzene with the QCM method at the mean temperature and at 298.15 K.

Triphenylbenzene	<*T*> / K	m	R^2	$\Delta_{cr}^{g}H_m^{\circ}$ (<*T*>) / kJ·mol^{-1}	$\Delta_{cr}^{g}H_m^{\circ}$ (*T* = 298.15 K) / kJ·mol^{-1}
Essay 1	413	-14830 ± 187	0.9995	123.3	129.6
Essay 2	416	-15329 ± 368	0.9977	127.5	133.9
Mean	-	-	-	-	131.8

Table 4.18 – Obtained and Literature Standard molar enthalpy of sublimation at the temperature of 298.15 K triphenylbenzene.

Triphenylbenzene	$\Delta_{cr}^{g}H_m^{\circ}$ (*T* = 298.15 K) / kJ·mol^{-1}	$\Delta_{cr}^{g}H_m^{\circ}$ (*T* = 298.15 K) Lit / kJ·mol^{-1}	$K_{instrum}$
Mean	131.8	149.2	1.1323

*Thermochimica Acta 331 (1999) 93-204 (pg 158)

4.1.6. Isothermal Thermogravimetry

Bathophenanthroline was also submitted to vapour pressure analysis with isothermal thermogravimetry aiming at determining its heat of vaporization. In this section the experimentally obtained and treated results are presented.

The values for d*m*/d*t*, *T*, 1/*T*, and ln Q are registered in table 4.19 and in figure 4.24 a graphical representation of ln Q vs 1/*T*. As described in chapter three, from this plot it is possible to only determine the enthalpy of vaporization at mean temperature, $\Delta_{l}^{g}H_m^{\circ}$ (<*T*>) as it is done under non-equilibrium conditions. It is possible to adjust the enthalpy of vaporization to the reference temperature of 298.15 K, $\Delta_{l}^{g}H_m^{\circ}$. These are registered in table 4.20.

Table 4.19 - Experimentally and treated results obtained for bathophenanthroline with the I-TG method.

d*m*/d*t*	*T* (K)	1/*T* (K^{-1})	ln *Q*
7.08E-11	519.15	0.00193	-12.31
9.94E-11	524.15	0.00191	-11.96
1.24E-10	530.15	0.00189	-11.74
1.66E-10	535.15	0.00187	-11.44
2.26E-10	541.15	0.00185	-11.12
2.76E-10	547.15	0.00183	-10.92
3.33E-10	552.15	0.00181	-10.73

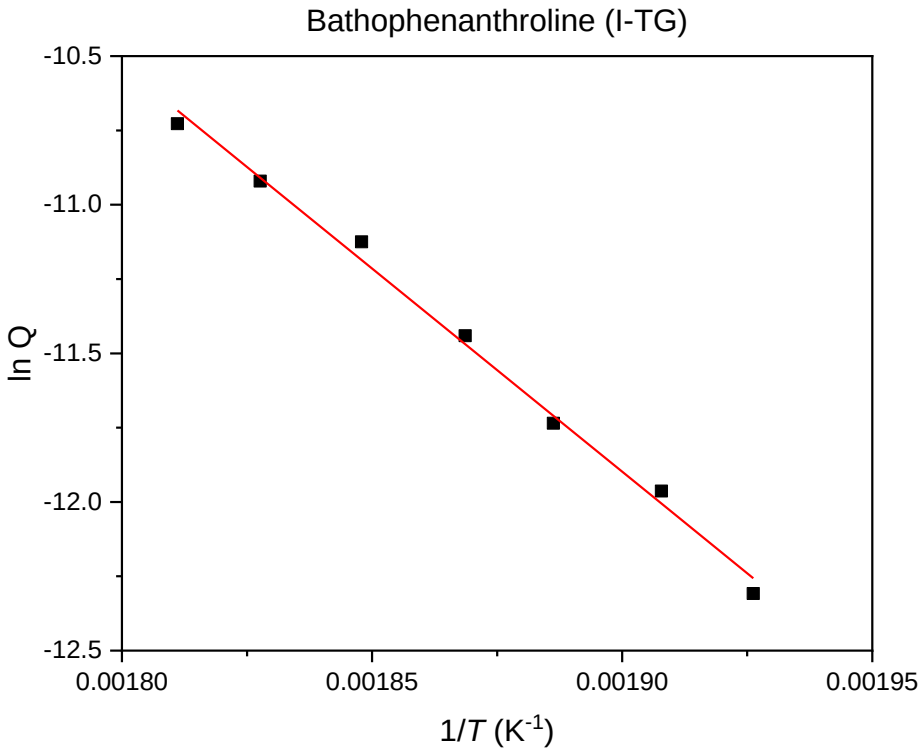

Figure 4.24 - Graphical representation of ln Q vs 1/*T* obtained through the QCM method for bathophenanthroline.

Table 4.20 - Clausius-Clapeyron equations parameters obtained for bathophenanthroline with the I-TG method at the mean temperature and at 298.15 K.

<*T*> / **K**	**m**	**R^2**	**$\Delta_l^g H_m^\circ$ (<*T*>)** / **kJ·mol^{-1}**	**$\Delta_l^g H_m^\circ$ (*T* = 298.15 K)** / **kJ·mol^{-1}**
544	-13668 ± 471	0.9941	113.6 ± 3.9	149.1 ± 3.9

As a way of verifying the obtained value, it is possible to use the heat of fusion and heat of sublimation values to calculate the heat of vaporization at 298.15 K. By subtracting one value to the other, $\Delta_l^g H_m^\circ = \Delta_{cr}^g H_m^\circ - \Delta_{cr}^l H_m^\circ$, a value of (153.4 ± 1.9) kJ·mol^{-1} is obtained. It is evident from this calculation that there is an agreement due to an overlap of their experimental errors. Several experimental factors can influence the determination of these parameters including temperature control, the sensitivity of the balance, and atmosphere control, all of which are crucial.

The apparatus used for this study has a high thermal inertia. This means that when heating a sample, it tends to overshoot the programmed temperature and it has some difficulties in maintaining the temperature stable. These reasons greatly affect the determination of temperature which directly affects 1/*T*. A lower heating rate is always

recommended. The sensitivity of scale also affects the results of these experiments as this device is not designed with this thermogravimetric purpose in mind. Larger isothermal times are recommended as a way to overcome the issue of the sensitivity of the mass detector. But one needs also to consider the limits of the sample loaded into the crucible.

These factors and perhaps others that remain unknown, dictate the necessity of introducing an instrumental constant to correct the obtained ln Q vs $1/T$ slope. This constant needs to be obtained by performing calibration experiments with test samples and comparing the obtained value with one found in literature. Time limitations and the lack of an appropriate test sample are the reasons why this effort was not undertaken.

4.2. Bathocuproine

The results pertaining to bathocuproine (figure 4.25) are presented and further discussed under this section.

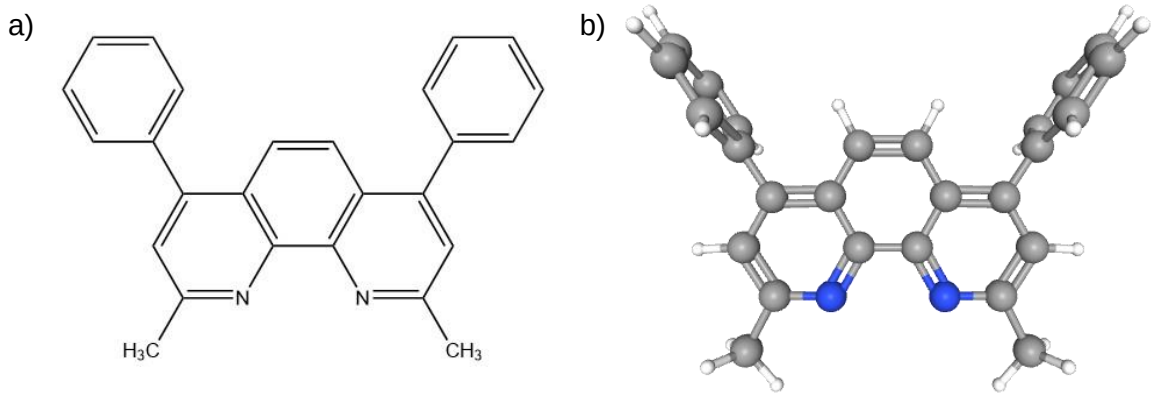

Figure 4.25 - a) Structural formula of bathocuproine. b) 3D representation of bathocuproine.

As explored in this first chapter, this molecule has several applications in the field of organic semiconductor devices particularly as a hole blocking material. To the best of my knowledge, there is no thermophysical information regarding this molecule in literature and as such, this work aims at providing a complete thermophysical characterization.

4.2.1. Sample Details: Source and Characterization

This section aims to present the characterization and, when appropriate, further treatment of the commercially obtained samples of bathocuproine. In table 4.21, it is possible to find details about the sample, its source, and the results purity and water content analysis.

Table 4.21 - Purification and source details of bathocuproine.

Compound	Bathocuproine	
[IUPAC name]	[2,9-dimethyl-4,7-diphenyl-1,10-phenanthroline]	
[CAS RN]	[4733-39-5]	
Molecular Formula	$C_{26}H_{20}N_2$	
Molecular Weight	360.4 $g.mol^{-1}$	
Source/Batch	Acros Organics	ThermoFisher Scientific
	1	2
Initial purity[a]	0.986	0.976
Appearance	Cream powder	Pale brown powder
Actual purity[b]	0.9978	0.9993
Purification method	Sublimation	-
Final mass fraction purity	-	-
Analysis method	GC-FID	GC-FID
% H_2O[c]	0.0675	-

[a]According to the analysis certificate of the supplier.

[b]Obtained from Gas chromatography (GC) analysis (with FID);

[c]Determined via Karl-Fischer Titration.

Gas-chromatography analysis revealed that the purity of the first sample was sufficient for the thermophysical studies conducted in this work. Still, the purification process resulted in a significant colour change from cream to a bright orange. The GC analysis indicated possible decomposition, as evidenced by a decrease in the purity of the sample.

To clear the questions raised beforehand, FTIR analysis was used to see if any chemical or physical change occurs. In figure 4.26, it is possible to see the complete FTIR spectrum of bathocuproine from the original sample and compare it with the sample purified by sublimation and in figure 4.27 the zoomed fingerprint region. The FTIR measurements were conducted on a PerkinElmer Spectrum Two (ATR module) with four scans per spectrum and data was analysed using the PerkinElmer software Spectrum. Sample FTIR analysis was conducted at FCUP|DQB Lab& Services.

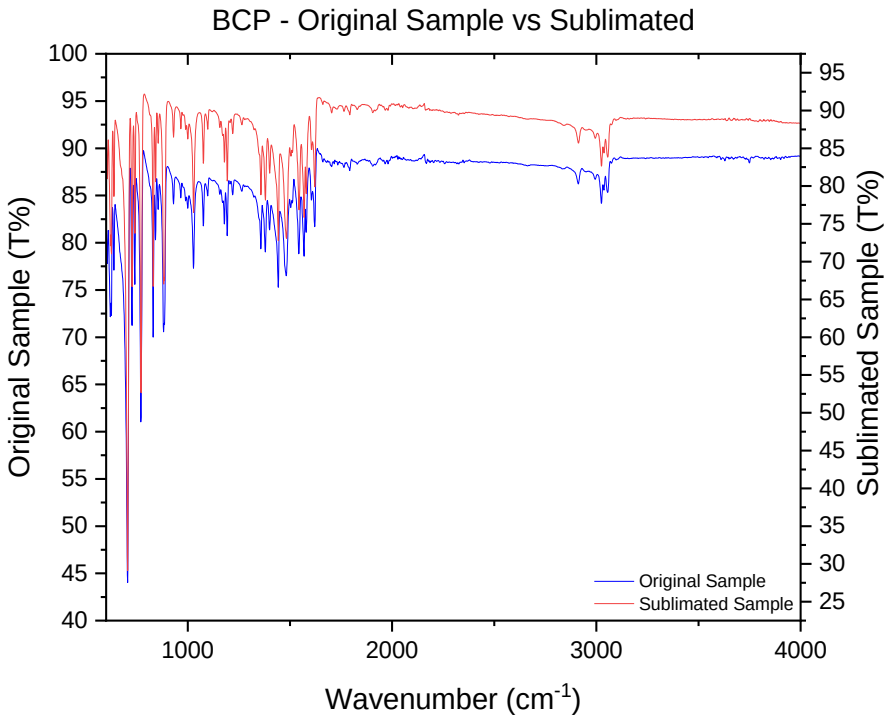

Figure 4.26 - Bathocuproine FTIR spectra. Original Sample versus Sublimated sample.

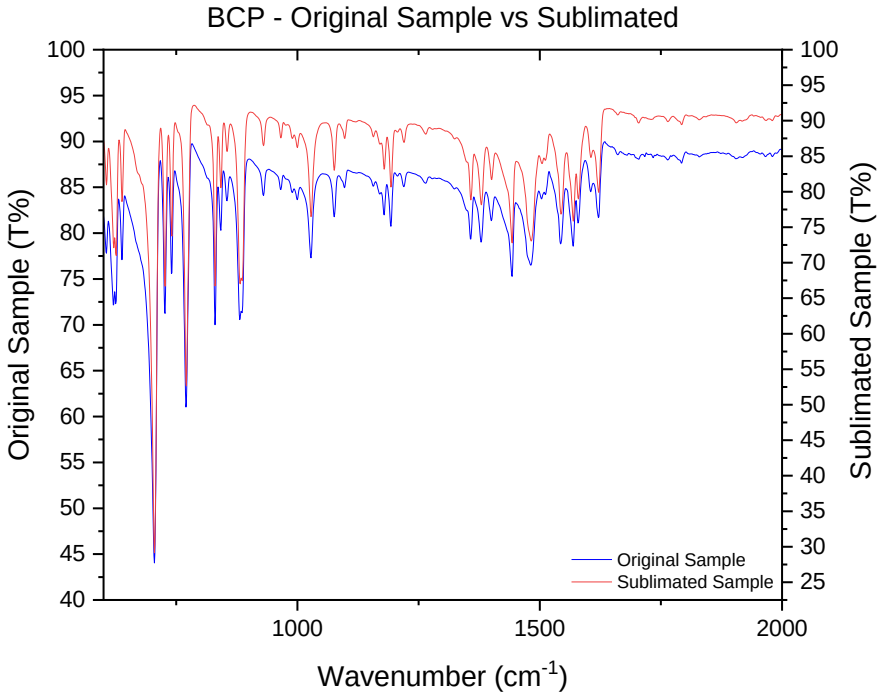

Figure 4.27 - Bathocuproine FTIR spectra. Original Sample versus Sublimated sample. (Fingerprint region)

As can be observed, no significant differences are found in the spectra. This suggests that a possible polymorph might have formed due to high temperatures, or decomposition occurred resulting in the formation of a chemically similar sample with identical vibrational frequencies. Further discussion on this topic will be presented in the DSC, TG and KEM subsections of this chapter.

The second batch exhibited a higher purity level (≤0.9990) than required for all studies, making it the recommended choice. However, when the first DSC measurements of the sample were conducted, it became apparent that the signal was not as clear as the less pure batch, indicating a potential metallic contamination as suggested by NMR analysis. To confirm this, further ICP-MS analysis is recommended, especially since atomic absorption spectroscopy did not detect any metals.

Despite the lower purity, the first sample was used for thermophysical analysis. Karl-Fischer analysis also indicated that a small amount of water is present and that it is not hygroscopic in nature.

4.2.2. Thermal Analysis

The present section presents and discusses the experimental results from DSC and TG analysis conducted on the previously mentioned sample. Various scans were conducted under different conditions, including different scanning rates and temperature programmes, which will be specified for each case.

An initial 10 $K \cdot min^{-1}$ scan was conducted on the original sample to determine if any solid-solid transitions are present as different crystalline states have different thermophysical and thermochemical properties. In figure 4.28 we can find the DSC curve that refers to that scan. As it is possible to observe, only one process is identified. A single and sharp endothermic peak that can be ascribed to fusion is shown.

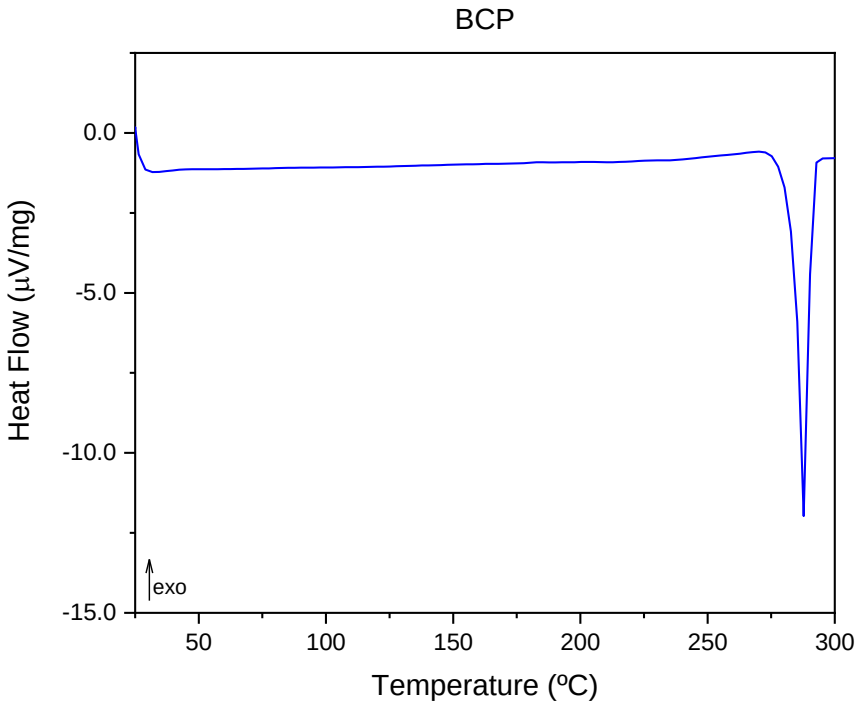

Figure 4.28 – DSC curve of a 10K·min-1 scan of the original bathocuproine sample. Analysis conducted with a hermetically sealed aluminium crucible under a constant nitrogen flow.

From this scan, a single fusion event was identified. The shape of the peak indicates that fusion happens in one single quick step for the only crystalline form that can be identified. As there only is a single fusion event, experiments to determine the temperature and heat of fusion can be easily carried out. However, note that a small exothermic increase in the heat flow signal occurs just before fusion. This means that the sample may start to undergo thermal decomposition.

4.2.2.1. Heat and Temperature of Fusion

The essays to determine the heat and temperature of fusion were conducted in the [533.15 – 573.15] K interval at a 2 $K \cdot min^{-1}$ heating rate. In addition, a hermetically sealed aluminium crucible was used under a N_2 flow. From four different essays with fresh samples a value of (554.83 ± 0.74) K was obtained for the temperature of fusion and a value of (40.5 ± 1.6) $kJ \cdot mol^{-1}$ for the standard molar enthalpy of fusion at the fusion temperature.

Table 4.22 - Experimentally obtained values for the temperature and heat of fusion of bathocuproine.

Essay	Bathocuproine	
	T_{fusion} (K)	$\Delta_{cr}^{l}H_{m}^{\circ}$ <T_{fusion}> (kJ·mol^{-1})
1	554.52	40.46
2	555.01	39.84
3	555.01	40.60
4	554.79	41.02
Average Values	⟨554.83 ± 0.74⟩	⟨40.5 ± 1.6⟩
$\Delta_{cr}^{l}H_{m}^{\circ}$ (298.15 K) (kJ·mol^{-1})	26.5 ± 1.6	

In figure 4.29 is possible to see the peak of fusion. As said before, it is a single however elongated endothermic peak which indicates the presence of a single crystalline form. The elongated nature may indicate that another process may be occurring simultaneously. This process seems to be decomposition.

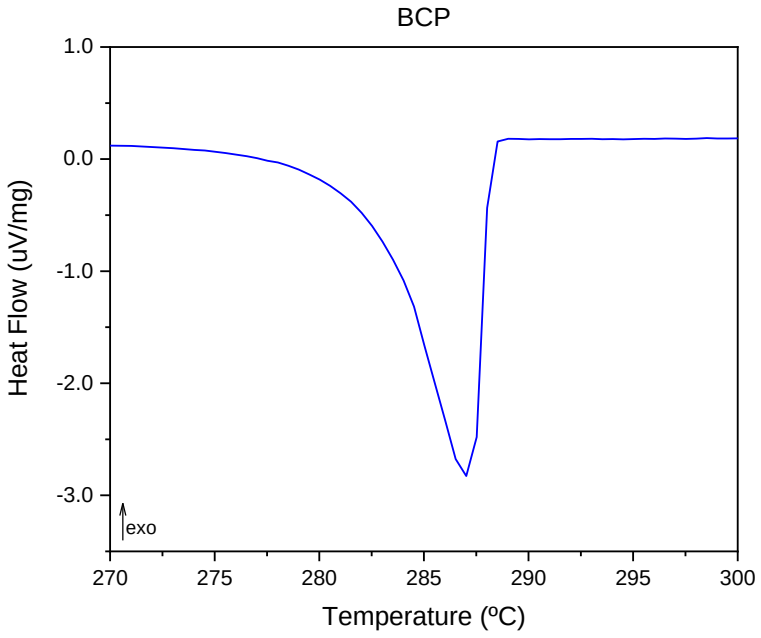

Figure 4.29 - DSC curve of the fusion process of bathocuproine.

4.2.2.2. Thermal Behaviour Analysis

Additional scans were conducted with the purpose of ascertaining if any other thermophysical processes occurred in the liquid and solid phases.

A scan with a rate of 10 $K \cdot min^{-1}$ was performed between [573.15 - 213.15] K and subsequently between [213.15 – 573.15] K. Unlike bathophenanthroline, bathocuproine does not exhibit any unusual thermophysical events. Only a single crystallization event is observed, as shown in its DSC curve in figure 4.30.

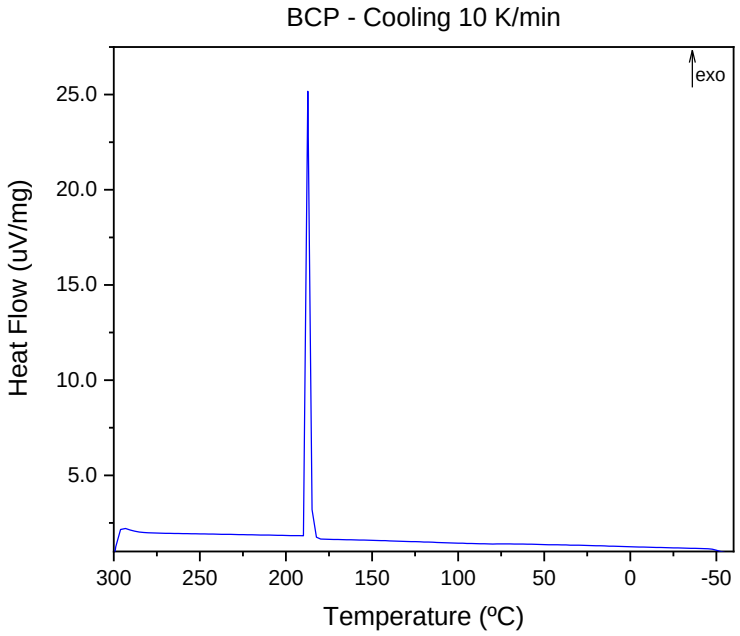

Figure 4.30 - DSC curve of the thermal behaviour analysis of bathocuproine. Cooling section. Hermetically sealed Al crucible under N_2 flow.

Further analysis also indicates that no significant changes occur in the size, onset, and shape of the fusion peak between different cycles of the previously detailed experiment, as shown in its DSC curve in figure 4.31.

Additional analysis was also done to see if any changes happened in the DSC curve after the sample underwent purification through high-temperature sublimation. As observed in figure 4.32, there is no change in the onset point of the fusion process. However, a change in the peak suggests that some chemical change may have occurred in the sample.

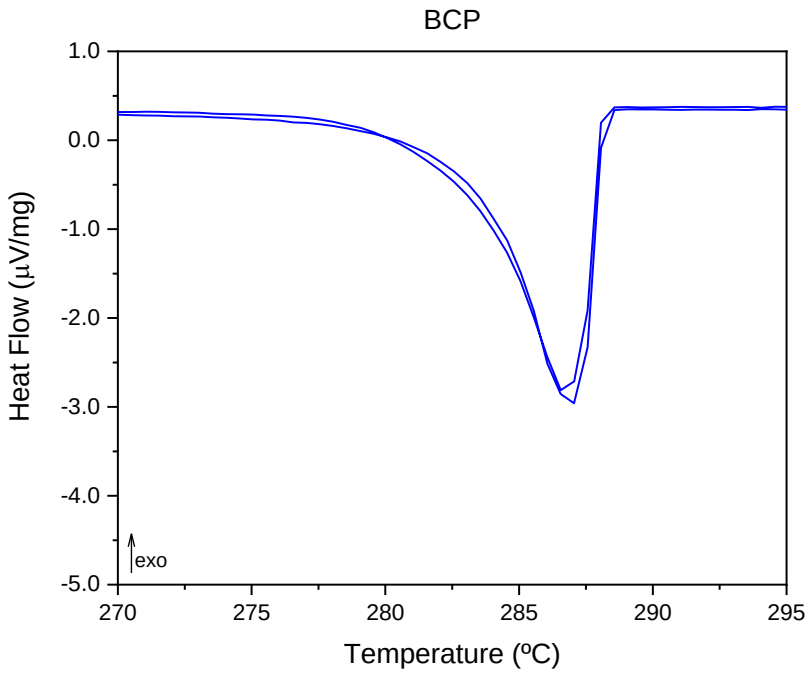

Figure 4.31 - DSC curve of the fusion process of bathocuproine between two heating and cooling cycles.

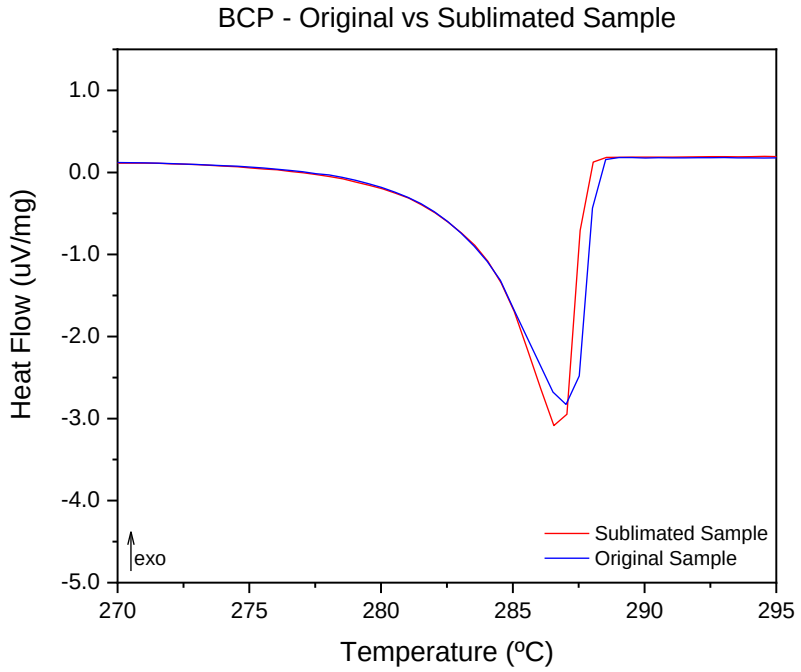

Figure 4.32 - DSC curve of the fusion process of bathocuproine. Original vs sublimated sample.

4.2.2.3. Simultaneous Thermal Analysis

Simultaneous heat flow and mass measurements were undertaken to ascertain the thermal behaviour of bathophenanthroline under open crucible and synthetic air (an 80/20 nitrogen/oxygen mixture). These conditions are more approximate to real conditions. The device described in chapter three covers a temperature range from [RT – 873.15] K, figure 4.33 displays a full thermogram within the available range.

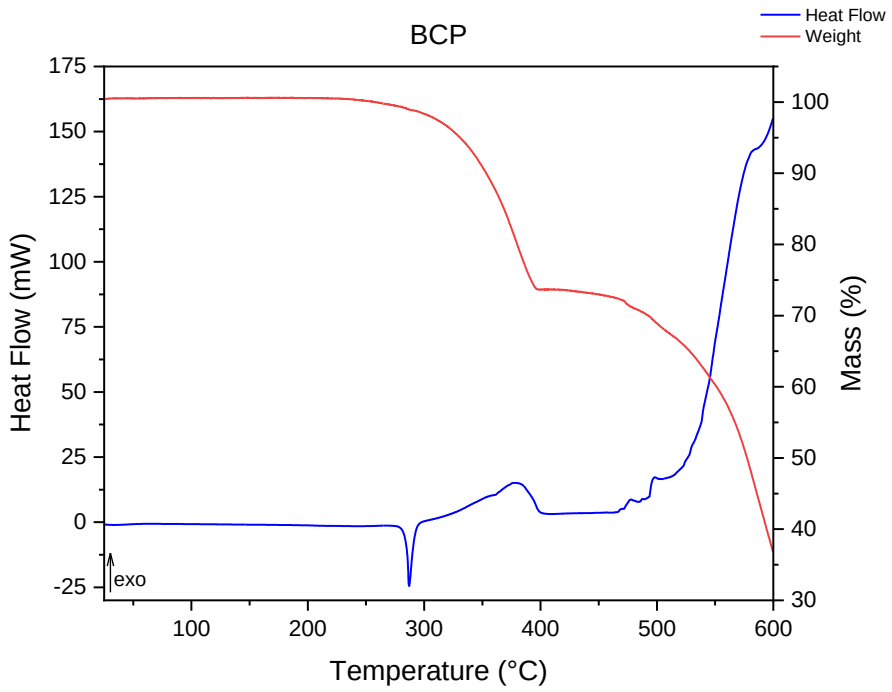

Figure 4.33 – DSC and TG curves of bathocuproine under open crucible and synthetic air conditions. [RT - 873.15] K range.

Before fusion, a decrease in the heat flow and sample mass signals is observed. This could either be to the presence of water on the sample, circa 1 %. However, Karl-Fischer titration experiments indicate that the amount of water present is much less than that (≈ 0.063 %). This suggests that decomposition may be occurring on our sample. This hypothesis is further supported by the fact that a constant mass loss and increase in the heat flow signal are observed during fusion. This is shown in figure 4.34.

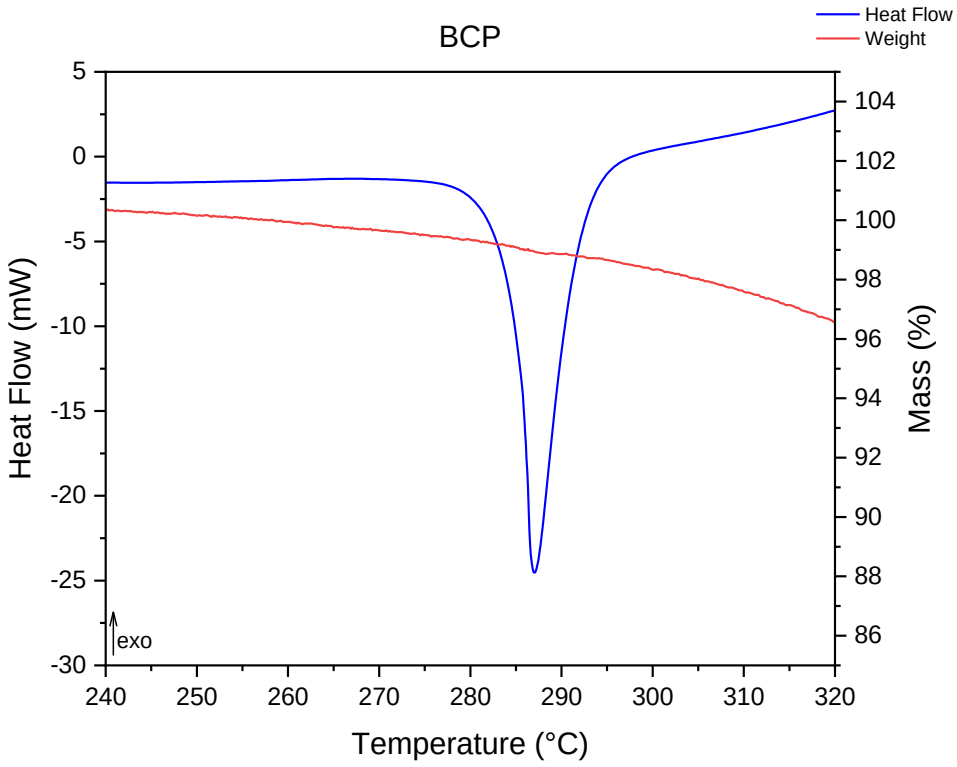

Figure 4.34 – DSC and TG curves of bathocuproine under open crucible and synthetic air conditions. Just before and after fusion.

After fusion, a constant increase in the heat flow of the sample is observed accompanied with an approximate mass loss of 26 %. The heat flow change is characteristic for the continuous decomposition of the sample. The mass change is approximately equivalent to the loss of a phenyl group and a methyl group. The decrease in the signal is constant until it reaches a minimum. This is indicative of the formation of an intermediate. Their possible molecular structures are shown in figure 4.35. Further experiments with TG-MS or TG-FTIR could elucidate the chemical nature of the intermediary state.

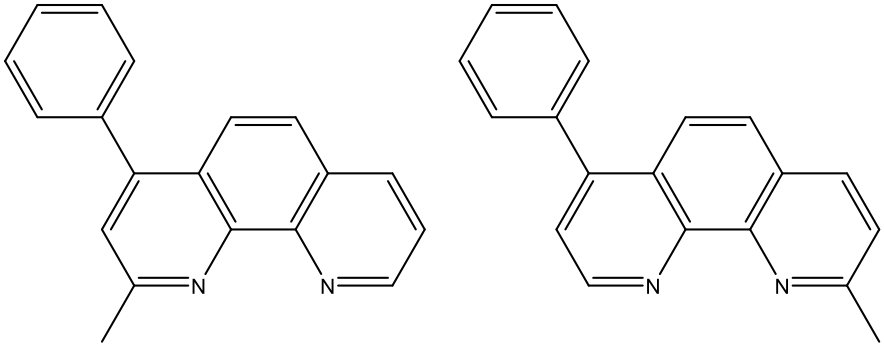

Figure 4.35 - Possible molecular structure of the intermediate molecules formed after thermal decomposition.

After 743 K, several decomposition steps are observed: First two small steps followed by a massive exothermic signal. The proximity of these events makes their distinction difficult. The experiments ends with an exothermic signal that cannot be fully accounted for as the device has reached its maximum working temperature. This is detailed in figure 4.36. Complete mass loss was not achieved, but if higher temperatures were attained, a zero-mass percentage could be reached, or carbon residues would remain.

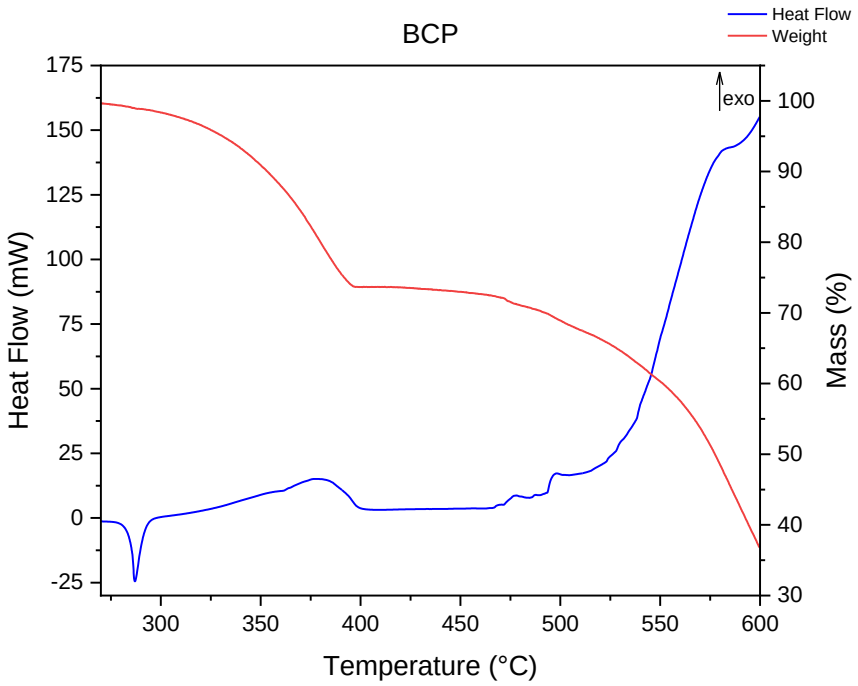

Figure 4.36 – DSC and TG curves of bathocuproine under open crucible and synthetic air conditions. [448.15 - 873.15] K range.

This experiment was repeated several times, and the observed behaviour is reproducible. Note that the instability of the sample after fusion rules out the possibility of conducting vapour pressure measurements to determine enthalpy of vaporization, as was done for bathophenanthroline.

4.2.3. Vacuum Drop-Microcalorimetry

The discussed sample was submitted to direct sublimation analysis using Calvet microcalorimetry. Tests with the sample indicated that the programmed working temperature of the device should be 533.15 K. The experimentally obtained results, along with further corrections for instrumental constant, are registered in table 4.23, along with the final result from the mean of six independent essays.

Table 4.23 - Experimentally obtained results on the sublimation study of bathocuproine with the vacuum drop-microcalorimetry technique.

Bathocuproine	**1**	**2**	**3**	**4**	**5**	**6**	**7**
***T*/ K**	541.08	541.12	541.11	541.13	541.02	541.02	541.12
T_{amb}/ K	298.35	298.15	298.15	298.35	298.35	298.15	298.05
$m_{samplecap}$/ mg	23.9413	22.3607	22.5444	21.5358	21.7837	24.2976	24.9127
m_{ref}/ mg	23.9004	22.3296	22.5668	21.5715	21.7284	24.1926	24.9887
m_{sample}/ mg	4.148	4.088	3.475	3.092	3.617	3.777	3.971
ΔH_{corr}(blanks)/ mJ	42.225	49.191	57.567	63.155	47.027	30.271	58.654
$\Delta H_{observed}$/ J	3.120	3.044	2.568	2.262	2.688	2.866	2.994
$\Delta H_{corrected}$/ J	3.162	3.093	2.626	2.325	2.735	2.897	3.053
$\Delta^{g,T}_{cr,298.15}H^{\circ}_{m}$ /kJ·mol^{-1}	295.9	293.6	293.2	291.9	293.4	297.6	298.4
$\Delta^{T}_{298.15}H^{\circ}_{m}$ /kJ·mol^{-1}	87.9	87.9	87.9	87.9	87.9	87.9	87.9
$\Delta^{g}_{cr}H^{\circ}_{m}$(298.15 K) /kJ·mol^{-1}	208.0	205.7	205.3	203.9	205.5	209.8	210.5
$<\Delta^{g}_{cr}H^{\circ}_{m}(298.15\ K)> = 206.9 \pm 3.2$ kJ·mol^{-1}							

The instrumental constant used in this determination was obtained with *in situ* experiments with 1,3,5-triphenylbenzene.

4.2.3.1. Calibration with 1,3,5-triphenylbenzene for bathophenanthroline and tests with 9-acridanone

A molecule with similar vapour pressure was selected to do in situ calibration for the selected temperature. The results for the 1,3,5-triphenylbenzene calibration are in table 4.24. The instrumental constant is obtained from the mean of seven different essays.

Table 4.24 - Experimentally obtained results on the calibration experiments with triphenylbenzene with the vacuum drop-microcalorimetry technique at 533.15 K.

1,3,5-Triphenylbenzene	**1**	**2**	**3**	**4**	**5**	**6**	**7**
***T*/ K**	541.01	540.88	541.08	541.02	540.88	540.93	541.12
T_{amb}/ K	298.45	297.95	298.25	298.05	298.05	298.15	298.15
$m_{samplecap}$/ mg	23.4689	23.9008	23.4314	23.6251	23.2601	22.2005	22.1245
m_{ref}/ mg	23.4577	23.8705	23.3842	23.5367	23.1841	22.2188	21.9900
m_{sample}/ mg	4.179	3.956	4.553	5.047	3.687	3.521	3.908
ΔH_{corr}(blanks)/ mJ	48.777	44.159	42.883	35.319	38.619	58.005	32.601
$\Delta H_{observed}$/ J	3.214	3.066	3.499	4.018	2.921	2.717	3.002
$\Delta H_{corrected}$/ J	3.262	3.110	3.542	4.054	2.960	2.775	3.035
$\Delta^{g,T}_{cr,298.15}H^{\circ}_{m}$ /kJ·mol^{-1}	239.2	240.9	238.3	246.1	246.0	241.5	238.0
$\Delta^{g,T}_{cr,298.15}H^{\circ}_{m}$ /kJ·mol^{-1} (expected)	259.9	259.8	259.9	259.9	259.8	259.8	259.9
K	1.0865	1.0786	1.0905	1.0560	1.0562	1.0761	1.0924
<K> = 1.0766 ± 0.0115							

Similarly to the essays for bathophenanthroline, the obtained instrumental constant was higher than usual for this device. The same reasoning presented in section 4.1.3. can be used here. The high temperature and the heat loss through the top section should be the main reasons why the instrumental constant is high. As it was done for bathophenanthroline, 9-acridanone was used to confirm the obtained instrumental constant. The results are presented in table 4.25.

Table 4.25 - Experimentally obtained results on the test experiments with 9-acridanone with the vacuum drop-microcalorimetry technique at 533.15 K.

Essay for BCP	**1**	**2**	**3**	**4**	**5**	**6**
***T*/ K**	540.88	541.02	541.12	541.08	541.12	541.12
T_{amb}**/ K**	298.05	298.15	298.05	298.25	298.15	298.05
$m_{samplecap}$**/ mg**	22.4376	22.6858	22.4731	22.9955	23.3841	24.1573
m_{ref}**/ mg**	22.3295	22.6542	22.5660	22.8472	23.4580	24.1918
m_{sample}**/ mg**	1.9627	3.4798	3.4564	2.2362	2.3647	2.3931
ΔH_{corr}**(blanks)/ mJ**	42.890	54.035	81.914	26.245	63.842	43.992
$\Delta H_{observed}$**/ J**	1.745	3.225	3.313	1.888	2.214	2.316
$\Delta H_{corrected}$**/ J**	1.788	3.279	3.395	1.914	2.278	2.360
$\Delta^{g,T}_{cr,298.15}H^{\circ}_{m}$ **/kJ·mol^{-1}**	65.3	65.3	65.3	65.3	65.3	65.3
$\Delta^{T}_{298.15}H^{\circ}_{m}$ **/kJ·mol^{-1}**	191.4	198.0	206.4	179.9	202.4	207.3
$\Delta^{g}_{cr}H^{\circ}_{m}$**(298.15 K) /kJ·mol^{-1}**	126.2	132.7	141.1	114.6	137.1	142.0
$<\Delta^{g}_{cr}H^{\circ}_{m}$(298.15 K)> = 132.3 ± 6.1 kJ·mol^{-1}						
$<\Delta^{g}_{cr}H^{\circ}_{m}$(298.15 K)>lit = 131.8 ± 2.9 kJ·mol^{-1}						

4.2.4. Knudsen Effusion Method

Bathocuproine was also submitted to vapour pressure studies with the two techniques described on chapter three. In this section the experimental and treated results are presented along with their interpretation and comments. Further discussion will be held on the “vapour pressure analysis” section at the end of this chapter.

4.2.4.1. Knudsen Effusion Mass Loss

In table 4.26 the obtained and treated results for bathocuproine with the KEML method are registered. These results include the temperature and accompanying vapour pressures along with the calculated 1/*T* and ln *p*. The latter values are used in a graphical representation of the Clausius-Clapeyron slope from which parameters *a* and *b* can be obtained (figure 4.37). As described in chapter three, from these values it is possible to calculate the vapour pressure at the mean temperature, *p*(<*T*>), the enthalpy of

sublimation at mean temperature, $\Delta_{cr}^{g}H_{m}^{\circ}$ (<*T*>), and the entropy of sublimation at mean temperature, $\Delta_{cr}^{g}S_{m}^{\circ}$ (<*T*>). These parameters are in table 4.27.

Considering the thermodynamic parameters obtained at the average temperature, it is possible to adjust the values to the reference temperature of 298.15 K, $\Delta_{cr}^{g}H_{m}^{\circ}$, $\Delta_{cr}^{g}S_{m}^{\circ}$. These latter parameters can be used Gibbs free energy of the sublimation process at 298.15 K, $\Delta_{cr}^{g}G_{m}^{\circ}$. The plot described earlier can also be used to extrapolate the vapour pressure at the reference temperature. Values registered in table 4.28.

It is important to mention that during the measurements for bathocuproine, an error with the program that controls the KEML device appeared and as such, due to this error and time restraints, a small number of measurements were done on this sample.

Table 4.26 - Experimental and treated results obtained for bathocuproine through the KEML method.

***T* (K)**	***p* (Pa)**	**1/*T* (K^{-1})**	**ln (*p*/Pa)**
457	0.059	0.00219	-2.83
461	0.096	0.00217	-2.34
465	0.128	0.00215	-2.06
468	0.193	0.00214	-1.65
469	0.233	0.00213	-1.46
472	0.282	0.00212	-1.27
473	0.333	0.00211	-1.10
476	0.428	0.00210	-0.85
477	0.516	0.00210	-0.66
$\langle T \rangle$ = 467 K			

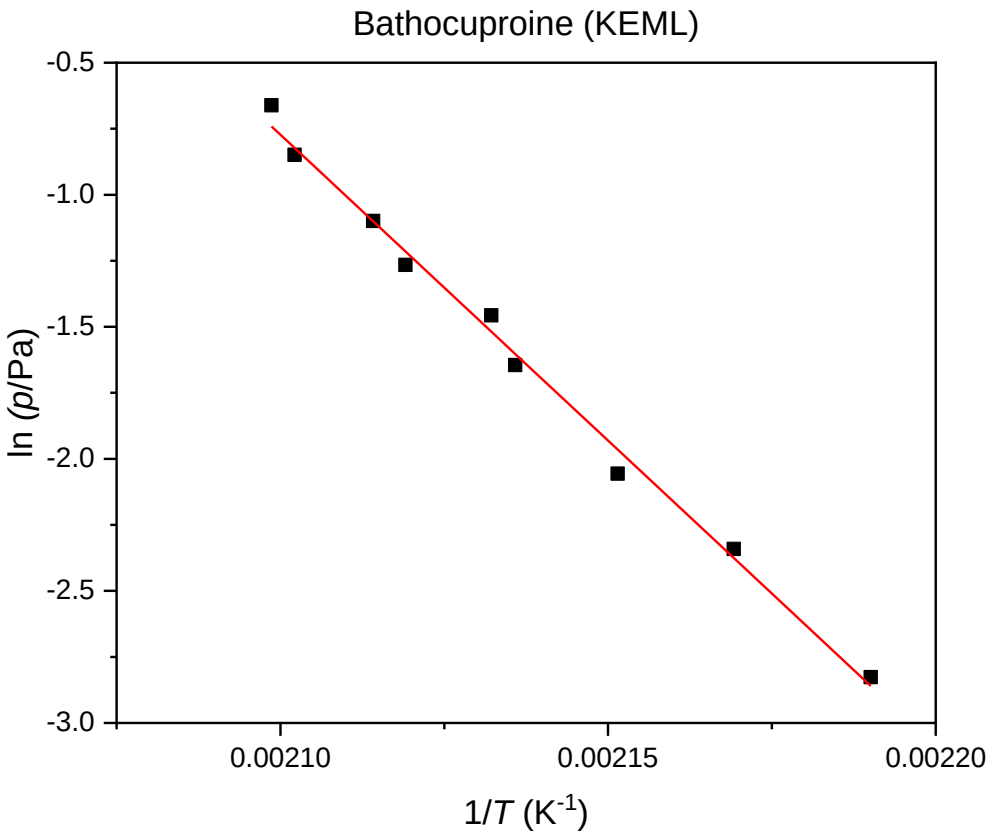

Figure 4.37 - Graphical representation of ln *p* vs 1/*T* obtained through the Knudsen effusion mass loss method for bathocuproine.

Table 4.27 - Clausius-Clapeyron equations parameters obtained for bathocuproine with the KEML method at the mean temperature.

Technique	a	b	R^2	p(<*T*>)	$\Delta_{cr}^{g}H_m^{\circ}$ (<*T*>)	$\Delta_{cr}^{g}S_m^{\circ}$ (<*T*>)
				Pa	kJ·mol^{-1}	J·K^{-1}·mol^{-1}
KEML	47.87±1.49	-23161±696	0.9937	0.154	192.6 ± 5.8	412.6 ± 12.4

Table 4.28 - Standard molar enthalpy, entropy and Gibbs free energy and vapour pressure at the temperature of 298.15 K for bathocuproine obtained with the KEML method.

Compound	$\Delta_{cr}^{g}H_m^{\circ}$ /kJ·mol^{-1}	$\Delta_{cr}^{g}S_m^{\circ}$ /J·K^{-1}·mol^{-1}	$\Delta_{cr}^{g}G_m^{\circ}$ /kJ·mol^{-1}	*p* / Pa
Bathocuproine	204.1 ± 5.8	248.6 ± 12.3	129.9 ± 7.5	1.07 x 10^{-11}

4.2.4.2. Knudsen Effusion Mass Spectrometry

In table 4.29 the experimentally obtained and treated results for bathocuproine with the KEMS method are registered. However, it is important to note that the apparatus used for this study has a major limitation for studying organic samples such as bathocuproine as mentioned before. Its original design is for high temperature chemistry and as such, it takes a long time to stabilize at low temperatures. So, it is practically impossible to measure a significant number of experimental points. This fact is the origin of the small number of points and the large experimental error. But, as mentioned in previous sections, it is an incredibly sensitive device.

The KEMS results include the temperature and accompanying vapour pressures along with the calculated $1/T$ and $\ln p$. The latter values are used in a graphical representation of the Clausius-Clapeyron slope from which parameters a and b can be obtained (figure 4.38). As described in chapter three, from these values it is possible to calculate the vapour pressure at the mean temperature, $p(<T>)$, the enthalpy of sublimation at mean temperature, $\Delta_{cr}^{g}H_{m}^{\circ}$ ($<T>$), and the entropy of sublimation at mean temperature, $\Delta_{cr}^{g}S_{m}^{\circ}$ ($<T>$). These parameters are in table 4.30.

Considering the thermodynamic parameters obtained at the average temperature, it is possible to adjust the values to the reference temperature of 298.15 K, $\Delta_{cr}^{g}H_{m}^{\circ}$, $\Delta_{cr}^{g}S_{m}^{\circ}$. These latter parameters can be used Gibbs free energy of the sublimation process at 298.15 K, $\Delta_{cr}^{g}G_{m}^{\circ}$. The plot described earlier can also be used to extrapolate the vapour pressure at the reference temperature. These parameters are presented in table 4.31 along with the appearance potential of our sample which was corrected by measuring the appearance potential of water, which is a known constant. It is also represented in figure 4.39.

For the determination of the instrumental constant to correct the experimentally obtained vapour pressure values for bathocuproine. The determination of the instrumental constant is done by measuring the vapour pressure values of triphenylbenzene and compare them with values from literature. As explained in section 3.1.5, this is done as the experimental conditions of Knudsen effusion mass spectrometry change from experiment to experiment.

Table 4.29 - Experimental and treated results obtained for bathocuproine through the KEMS method.

Essay 1			
***T* (K)**	***p* (Pa) ***	**1/*T* (K^{-1})**	**ln (*p*/Pa)**
352	7.08E-08	0.00284	-16.46
360	3.38E-07	0.00278	-14.90
369	1.48E-06	0.00271	-13.42
378	5.77E-06	0.00265	-12.06
$\langle T \rangle$ = 365			
Essay 2			
***T* (K)**	***p* (Pa) ***	**1/*T* (K^{-1})**	**ln (*p*/Pa)**
350	2.26E-07	0.00286	-15.30
359	1.08E-06	0.00279	-13.74
369	5.61E-06	0.00271	-12.09
377	1.72E-05	0.00265	-10.97
$\langle T \rangle$ = 364			

*Obtained with an instrumental constant from triphenylbenzene; sigma (bathophenanthroline) = 3*sigma (benzene) + 2 sigma (pyridine) ≅5*sigma (benzene) = 75

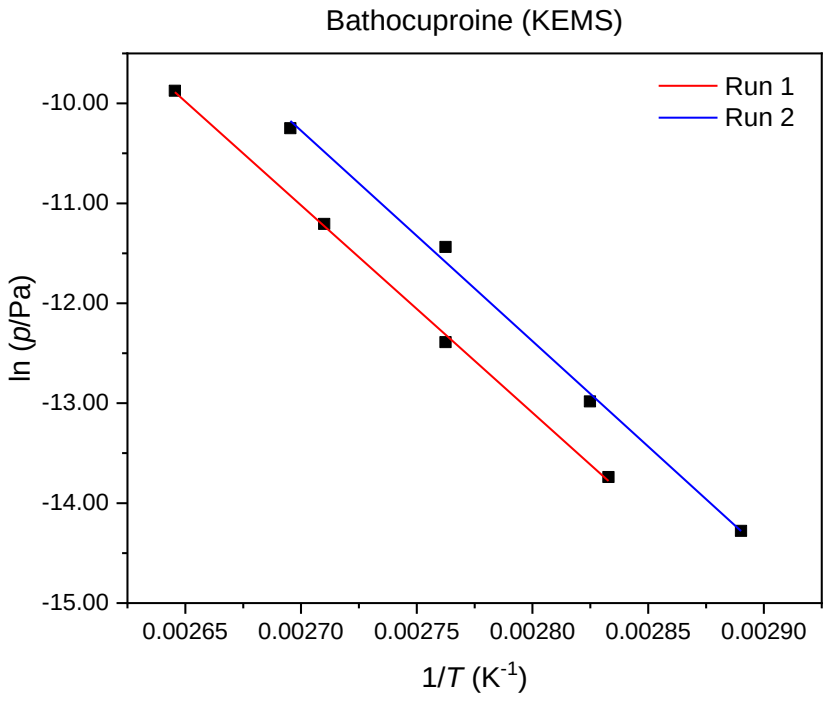

Figure 4.38 - Graphical representation of ln *p* vs 1/*T* obtained through the Knudsen effusion mass spectrometry method for bathocuproine.

Table 4.30 - Clausius-Clapeyron equations parameters obtained for bathocuproine with the KEML method at the mean temperature.

KEMS	a	b	R^2	p(<*T*>)	$\Delta_{cr}^{g}H_m^{\circ}$ (<*T*>)	$\Delta_{cr}^{g}S_m^{\circ}$ (<*T*>)
				Pa	kJ·mol^{-1}	J·K^{-1}·mol^{-1}
Essay 1	47.35±1.61	-22439±587	0.9986	7.26 x 10^{-7}	186.6 ± 4.9	511.5 ± 13.4
Essay 2	45.50±0.99	-21271±362	0.9994	1.87 x 10^{-6}	176.9 ± 3.0	486.2 ± 8.3

Table 4.31 - Standard molar enthalpy, entropy and Gibbs free energy and vapour pressure at the temperature of 298.15 K for bathocuproine obtained with the KEML method.

Essay	$\Delta_{cr}^{g}H_m^{\circ}$ /kJ·mol^{-1}	$\Delta_{cr}^{g}S_m^{\circ}$ /J·K^{-1}·mol^{-1}	$\Delta_{cr}^{g}G_m^{\circ}$ /kJ·mol^{-1}	*p* / Pa	AE_0 /eV
1	191.1 ± 4.9	419.1 ± 13.4	65.9 ± 2.7	2.99 x 10^{-12}	-
2	176.9 ± 3.0	400.7 ± 8.3	61.9 ± 1.6	1.64 x 10^{-11}	-
Mean	184.6 ± 2.6	406.0 ± 7.0	62.9 ± 1.4	9.68 x 10^{-12}	8.9

The value obtained with KEMS are not in agreement with the values obtained with the mass loss and VDM methods. Particularly the value from the second essay. The small number of experimentally obtained points can explain some of the underestimation of the thermodynamic parameters but also wrong temperature measurements as explained in section 4.1.4.2. As such, the mean from both essays is not recommended but rather only the use of the first.

Table 4.32 - Instrumental constant values obtained with triphenylbenzene.

T (K)	*p* (bar)*	$K_{instrum}$
372	2.87e-8	0.0089
354	2.57e-9	0.0124
345	7.07e-10	0.0106

*Values from Verevkin et al. JCT (1997) 29, 1495.

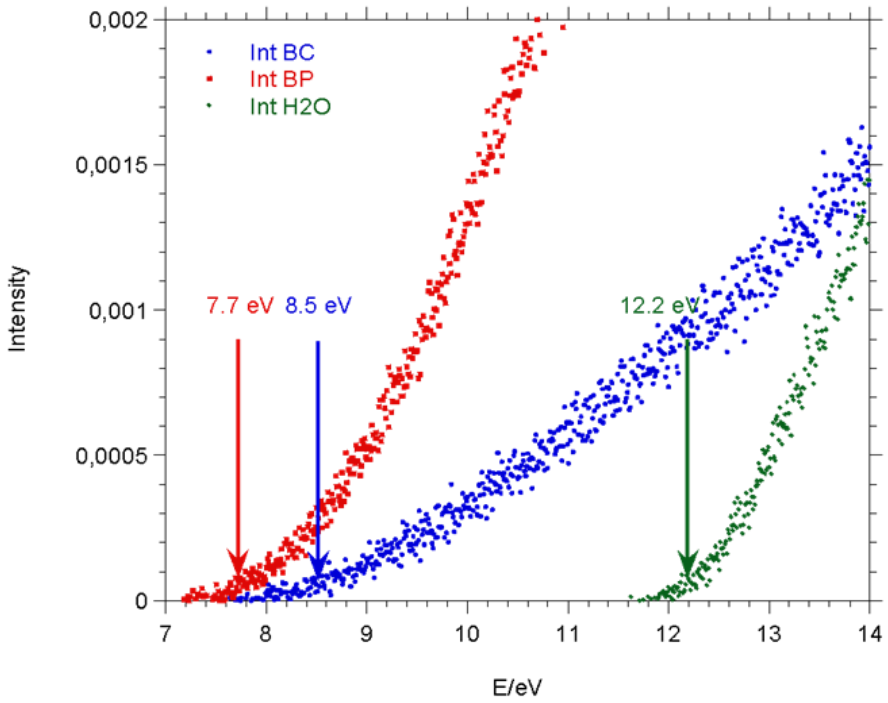

Figure 4.39 - Ionization intensity measurements for the determination of the appearance potential of bathocuproine

During KEMS experiments, the only significant mass spectrometry signals detected were the ones corresponding to the mass of bathocuproine and its isotopes. Therefore, it can be inferred that no decomposition occurs, only sublimation. However, a change in the colour of the sample from cream to orange was observed. To investigate this change, X-ray crystallography and FTIR experiments were conducted. The results are presented in figure 4.40 and 4.41, respectively. No alterations in the sample were observed in the XRD and FTIR results. The change in colour could be due to a change in the crystalline structure significant enough to affect the interactions with radiation, but not enough to be detected via powder XRD experiments.

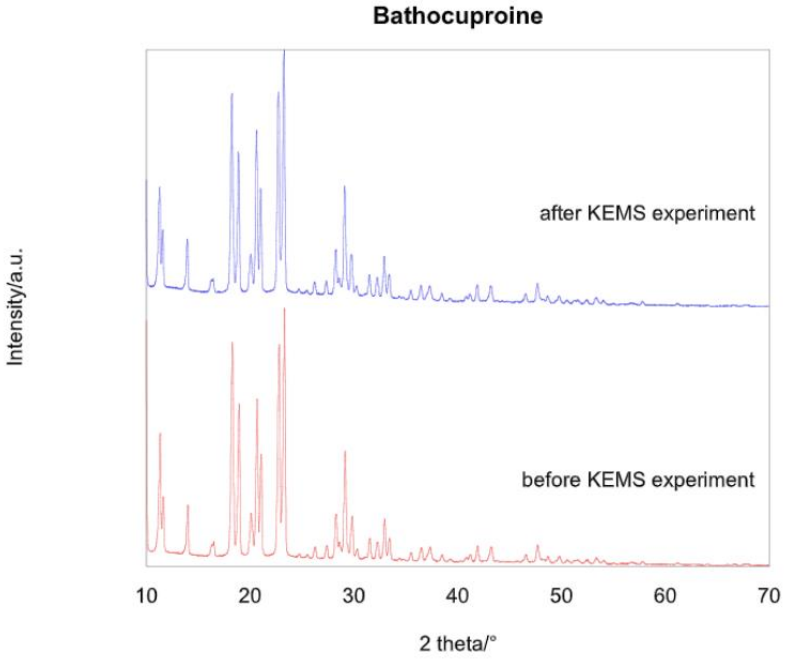

Figure 4.40 - XRD spectra of bathocuproine before and after a KEMS experiment.

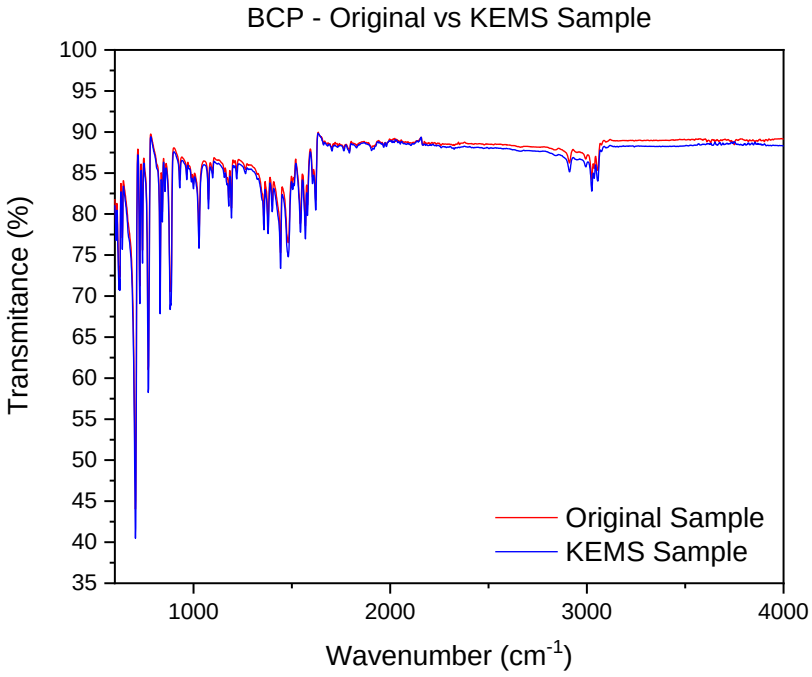

Figure 4.41 - FTIR spectra of a bathocuproine sample from before and after a KEMS experiment.

4.2.5. Quartz Crystal Microgravimetry

Bathocuproine was also submitted to vapour pressure analysis with the quartz crystal microgravimetric technique described on section 3.2. As already mentioned, this technique can only determine the heat of sublimation due to the non-equilibrium conditions.

In this section the raw and treated results are presented. The values for df/dt, *T*, 1/*T*, and ln Q are registered in table 4.33. In figure 4.42 there is a graphical representation of the ln Q *vs* 1/*T* plot. As described in chapter three, from these values it is possible to calculate the enthalpy of sublimation at mean temperature, $\Delta_{cr}^{g}H_{m}^{\circ}$ (<*T*>), and from that the enthalpy of sublimation at the reference temperature of 298.15 K, $\Delta_{cr}^{g}H_{m}^{\circ}$. Tables 4.44 and 4.45.

The initial results obtained with this technique were significantly different from those obtained with the other vapour pressure techniques. The reasoning for the tests and further corrections are described on section 4.1.5. The information presented there applies here without any change.

Table 4.33- Experimentally and treated results obtained for bathocuproine with the QCM method.

Essay 1			
d*f*/d*t*	***T* (K)**	**1/*T* (K^{-1})**	**ln *Q***
0.0726	468	0.00214	0.452
0.0562	465	0.00215	0.192
0.0430	462	0.00217	-0.079
0.0324	459	0.00218	-0.364
0.0255	456	0.00219	-0.607
0.0189	453	0.00221	-0.909
Essay 2			
d*f*/d*t*	***T* (K)**	**1/*T* (K^{-1})**	**ln *Q***
0.0496	466	0.00215	0.068
0.0381	463	0.00216	-0.199
0.0284	460	0.00217	-0.497
0.0212	457	0.00219	-0.789
0.0162	454	0.00220	-1.065

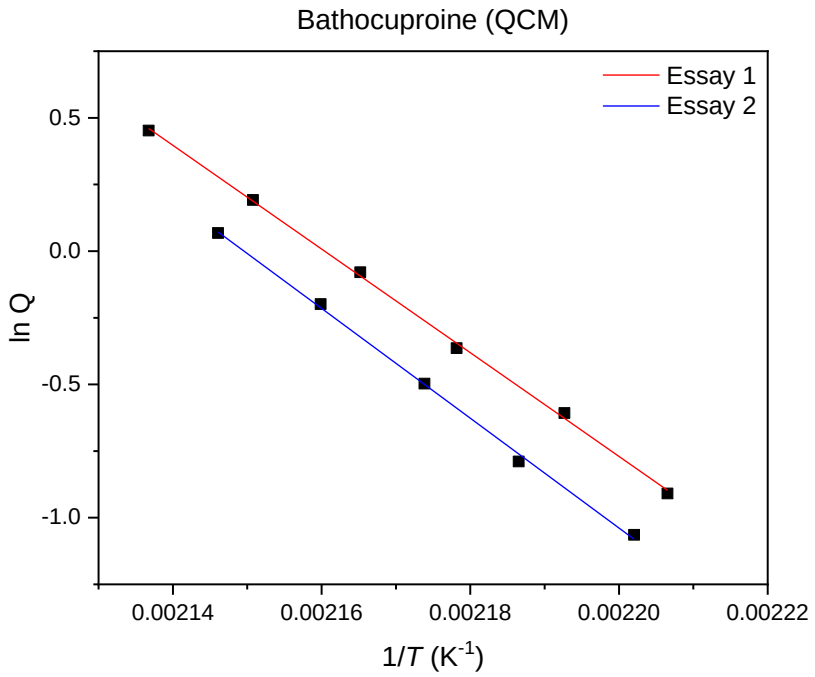

Figure 4.42 - Graphical representation of ln Q vs 1/*T* obtained through the QCM method for bathocuproine.

Table 4.34 - Clausius-Clapeyron equations parameters obtained for bathocuproine with the QCM method at the mean temperature.

Bathocuproine	**<*T*>**	**m**	**R^2**	**$\Delta_{cr}^{g}H_m^{\circ}$ (<*T*>)**
				kJ·mol^{-1}
Essay 1	462	-19453 ± 292	0.9991	161.7 ± 2.4
Essay 2	460	-20589 ± 470	0.9985	161.2 ± 3.9

Table 4.35 - Standard molar enthalpy at the mean temperature and at the temperature of 298.15 K before and after correction for bathocuproine obtained with the QCM method.

Essay	**$\Delta_{cr}^{g}H_m^{\circ}$ (<*T*>)**	**$\Delta_{cr}^{g}H_m^{\circ}$ (*T* = 298.15 K)**	**$\Delta_{cr}^{g}H_m^{\circ}(T = 298.15\ K)_{corr}$ ***
	kJ·mol^{-1}	**kJ·mol^{-1}**	**kJ·mol^{-1}**
Essay 1	161.7 ± 2.4	172.9 ± 2.4	195.4 ± 2.4
Essay 2	161.2 ± 3.9	182.2 ± 3.9	205.9 ± 3.9
Mean	-	177.6 ± 2.1	198.3 ± 2.1

*Correction with an instrumental constant from triphenylbenzene.

4.3. Vapour Pressures and Enthalpies of Sublimation

The present section aims at discussing the standard molar enthalpy of sublimation at the reference temperature of 298.15 K, $\Delta_{cr}^{g}H_{m}^{\circ}$, results obtained for bathophenanthroline and bathocuproine with the various techniques. The values gathered for bathophenanthroline are registered in table 4.36.

Table 4.36 - Collection of the standard molar enthalpy of sublimation at the reference temperature of 298.15 K obtained for bathophenanthroline.

Bathophenanthroline	$\Delta_{cr}^{g}H_{m}^{\circ}$ **/kJ·mol^{-1}**
KEML	183.8 ± 2.8
KEMS	176.9 ± 3.4
QCM	182.4 ± 2.7
VDM	183.7 ± 4.2
I-TG + DSC	179.3 ± 5.3
Recommended Value from KEML & VDM	183.8 ± 2.2

The value of the standard molar enthalpy of sublimation at the reference temperature of 298.15 K obtained with the KEML method is in excellent agreement with the value obtained via the VDM method. So, the mean of the two values is recommended for use.

The value obtained with KEMS for the reference temperature is not entirely in agreement with the values obtained with the mass loss and VDM methods. The small number of experimentally obtained points can explain some of the underestimation of the thermodynamic parameters. However, another factor that can also affect is the measurement of temperature. For this technique, the thermocouple that was used is more appropriate for higher temperatures and thus, it takes a long time to have a stable measurement at the working temperatures for this sample. So, replacement of the thermocouple for one more appropriate for this temperature range is advised. Additionally, it has a different placement from experiment to experiment as the Knudsen cell is completely removed when a new sample is inserted. This can potentially affect the measurement of *T* and thus affecting the ln p vs 1/*T* plot although it is unlikely that it does. Higher temperatures on the KEMS experiments should yield more and better results.

In figure 4.43, a visual representation of the natural logarithm of the vapour pressures measured by both Knudsen effusion methods is shown. Although they seem to align,

when further examining the tendency and origin of both linear regressions, a significant difference appears which is then seen in the end results.

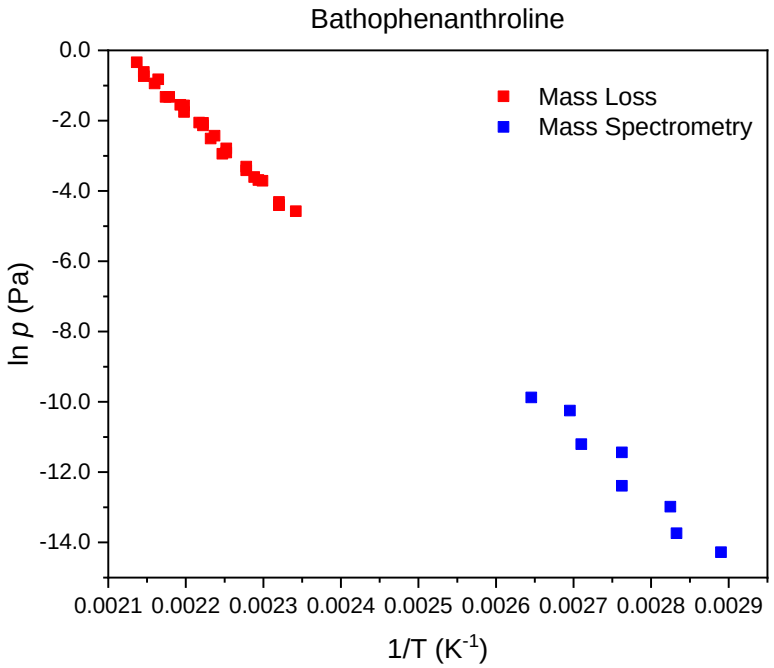

Figure 4.43 - Visual representation of the natural logarithm of the vapour pressures measured by both Knudsen effusion methods for bathophenanthroline.

The value obtained by QCM is in good agreement with both the KEML and VDM methods. However, the large correction that was introduced with the corrections constant makes its use not recommended. The improvements on the device described in section 4.1.5 should help with the production of better results.

In the case of the enthalpy of sublimation obtained from the addition of the enthalpies of fusion and vaporization. Although being in agreement, the value obtained has a large experimental error due to the use of two techniques for these determinations. This leads to the value not being considered. The reasoning for the large error has been explored in section 4.1.6.

Regarding bathocuproine, the experimentally obtained results for the standard molar enthalpy of sublimation at the reference temperature of 298.15 K are registered in table 4.37.

Table 4.37 - Collection of the standard molar enthalpy of sublimation at the reference temperature of 298.15 K obtained for bathocuproine.

Bathocuproine	$\Delta_{cr}^{g} H_{m}^{\circ}$ /kJ·mol^{-1}
KEML	204.1 ± 5.8
KEMS	184.0 ± 2.6
QCM	198.3 ± 2.1
VDM	206.9 ± 3.2
Recommended Value from KEML and VDM	206.2 ± 2.8

The value obtained with KEML agrees with the value obtained by VDM although the agreement is not as good as the one for bathophenanthroline. Note that the software error mentioned in section 4.2.4.1 may be the main reason for the difference, but decomposition cannot be discarded. So, the mean of the two values is recommended for use.

The value obtained with KEMS for the reference temperature is not entirely in agreement with the values obtained with the mass loss and VDM methods. The reasons were detailed above when discussing bathophenanthroline.

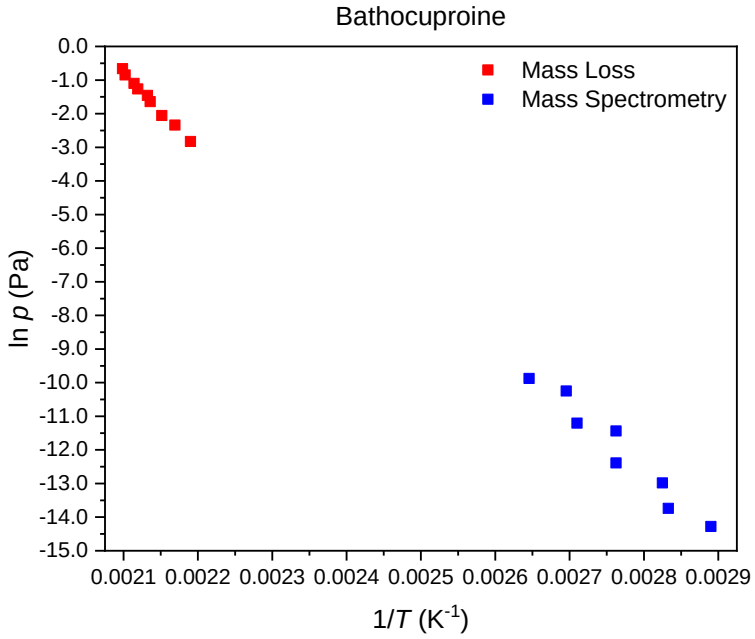

Figure 4.44 - Visual representation of the natural logarithm of the vapour pressures measured by both Knudsen effusion methods for bathocuproine.

In figure 4.44, a visual representation of the natural logarithm of the vapour pressures measured by both Knudsen effusion methods is shown. A clear difference in alignment is seen.

The value obtained with QCM agrees with the value obtained by KEML and VDM although the agreement is not as good as the one for bathophenanthroline. Note that the small number of experimental points is one of the main reasons for the difference. The necessity of a better calibration experiment is noteworthy.

It is however important to note that experiments done at higher temperatures may subject the sample to some thermal decomposition. DSC and TG data support the decomposition hypothesis although at a much higher temperature than the one used for most effusion experiments.

5. Final Remarks and Future Perspectives

Throughout chapter four, the results from the thermophysical studies of bathophenanthroline and bathocuproine are presented and discussed. A thorough analysis of the thermophysical nature of these samples has been undertaken filling a void in the available literature on phenanthroline derivatives.

In this chapter, a summary of the thermophysical studies is presented. Followed by remarks on the enthalpic effects of the addition of the phenyl and methyl groups. It ends with the prospects into the future of this work.

5.1. Thermophysical Studies

The main goal of this work, as mentioned before, is to provide phase change data and thermophysical parameters for two molecules of the phenanthroline molecular family. In the process complete the thermophysical cycle in figure 5.1. All of the results from the processes represented in the thermophysical cycle are registered in table 5.1.

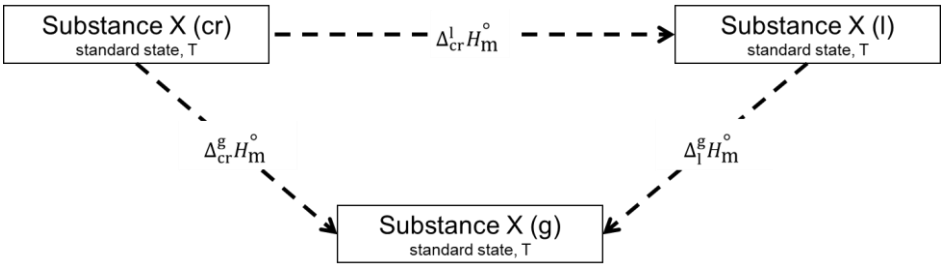

Figure 5.1 - Thermophysical cycle of the relations of phase transition.

Table 5.1 - Standard molar enthalpies of phase transition at the reference temperature of 298.15 K.

Bathophenanthroline		
$\Delta^{l}_{cr}H^{\circ}_{m}$ /kJ·mol^{-1}	$\Delta^{g}_{l}H^{\circ}_{m}$ /kJ·mol^{-1}	$\Delta^{g}_{cr}H^{\circ}_{m}$ /kJ·mol^{-1}
30.4 ± 0.4	153.4 ± 1.9	183.8 ± 2.2
Bathocuproine		
$\Delta^{l}_{cr}H^{\circ}_{m}$ /kJ·mol^{-1}	$\Delta^{g}_{l}H^{\circ}_{m}$ /kJ·mol^{-1}	$\Delta^{g}_{cr}H^{\circ}_{m}$ /kJ·mol^{-1}
26.5 ± 1.6	179.7 ± 4.1	206.2 ± 2.8

In the case of bathophenanthroline, a high standard molar enthalpy of sublimation at the reference temperature of 298.15 K was determined. This is a direct indication of the strong intermolecular forces present in the crystalline phase. This stability passes from the crystalline phase unto the liquid phase which remains stable until approximately 700 K. The temperature at which vaporization ends and decomposition starts as shown from the DSC and TG experiments. This is also confirmed by the large standard molar enthalpy of vaporization at the reference temperature of 298.15 K obtained by both the I-TG method and calculating it through the heat of fusion and the heat of sublimation.

It is also important to mention that bathophenanthroline shows several curious thermophysical behaviours on the condensed phases. The formation of a metastable phase and a subsequent cold crystallization are not entirely common in small organic molecules, but it seems to be a characteristic of the kinetic thermal behaviour of bathophenanthroline.

In the case of bathocuproine, an increase in the enthalpy of sublimation is observed. This is most likely due to the insertion of the two methyl groups, which likely contribute to the stabilization of the electronic structure, particularly due to their proximity to the nitrogen atoms introduced in the 1 and 10 positions of the structure. However, from DSC and TG experiments, it is evident that the sample becomes unstable at temperatures near fusion. Decomposition starts to occur during these experiments, and after fusion, it only intensifies. The loss of a methyl and a phenyl group is observed, and the formation of an intermediary compound further supports this hypothesis. Nevertheless, the high enthalpy of sublimation indicates the presence of strong intermolecular forces in the crystalline phase.

5.2. Ongoing Works and Future Perspectives

Experimental thermochemical works to determine the massic energies of combustion are ongoing. These measurements are being undertaken with static bomb combustion calorimetry in oxygen. This can be used to derive the standard molar enthalpy of formation in the crystalline phase at 298.15 K, $\Delta_f H^\circ(\mathrm{cr})$. From the latter thermochemical parameter and from the enthalpies of phase transition the values for the enthalpy of formation in the liquid and gas phases can be calculated.

This extensive thermodynamic study allows the creation of a comprehensive thermodynamic profile of the molecules under investigation. The phase transition and

formation processes mentioned earlier are depicted in a thermodynamic cycle, as shown in figure 5.2.

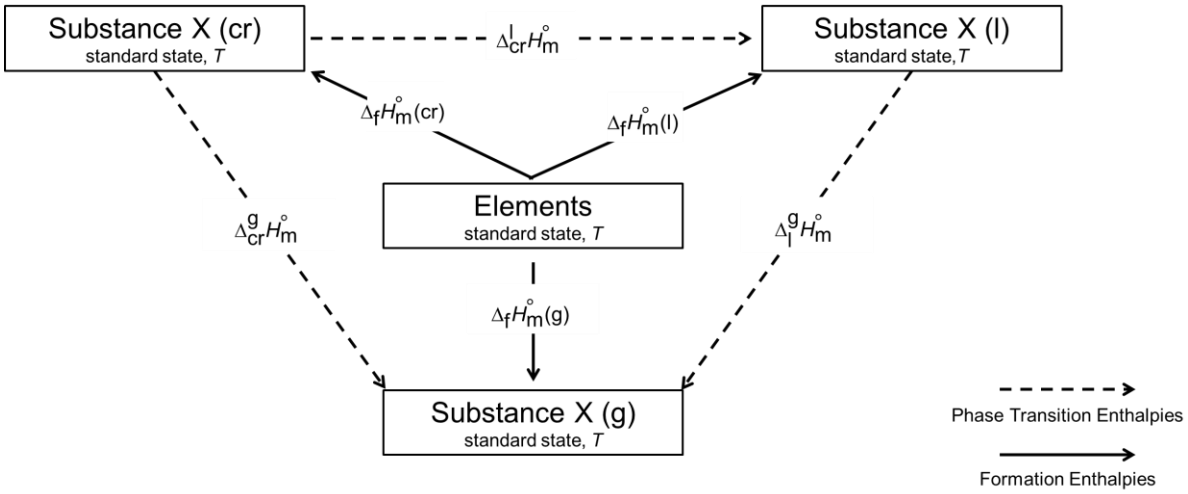

Figure 5.2 - Thermodynamic cycle illustrating the relations of formation and phase transition of a given substance.

Along with the experimental study, a computational approach is being used to predict, with a reasonable degree of accuracy, the gas-phase molar enthalpy of formation. The enthalpy of formation of the molecules under study is estimated using composite methods, along with appropriate gas-phase hypothetical reactions. The G3(MP2)B3 [65] and G4(MP2) [66] methods, based on the Gaussian-3/4 theories, are composite methods that involves a series orbital calculations to determine the total energy of a particular molecular species.

By employing a series of hypothetical isodesmic reactions and incorporating experimentally determined values of the standard molar enthalpy of formation in the gas phase for auxiliary molecules, the theoretical molar enthalpy of formation in the gas can be estimated and compared with the experimentally determined values.

This thermodynamic study is part of an ongoing research that aims at characterizing the enthalpic relationship between the various phenanthrolines like the one described below.

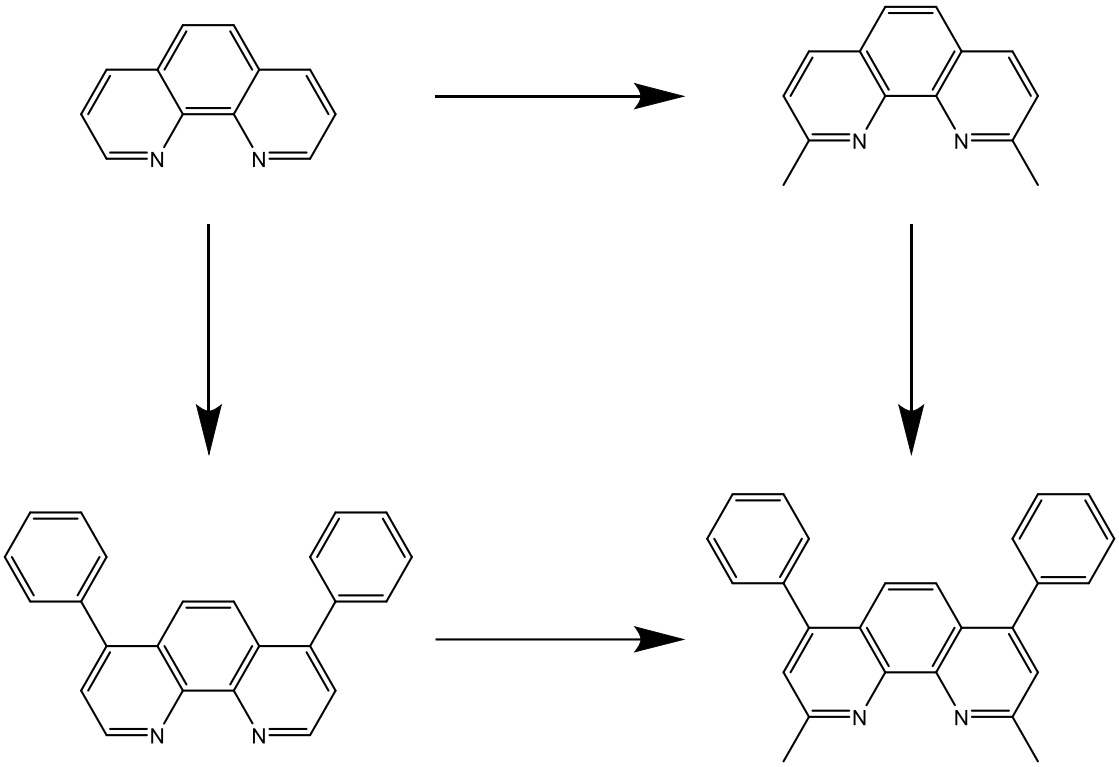

Figure 5.3 - Scheme of the enthalpic relations between various phenanthrolines.

This study can also be extended other phenanthrolines that have various others functional groups in the same or different positions on the molecules. It is also important to mention that these molecules are known ligands and as such, with the appropriate techniques, this study can also comprehend the metallic complexes formed between the phenanthrolines and several metal atoms.

Further spectroscopic studies such as UV-Vis spectroscopy and fluorescence spectroscopy also provide important data for their use in OSCs. Computational studies can also help in comprehending the electronic nature of the phenanthroline molecular family.

So, through the work developed for this thesis and the ongoing/future experiments, a better understanding of the chemical and physical transformations of this molecular family providing a contribution to the development of charge carrier transporting molecular materials through the general better understanding of the stability of these substances on the condensed phases.

6. References

(1) Sammes, P. G.; Yahioglu, G. 1,10-Phenanthroline: A Versatile Ligand. Chemical Society Reviews 1994, 327-334.

(2) Halcrow, B. E.; Kermack, W. O. 43. Attempts to find new antimalarials. Part XXIV. Derivatives of o-phenanthroline (7 : 8 : 3′ : 2′-pyridoquinoline). Journal of the Chemical Society 1946, 155-157.

(3) Bencini, A.; Lippolis, V. 1,10-Phenanthroline: A versatile building block for the construction of ligands for various purposes. Coordination Chemistry Reviews 2010, 254 (17-18), 2096-2180. DOI: 10.1016/j.ccr.2010.04.008.

(4) Accorsi, G.; Listorti, A.; Yoosaf, K.; Armaroli, N. 1,10-phenanthrolines: versatile building blocks for luminescent molecules, materials and metal complexes. Chem Soc Rev 2009, 38 (6), 1690-1700. DOI: 10.1039/b806408n From NLM PubMed-not-MEDLINE.

(5) Wu, F.; Xie, J.; Zhu, Z. 1,10-Phenanthroline: A versatile ligand to promote copper-catalyzed cascade reactions. Applied Organometallic Chemistry 2020, 34 (11). DOI: 10.1002/aoc.5926.

(6) Belcher, R. The application of chelate compounds in analytical chemistry. Pure and Applied Chemistry 1973.

(7) Amini, M.; Najafi, S.; Janczak, J. Copper (I) complex of 2,9-dimethyl-1,10-phenanthroline: Synthesis, structure, and catalytic properties. Inorganica Chimica Acta 2018, 482, 333-339. DOI: 10.1016/j.ica.2018.06.032.

(8) Pouretedal, H. R.; Keshavarz, M. H. Copper(I)-bathocuproine complex as carrier in iodide-selective electrode. Talanta 2004, 62 (1), 221-225. DOI: 10.1016/S0039-9140(03)00398-9 From NLM PubMed-not-MEDLINE.

(9) White, M. A. Physical properties of materials; CRC Press, 2019.

(10) Callister, W. D. Materials science and engineering : an introduction; John Wiley & Sons New York, 1997.

(11) Simon, S. H. The Oxford solid state basics; Oxford University Press Oxford, 2016.

(12) Shirota, Y.; Kageyama, H. Charge Carrier Transporting Molecular Materials and Their Applications in Devices. Chem. Rev. 2007, (107), 953-1010.

(13) Giannini, S.; Blumberger, J. Charge Transport in Organic Semiconductors: The Perspective from Nonadiabatic Molecular Dynamics. Acc Chem Res 2022, 55 (6), 819-830. DOI: 10.1021/acs.accounts.1c00675 From NLM Medline.

(14) Haneef, H. F.; Zeidell, A. M.; Jurchescu, O. D. Charge carrier traps in organic semiconductors: a review on the underlying physics and impact on electronic devices. Journal of Materials Chemistry C 2020, 8 (3), 759-787. DOI: 10.1039/c9tc05695e.
(15) Fratini, S.; Nikolka, M.; Salleo, A.; Schweicher, G.; Sirringhaus, H. Charge transport in high-mobility conjugated polymers and molecular semiconductors. Nat Mater 2020, 19 (5), 491-502. DOI: 10.1038/s41563-020-0647-2 From NLM PubMed-not-MEDLINE.
(16) Ji, T.; Wang, Y.-K.; Feng, L.; Li, G.-H.; Wang, W.-Y.; Li, Z.-F.; Hao, Y.-Y.; Cui, Y.-X. Charge transporting materials for perovskite solar cells. Rare Metals 2021, 40 (10), 2690-2711. DOI: 10.1007/s12598-021-01723-2.
(17) Bhatt, M. D.; Suzuki, S.; Sakurai, T.; Akimoto, K. Interaction of bathocuproine with metals (Ca, Mg, Al, Ag, and Au) studied by density functional theory. Applied Surface Science 2010, 256 (9), 2661-2667. DOI: 10.1016/j.apsusc.2009.11.044.
(18) Andrea Listorti; Alessandra Degli Esposti; Ravuri S. K. Kishore; Venkateshwarlu Kalsani; Michael Schmittel; Armaroli, N. 1,10-Phenanthrolines with Tunable Luminescence upon Protonation: A Spectroscopic and computational study. J. Phys. Chem. A 2007, 111, 7707-7718.
(19) Armaroli, N.; Eckert, J.-F.; Nierengarten, J.-F. Controlling the energy-transfer direction: an oligophenylenevinylene–phenanthroline dyad acting as a proton triggered molecular switch. Chemical Communications 2000, (21), 2105-2106. DOI: 10.1039/b006174n.
(20) Bazzicalupi, C.; Bencini, A.; Berni, E.; Bianchi, A.; Borsari, L.; Giorgi, C.; Valtancoli, B.; Lodeiro, C.; Lima, J. C.; Parola, A. J.; et al. Protonation and coordination properties towards Zn(II), Cd(II) and Hg(II) of a phenanthroline-containing macrocycle with an ethylamino pendant arm. Dalton Trans 2004, (4), 591-597. DOI: 10.1039/b315608g From NLM Medline.
(21) Kim, M.; Kim, J.; Son, H.; Jang, J.-H.; Yi, M. Performance Enhancement of Organic Thin-Film Transistors Using Bathophenanthroline:Cs Electron Injection Layer. Japanese Journal of Applied Physics 2010, 49 (10R). DOI: 10.1143/jjap.49.101601.
(22) Masumoto, Y.; Mori, T. Application of organic bathocuproine-based alloy film to organic light-emitting diodes. Thin Solid Films 2008, 516 (10), 3350-3356. DOI: 10.1016/j.tsf.2007.11.082.
(23) Liu, J.; Liu, X.; Chen, C.; Han, S.; Wang, N.; Du, S.; Tong, J.; Li, J.; Xia, Y. Construction of effective organic solar cell using phenanthroline derivatives as cathode interface layer. Optical Materials 2021, 122. DOI: 10.1016/j.optmat.2021.111647.

(24) Farinhas, J.; Ferraria, A. M.; do Rego, A. M. B.; Morgado, J.; Charas, A. Understanding the Role of Phenanthroline as Interlayer in Bulk Heterojunction Organic Photovoltaic Cells. ChemistrySelect 2016, 1 (18), 5638-5646. DOI: 10.1002/slct.201600574.
(25) Bonicelli, M. G.; Catalani, A.; Mariano, G.; Vecchio, S. Heat capacities and molar enthalpies and entropies of fusion for anhydrous 1,10-phenanthroline and 2,9-dimethyl-1,10-phenanthroline. Thermochimica Acta 2007, 466 (1-2), 69-71. DOI: 10.1016/j.tca.2007.10.001.
(26) Lipkind, D.; Hanshaw, W.; Chickos, J. S. Hypothetical Thermodynamic Properties. Subcooled Vaporization Enthalpies and Vapor Pressures of Polyaromatic Heterocycles and Related. J. Chem. Eng. Data 2009, (54), 2930-2943.
(27) Brunetti, B.; Ciccioli, A.; Lapi, A.; Buzyurov, A. V.; Nagrimanov, R. N.; Varfolomeev, M. A.; Ciprioti, S. V. Sublimation Study of Six 5-Substituted-1,10-Phenanthrolines by Knudsen Effusion Mass Loss and Solution Calorimetry. Entropy (Basel) 2022, 24 (2). DOI: 10.3390/e24020192 From NLM PubMed-not-MEDLINE.
(28) Clausius, R. Mechanical Theory of Heat. 1879.
(29) Gibbs, J. W. Equilibrium of Heterogeneous Substances. 1875-1878.
(30) Atkins, P.; Paula, J. d.; Keeler, J. Atkins' Physical Chemistry; Oxford University Press, 2018.
(31) Quantities, Units and Symbols in Physical Chemistry; 2007.
(32) Martinho Simões, J. A.; Minas da Piedade, M. E. Molecular Energetics: Condesed Phase Thermochemical Techniques; Oxford University Press, 2008.
(33) Lever, T.; Haines, P.; Rouquerol, J.; Charsley, E. L.; Van Eckeren, P.; Burlett, D. J. ICTAC nomenclature of thermal analysis (IUPAC Recommendations 2014). Pure and Applied Chemistry 2014, 86 (4), 545-553. DOI: 10.1515/pac-2012-0609.
(34) Curtiss, L. A.; Redfern, P. C.; Raghavachari, K. Gn theory. WIREs Computational Molecular Science 2011, 1 (5), 810-825. DOI: 10.1002/wcms.59.
(35) Alcácer, L. Introdução à Química Quântica Computacional; IST Press, 2007.
(36) Chickos, J. S.; Hesse, D. G.; Liebman, J. F. A Group Additivity Approach for the Estimation of Heat Capacities of Organic Liquids and Solids at 298 K. Structural Chemistry 1993, 4 (4), 261-269.
(37) Chickos, J. S.; Hosseini, S.; Hesse, D. G.; Liebman, J. F. Heat Capacity Corrections to a Standard State: A Comparison of New and Some Literature Methods for Organic Liquids and Solids. Structural Chemistry 1993, 4 (4), 271-278.
(38) Knudsen, M. Ann. Phys. 1909, 29, 179.

(39) Knudsen, M. Ann. Phys. 1909, 28, 999.
(40) Knudsen, M. Ann. Phys. 1909, 28, 75.
(41) Ribeiro da Silva, M. A. V.; Monte, M. J. S.; Santos, L. M. N. B. F. The design, construction, and testing of a new Knudsen effusion apparatus. The Journal of Chemical Thermodynamics 2006, 38 (6), 778-787. DOI: 10.1016/j.jct.2005.08.013.
(42) Santos, L. M. N. B. F.; Ferreira, A. I. M. C. L.; Štejfa, V.; Rodrigues, A. S. M. C.; Rocha, M. A. A.; Torres, M. C.; Tavares, F. M. S.; Carpinteiro, F. S. Development of the Knudsen effusion methodology for vapour pressure measurements of low volatile liquids and solids based on a quartz crystal microbalance. The Journal of Chemical Thermodynamics 2018, 126, 171-186. DOI: 10.1016/j.jct.2018.07.004.
(43) Brunetti, B.; Ciccioli, A.; Gigli, G.; Lapi, A.; Misceo, N.; Tanzi, L.; Vecchio Ciprioti, S. Vaporization of the prototypical ionic liquid BMImNTf(2) under equilibrium conditions: a multitechnique study. Phys Chem Chem Phys 2014, 16 (29), 15653-15661. DOI: 10.1039/c4cp01673d From NLM PubMed-not-MEDLINE.
(44) Copland, E. H.; Jacobson, N. Measuring Thermodynamic Properties of Metals and Alloys With Knudsen Effusion Mass Spectrometry; National Aeronautic and Space Administration - NASA, 2010.
(45) Miller, M.; Armatys, K. Twenty Years of Knudsen Effusion Mass Spectrometry: Studies Performed in the Period 1990-2010. The Open Thermodynamics Journal 2013, 7, 2-9.
(46) de Maria, G.; Balducci, G.; Guido, M.; Piacente, V. Mass spectrometric investigation of the vaporization process of Apollo 12 lunar samples. Proceedings of the Lunar Science Conference 1971, 2, 1267.
(47) Jacobson, N.; Kobertz, D.; Sergeev, D. Introduction to proceedings of the workshop on Knudsen Effusion Mass Spectrometry. Calphad 2019, 65, 111-126. DOI: 10.1016/j.calphad.2019.01.004.
(48) Ciccioli, A.; Gigli, G. The uncertain bond energy of the NaAu molecule: experimental redetermination and coupled cluster calculations. J Phys Chem A 2013, 117 (23), 4956-4962. DOI: 10.1021/jp402374t From NLM PubMed-not-MEDLINE.
(49) Arnau, A. Piezoelectric transducers and applications; Springer, 2004.
(50) Lu, C.; Czanderna, A. Methods and Phenomena, Their Applications in Science and Technology. 1984.
(51) Steinem, C.; Janshoff, A. Piezoelectric sensors; Springer Science & Business Media, 2007.

(52) Sauerbrey, G. The Use of Quartz Oscillators for Weighing Thin Layers and for Microweighing. Zeitschrift für Physik 1959, 155 (2), 206-222.
(53) Mecea, V. M. Fundamentals of mass measurements. J. Therm. Anal. Calorim. 2006, 86, 9-16.
(54) Verevkin, S. P.; Ralys, R. V.; Zaitsau, D. H.; Emel'yanenko, V. N.; Schick, C. Express thermo-gravimetric method for the vaporization enthalpies appraisal for very low volatile molecular and ionic compounds. Thermochimica Acta 2012, 538, 55-62. DOI: 10.1016/j.tca.2012.03.018.
(55) Verevkin, S. P.; Zaitsau, D. H.; Emelyanenko, V. N.; Heintz, A. A new method for the determination of vaporization enthalpies of ionic liquids at low temperatures. J Phys Chem B 2011, 115 (44), 12889-12895. DOI: 10.1021/jp207397v From NLM PubMed-not-MEDLINE.
(56) Craig, D. Q. M.; Reading, M. Thermal Analysis of Pharmaceuticals; CRC Press, 2006.
(57) Prime, R. B.; Bair, H. E.; Vyazovkin, S.; Gallagher, P. K.; Riga, A. Thermogravimetric Analysis (TGA). In Thermal Analysis of Polymers, 2009; pp 241-317.
(58) Höhne, G.; Hemminger, W.; Flammersheim, H. J. Differential Scanning Calorimetry; 1996. DOI: 10.1007/978-3-662-03302-9.
(59) Abd-Elghany, M.; Klapötke, T. M. A review on differential scanning calorimetry technique and its importance in the field of energetic materials. Physical Sciences Reviews 2018, 3 (4). DOI: doi:10.1515/psr-2017-0103 (acccessed 2023-08-29).
(60) FAQ: Beginners Guide to Thermogravimetric Analysis; Perkin Elmer.
(61) Coats, A. W.; Redfern, J. P. Thermogravimetric analysis. A review. The Analyst 1963, 88 (1053). DOI: 10.1039/an9638800906.
(62) Vecchio, S.; Brunetti, B. Vapor Pressures and Standard Molar Sublimation Enthalpies of Three 6-Methylthio-2,4-di(alkylamino)-1,3,5-triazine Derivatives: Simetryn, Ametryn, and Terbutryn. J. Chem. Eng. Data 2007, 52, 1585-1594.
(63) Santos, L. M. N. B. F.; Schröder, B.; Fernandes, O. O. P.; Ribeiro da Silva, M. A. V. Measurement of enthalpies of sublimation by drop method in a Calvet type calorimeter: design and test of a new system. Thermochimica Acta 2004, 415 (1-2), 15-20. DOI: 10.1016/j.tca.2003.07.016.
(64) Geiseler, G. J. D. Cox und G. Pilcher: Thermochemistry of Organic and Organometallic Compounds. Academic Press, London and New York 1970. 643 Seiten. Preis: 170s. Berichte der Bunsengesellschaft für physikalische Chemie 1970, 74 (7), 727-727. DOI: https://doi.org/10.1002/bbpc.19700740727.

(65) Curtiss, L. A.; Redfern, P. C.; Raghavachari, K. Gaussian-3 (G3) theory for molecules containing first and second-row atoms. J Chem Phys 1998, 109, 7764. DOI: 10.1063/1.2436888.
(66) Curtiss, L. A.; Redfern, P. C.; Raghavachari, K. Gaussian-4 theory. J Chem Phys 2007, 126 (8), 084108. DOI: 10.1063/1.2436888 From NLM PubMed-not-MEDLINE.